CONTINUOUS LEACHING OF A REDUCED MANGANESE ORE

Clive John Jones

A Dissertation Submitted to the Faculty of Engineering, University of the Witwatersrand, Johannesburg in fulfillment of the requirements for the Degree of Master of Engineering.

Johannesburg 1983

ABSTRACT

A design procedure for agitated leaching vessels is not well-established. The majority of previous investigations have tended to concentrate on kinetic studies performed batchwise in which the information obtained is not directly useful in designing continuous systems. The leaching of a reduced manganese ore is chosen as the topic for investigation since the production of manganese is of great importance to both the electrolytic manganese metal and manganese dioxide industries.

The system chosen is complicated by the presence of iron, some of which leaches in the ferrous state but is oxidised by dispersing air in the tank to an insoluble ferric hydroxide. Manganous ions may also be oxidised to insoluble manganic hydroxide. The control of pH is important since if it falls below 5,5 a large amount of iron dossolves whereas above 6,5 the leaching rate is slow.

These factors are studied experimentally and a leaching model is proposed. An example of the use of this model in design of a leach process is given.

DECLARATION

I, the undersigned, Clive Jones, do hereby declare that the contents of this dissertation are solely my work except where specific acknowledgement is made. This dissertation has not been submitted for a degree at any other university or institution.

CLIVE JONES

Department of Chemical Engineering,
University of the Witwatersrand,
Johannesburg.

January, 1983

ACKNOWLEDGEMENTS

Thanks are due to the following people and institutions for making this dissertation possible:

Professor A.W.Bryson who as supervisor of this project rendered invaluable advice and assistance;

The Council for Mineral Technology (MINTEK) for providing a bursary and funds to finance this project and for analysing over three hundred liquid and solid samples;

The University of the Witwatersrand for providing laboratory and office facilities;

The workshop staff of the Chemical Engineering Department for setting up the apparatus;

Delta Manganese (Pty) Ltd. for providing an ore sample and technical assistance;

My fiancé, Diana , for typing this dissertation.

CONTENTS

CONTENTS continued

CONTENTS continued

NOTATION

Latin Symbols

		units
a	surface area per unit volume of fluid	m^2/m^3
A	liquid reactant (equation (2.19))	
B	solid reactant (equation (2.19))	
C_A	concentration of total NH_3^+ or concentration of species A	mol/l or g/l
C_{Ab}	bulk concentration of species A	"
C_{As}	surface concentration of species A	"
C_1	concentration of Mn^{2+}	"
C_2	concentration of H^+	"
C_3	concentration of NH_4^+	"
C_4	concentration of $MnNH_3^{2+}$	"
C_5	concentration of NH_3	"
C_m	concentration of total Mn	"
C_{ms}	equilibrium Mn concentration	"
C	liquid product (equation (2.19))	
d	mean equivalent spherical diameter	cm
D_A	effective diffusion coefficient in the ash layer	cm^2/sec
$E_D(t)dt$	residence time distribution	
g_0	inlet mass fraction	
g_1	outlet mass fraction	
k	rate constant	
k_g	mass transfer coefficient between liquid and solid	mol/cm^2 sec

Notation continued

k_m	mass transfer coefficient	cm/sec
k_s	first order rate constant	cm/sec
K, K_a, K_c, K_s	equilibrium constants, as defined by equations (2.4)-(2.6)	
K'_a, K'_c, K'_s	equilibrium ratios as defined by equations (2.7)-(2.9)	
l	size factor	
M	total mass of B in unreacted cores per unit volume of fluid	g/l
M_0	total mass of B per unit volume of fluid in the inlet stream	g/l
M_1	total mass of B per unit volume of fluid in the outlet stream	g/l
$(M)_{batch}$	mass of B per unit volume of fluid in a batch reactor operating with the same values of k, N, ϕ and Ψ.	g/l
n_b, n_c, n_D	stoichiometric coefficients, equation (2.13)	
N_i	moles of component i	
N	number of particles in a vessel per unit volume of fluid	no./l
p	surface to volume ratio	m^2/m^3
P	solid product, equation(2.19)	
Q_0	inlet solution flowrate	l/min
Q	outlet solution flowrate	l/min
r_A	rate of disappearance of reactant A	mol/m^3 min
r_c	radius of unreacted core	cm
R	radius of particle	cm

Notation continued

S_{ex}	external surface area of particle	cm^2
t	time	min
t^*	defined by equation (2.38)	min
T	temperature	K
v	volume of particle	cm^3
V_1	volume of leach reactor	l
W_0	inlet solid flowrate	g/min
W_1	discharge solid flowrate	g/min
X_B	fractional conversion of reactant B	

Greek Symbols

ε	$\psi(C_{As}, C_{Cs})$ i.e. function of the concentration of species A in the fluid phase at the outer surface of the particle	g/l
ϕ	shape factor	
λ	defined by equation (2.40)	min^{-1}
η	fractional leach efficiency	
ρ_B	density of B	g/cc
γ_1	activity coefficient of Mn^{2+}	
γ_2	activity coefficient of H^+	
γ_3	activity coefficient of NH_4^+	
γ_4	activity coefficient of $MnNH_3^{2+}$	
γ_5	activity coefficient of NH_3	
θ	fraction of surface covered by adsorbed A	
$\bar{t}$	residence time	min
δ	apparent film thickness for mass transfer	cm
τ	time for complete conversion	min

List of Tables

List of Tables continued

List of Figures

List of Figures continued

List of Figures Continued

1. INTRODUCTION

1.1 The History of Electrolytic Manganese

Initially, the production of electrolytic manganese was considered impossible (1,2). Metallurgical authorities came to this conclusion in the early Thirties, after extensive investigation of the electrolytic process.

From strictly theoretical considerations, manganese is too high in the electro-motive series to be readily deposited from aqeous solutions. Operating conditions must be carefully controlled witnin narrow operating bands, or hydrogen gas will be produced instead of metal.

Despite the difficulties in the production of manganese metal, there were strong incentives for developing a workable process. Manganese is widely used as a valuable alloying material for steel, aluminium and other metals and the higher quality alloys,such as stainless steel, cannot tolerate more than trace amounts of carbon, sulphur and phosphorous. This indicated that pure manganese, if commercially available, would become an important major constituent of both ferrous and nonferrous alloys.

In 1935, the U.S.Bureau of Mines under Dr. R.S.Dean (5) undertook a major program of electrometallurgical investigation, one of the first objectives being the production of pure manganese. In 1939, the Electro-Manganese Corporation was formed to develop the production of electrolytic manganese on a commercial scale, based on the U.S. Bureau of Mines laboratory process.

By 1942, the world's production capacity of electrolytic manganese was 365 tonnes per annum and by 1977 this had increased to 76900 tonnes per annum.(3)

1.2 Uses of Electrolytic Manganese

Electrolytic manganese due to its high purity can be used for virtually every application where manganese is required. In particular, it is used in both the ferrous and non-ferrous industries in the production of alloys such as stainless steel, High Strength Low Alloy (H.S.L.A), other special steels, aluminium, nickel, titanium, magnesium, silver, zinc and cobalt alloys. Manganese is also used extensively in the ferrite (magnetic ceramics) and chemical industries.

Potential market areas for electrolytic manganese include:

a) production of methylcyclopentadienyl manganese tricarbonyl(MMT) used as an anti-knock compound for petrol as well as a combustion improver in distillate fuels (electrolytic manganese is an ideal source of manganese for producing $MnCl_2$, which is used to produce MMT),

b) electrolytic manganese powder for purification in zinc electrowinning processes,

c) manganese-copper dampening alloys, and

d) production of high strength low alloy steels.

1.3 The Production of Electrolytic Manganese in South Africa

In 1954 the first electrolytic manganese in South Africa was produced by Harris (2,3) on an experimental basis at the University of the Witwatersrand, Johannesburg, South Africa. A pilot plant was subsequently erected at West Rand Cons in Krugersdorp. This plant produced electrolytic manganese from manganese hydroxide originating from uranium effluent.

In 1960, the plant (now known as EMCOR) started producing electrolytic manganese from manganese ores mined in the North Western Cape. These ores raised a whole series of new problems mostly connected with the relatively high iron content of the ores, which were subsequently solved.

In 1974, another company (Delta Manganese (Pty.) Limited, Nelspruit) commenced production of electrolytic manganese from manganese ore. This process is discussed below.

By 1977, South Africa was producing 50 per cent of the world's electrolytic manganese and supplied 75 to 80 per cent of the metal available for free trade(3).

1.4 The Delta Manganese Process

To understand fully the role of leaching in the production of electrolytic manganese, a brief description of the Delta Manganese process is presented. The flowsheet of the process is given in

Figure 1.1. The process consists essentially of four main steps:

a) reduction of the ore from manganese (IV) to manganese (II) to solubilize it in sulphuric acid,

b) leaching of the reduced ore in spent electrolyte using techniques to minimize the dissolution of iron (iron interferes with the electrowinning process in the cell house),

c) purification of the leach liquor to remove all the elements that will adversely affect the electrodeposition of manganese, and

d) electrolysis of the purified solution to plate pure manganese metal.

1.5 Type of Manganese Ore Used

Throughout this project, ore from the North Western Cape (via Delta Manganese) was used. The ore had already been processed in the first stage of the overall operation i.e. milled and reduced from manganese (IV) to manganese (II). A typical analysis of the ore is given in Table 1.1 (3).

Table 1.1

Typical Analysis of the Reduced Manganese Ore

Manganese (total)	54,0%
Iron	10,9%
Silica	4,1%
Nickel	26ppm
Cobalt	76ppm
Zinc	158ppm
Moisture content	0,4-0,8%

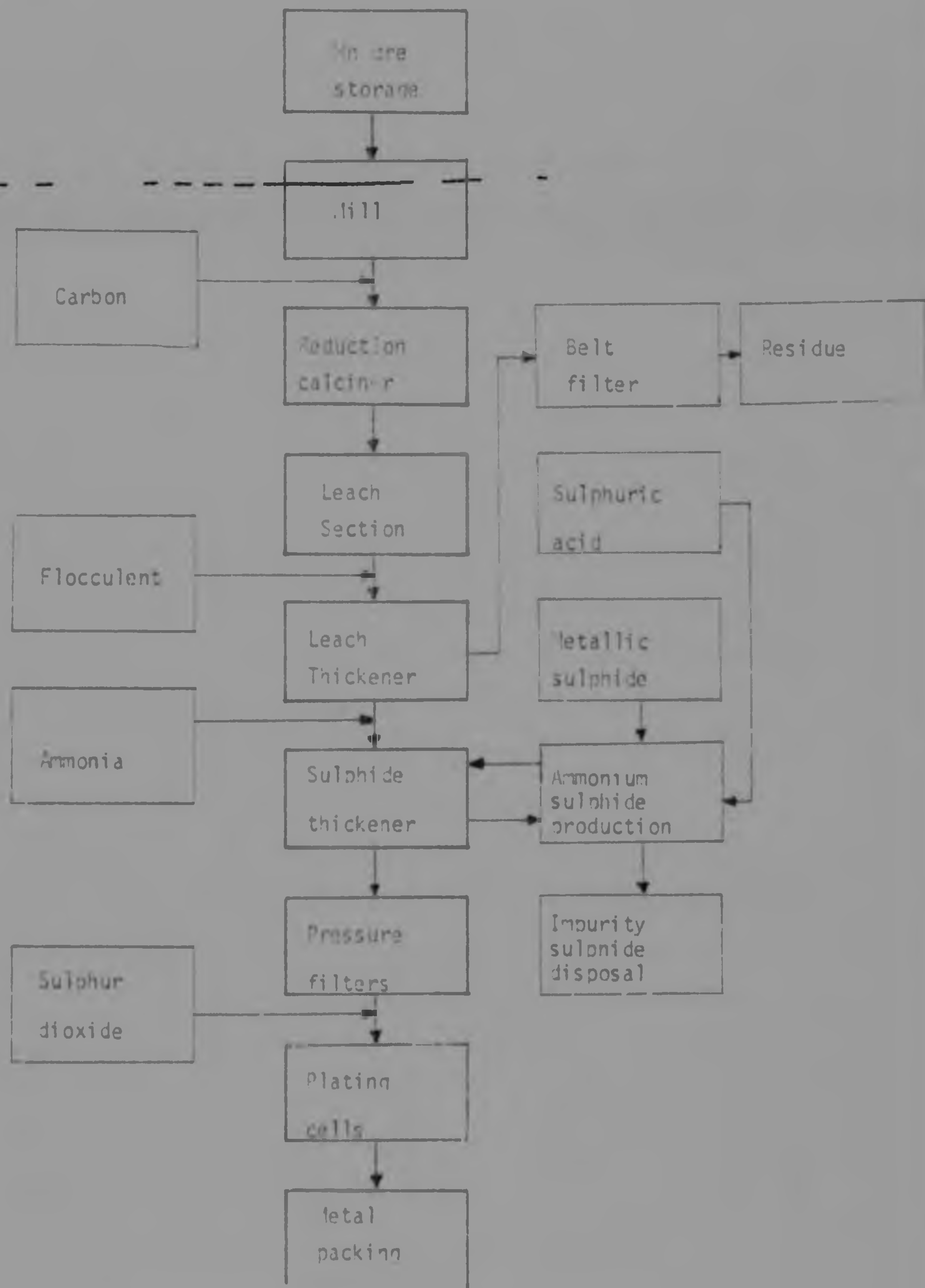

FIG.1.1:Flowsheet for the Production of Electrolytic Manganese at Delta Manganese

1.6 Aims of this Investigation

From the above discussion, it is clear that the production of manganese is of great importance to both the electrolytic manganese metal and manganese dioxide industries. In previous work (6,7) both the reduction of the manganese ore and the electrolysis of the purified solution to plate pure manganese metal have been modelled. Thus, the leaching of the reduced manganese ore was chosen as the topic for investigation.

The broad aim of this investigation is to determine the rates at which manganese leaches as a function of pH and concentration. Further, a design procedure for agitated leaching vessels is not well-established. Most kinetic studies are performed batchwise and this information is not always directly useful in designing continuous systems. It is for this reason that the leaching was performed continuously.

The system chosen is complicated by the presence of iron, some of which leaches in the ferrous state but is oxidised by dispersing air in the tank to an insoluble ferric hydroxide. Manganous ions may also be oxidised to insoluble manganic hydroxide. The control of pH is thus important since if the pH falls below 5,5 a large amount of iron will dissolve, which on subsequent precipitation forms a bulky precipitate which settles out very slowly and is difficult to filter and wash. If the pH goes above 6,5 the leaching rate becomes very slow.

These factors were studied experimentally and the results were then fitted to an appropriate design oriented model.

2. THEORETICAL ASPECTS OF REDUCED MANGANESE LEACHING

2.1 The Theory of Leaching (8,9)

Leaching is fundamentally a separation process. In this respect it is like all other unit operations in extractive metallurgy. Very rarely is leaching applied in such a way as to totally dissolve the raw material being treated. This means that leaching is almost always wedded to a liquid-solid separation plant, in which the solid is either an undissolved material, a precipitate that formed during leaching , or a combination of both. The solids that are rejected nearly always contain residual unleached values, partly as undecomposed minerals, partly as adsorbed or absorbed components in the precipitates, and partly as entrained leach solution. The presence of undecomposed mineral usually arises because the leaching process is kinetically slow, and when the residence time has been too short. The presence of adsorbed or absorbed metal in precipitates is due to thermodynamic conditions that partition the leached metal species between the two phases - the solid precipitate and the aqueous solution. The entrained leach solution is a result of an imperfect liquid-solid separation.

When leaching recoveries are less than 100%, the problem usually warrants investigation to ascertain whether it is a kinetic, a thermodynamic, or a physical problem. The investigation may give an indication of the most appropriate methods of improving the performance of the leaching operation.

2.2 Solution Production

The most common reagents used for leaching are acids, of which sulphuric acid is the most widely used, but hydrochloric acid also finds a limited application. Other reagents used include alkalies, oxidizing agents and reducing agents.

The use of a particular leaching agent or combination of leaching reagents is determined ultimately of course, by the overall economics of the process. A number of factors can be listed as being of major significance in evaluating leaching reagents:

a) The leach solution should be selective to the extent that it dissolves the desired metal values rapidly, and reacts with the valueless minerals slowly or most desirably, not at all.

b) The solubility of the leaching reagents should be sufficiently high to achieve adequate reaction rates. The solubility of the metal compounds produced should also be high to minimize the volume of solutions to be handled.

c) The leach solutions should present the minimum of problems with regard to corrosion of equipment.

d) The presence of residual amounts of the reagent in plant effluent should not be harmful to the environment.

e) The reagents should be available at low cost or such that they can be simply regenerated or converted to useful by-products.

2.3 The Leaching of Manganese

On the Delta Manganese plant, the manganese is leached from the reduced ore on a continuous basis with the spent electrolyte (anolyte) from the electrolytic cells. The leach solution used in this project was similar. It is an ammonium sulphate-manganese sulphate solution having a composition as indicated in Table 2.1.

Table 2.1.

Composition of the Anolyte solution

Ammonium sulphate	107	kg/m^3
Manganese (total)	12,2	kg/m^3
Sulphuric acid	31,3	kg/m^3
pH	< 1	

The reduced ore is added to the anolyte at such a rate as to control the pH at between 5,5 and 6,5. (In this investigation, the pH was varied between 2,0 and 7,5). If the pH falls below 5,5 a large amount of iron will be dissolved, which on subsequent precipitation forms a bulky precipitate which settles out very slowly and is difficult to filter and wash. If the pH goes above 6,5 the leaching rate becomes very slow. If the pH goes above 7,0 the reduced ore reacts with the ammonium sulphate liberating ammonia gas which will precipitate manganese hydroxide from the leach solution. The manganese hydroxide thus precipitated will react with air in the solution to form insoluble manganese dioxide which will be lost in the leach residue.

Bryson and Rodrigues (10) have shown that a manganese sulphate-ammonium sulphate solution in the pH range 6,0 to 8,0 will contain H_2O, Mn^{2+}, NH^+_4, $MnNH_3^+$, NH_3 and SO_4^{2-} as the major species. To determine the concentrations of various components from equilibrium constants (K), it is necessary to know activity coefficients. Since very little data is available for concentrated solution mixtures, equilibrium ratios K' have been measured or estimated by Rodrigues (7). At equilibrium if there is any MnO remaining, the surface of this MnO will probably be completely hydrolysed, i.e. in the form of $Mn(OH)_2$. The following equilibria can then be expected:

$$Mn^{2+} + 2H_2O = Mn(OH)_2(s) + 2H^+ \tag{2.1}$$

$$Mn^{2+} + NH_4^+ = MnNH_3^{2+} + H^+ \tag{2.2}$$

$$NH_3 + H^+ = NH_4^+ \tag{2.3}$$

The above reactions are then also the leach reactions. The following equilibrium coefficients then apply:

$$K_s = \frac{\gamma_2^2 C_2^2}{\gamma_2^2 C_1} = \frac{\gamma_2^2}{\gamma_2^2} K_s' \tag{2.4}$$

$$K_c = \frac{\gamma_2 \gamma_4 C_2 C_4}{\gamma_1 \gamma_3 C_2 C_5} = \frac{\gamma_2 \gamma_4}{\gamma_1 \gamma_3} K_c' \tag{2.5}$$

$$K_a = \frac{\gamma_3 C_3}{\gamma_2 \gamma_5 C_2 C_5} = \frac{\gamma_3}{\gamma_2 \gamma_5} K_a' \tag{2.6}$$

The equilibrium ratios for the above reactions have been modelled by Rodrigues (7) over the temperature range $295 < T < 330$ by the following equations:

$$K'_s = \frac{C_2^2}{C_1} = \exp\,(-65{,}17 + 0{,}1025T) \tag{2.7}$$

$$K'_c = \frac{C_2C_4}{C_1C_3} = \exp\,(-34{,}57 + 0{,}051T) \tag{2.8}$$

$$K'_a = \frac{C_3}{C_2C_5} = \exp\,(40{,}32 - 0{,}064T) \tag{2.9}$$

The following mass balances can also be written:

$$C_{ms} = C_1 + C_4 \tag{2.10}$$

$$C_A = C_3 + C_4 + C_5 \tag{2.11}$$

$$C_1 = \frac{C_2^2}{K'_s} \tag{2.12}$$

$$C_4 = C_{ms} - C_1 \tag{2.13}$$

$$C_3 = \frac{C_2C_4}{C_1K'_c} = \frac{C_2(C_{ms} - C_1)}{C_1K'_c} \tag{2.14}$$

$$C_5 = \frac{C_3}{C_2K'_a} = \frac{C_{ms} - C_1}{C_1K'_cK'_a} \tag{2.15}$$

And by rearranging equations (2.10) to (2.15):

$$C_A = \frac{C_2(C_{ms} - C_1)}{C_1K'_c} + C_{ms} - C_1 + \frac{C_{ms} - C_1}{C_1K'_cK'_a} \tag{2.16}$$

$$C_{ms} = \frac{C_A + C_2/K'_c + C_1 + 1/K'_cK'_a}{C_2/C_1K'_c + 1 + 1/C_1K'_cK'_a} \tag{2.17}$$

By substituting equation (2.17) into equation (2.16), the equilibrium manganese concentration (C_{ms}) is:

$$C_{ms} = \frac{C_1(C_A + C_2/K'_c + C_1 + 1/K'_cK'_a)}{C_2/K'_c + C_1 + 1/K'_cK'_a} \tag{2.18}$$

2.4 Theory of Non-Catalytic Liquid-Solid Reactions.

Although there has been a vast amount of research into non-catalytic liquid-solid reactions, information relating to reduced manganese leaching is scarce (1,2,3,4,11,12). Most studies on particulate systems have concentrated on the development of models to explain the reaction of the solid phase with the liquid phase.

The models reported in the literature range from simple models based on single rate controlling steps (14,15), through generalised models including the effects of convective mass transfer (17), reaction with porous solids (18) to quite sophisticated models incorporating pore size distributions (19,21) and simultaneous noncatalytic solid-fluid reactions(22). Models based on variable activation energies (23) and diffuse interfaces (24) have also been developed.

In this investigation some of these models are discussed and compared with experimental data.

Wen(14) has reviewed, in some detail, the processes involved in different types of solid-fluid reactions. For the most general case with both fluid and solid reactants and products, which is typical of leaching processes,

$$A(l) + n_b B(s) = n_c C(l) + n_D P(s) \qquad (2.19)$$

The reaction proceeds through five consecutive steps:

i) Diffusion of liquid reactant A through the film surrounding the particle to the surface of the solid B.

ii) Penetration and diffusion of A through the pores of the solid to the reaction sites.

iii) Reaction of A with B at this solid interface.

iv) Diffusion of C through the pores of the solid to the outer surface of the particle.

v) Diffusion of C across the boundary layer film surrounding the particle to the bulk liquid phase.

If the concentration driving force of any of the above processes is much larger than the others, then that process is the one which apparently controls the overall process. The other, faster, processes may be considered to be at equilibrium when formulating a model of the reaction system. If all of the concentration driving forces are of a similar magnitude then the contribution of each to the overall reaction rate must be included in the model.

2.5 The Unreacted Core Shrinking Model

The earliest heterogenous non-catalytic fluid-solid reaction model, proposed by Yagi and Kunii (13) has been discussed in some detail by Levenspiel (14) and Smith (15). This model, the so-called unreacted core shrinking model, which is depicted schematically in Figure 2.1 is based on the assumption that the reaction occurs only at a discrete interface between the solid reactant and product.

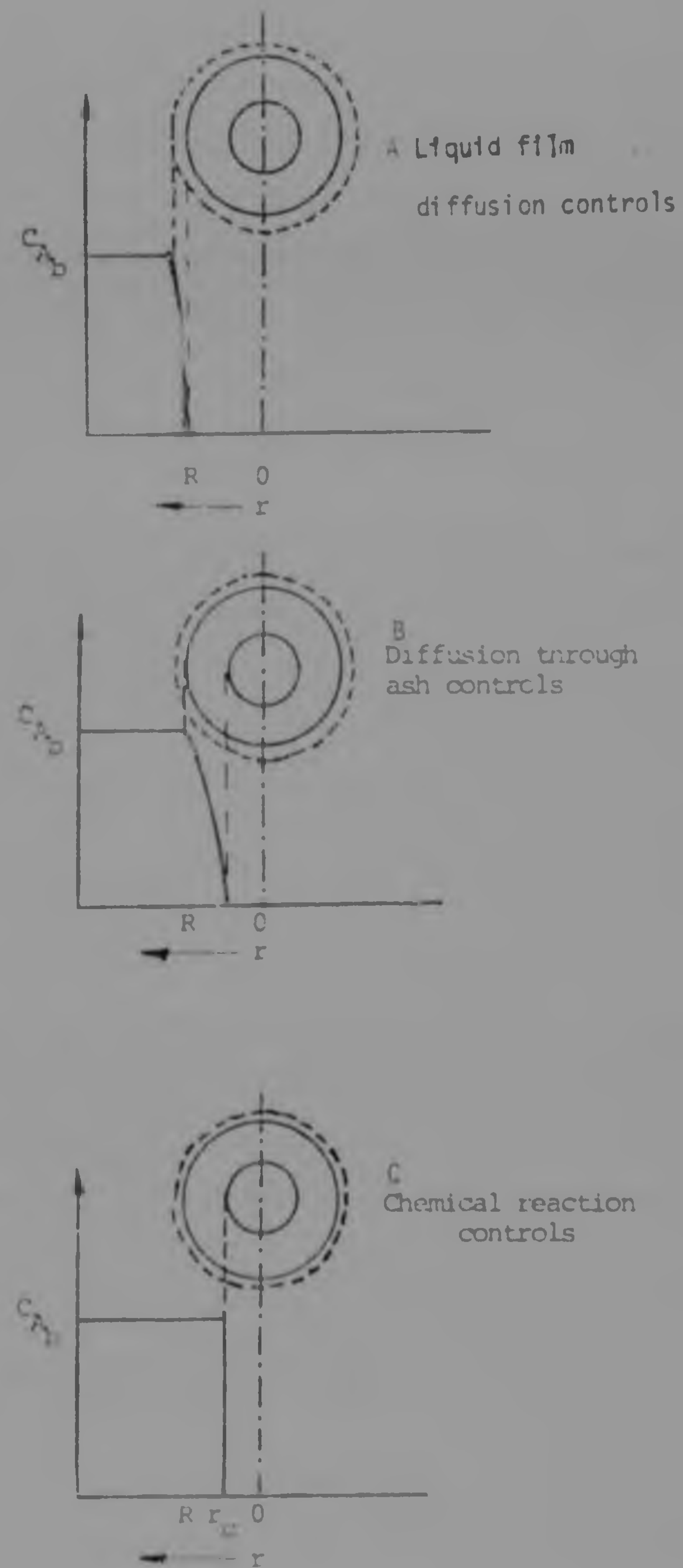

FIGURE 2.1.

SCHEMATIC REPRESENTATION OF THE UNREACTED CORE SHRINKING MODEL

This implies that the intrinsic reaction rate is very much faster than the rate of liquid diffusion in the unreacted core. This condition is realised in initially non-porous materials but the model is not applicable to the chemically controlled reaction of an initially porous solid, for in this case the liquid would diffuse throughout the solid particle before any appreciable conversion occurred, and the reaction would proceed homogeneously.

In view of the liquid concentration profiles in the solid particle defined by the assumptions in arriving at the unreacted core shrinking model, it is clear that at least for mass transfer and diffusion control of the reaction there will be only one reaction interface regardless of the number of solid phases present.

In the case of chemical reaction control ,the dense core could shrink, leaving behind a porous, grainy "ash" through which the liquid would diffuse witn no resistance. The remaining grains would now act as individual particles and react according to the unreacted core shrinking model, possibly becoming grainy in turn. Park and Levenspiel (30) have described a similar model, called the crackling core model.

2.5.1 Diffusion Through Liquid Film Controls

Whenever the resistance of the liquid film controls, the concentration profile of liquid reactant A will be as shown in Figure 2.1(a). From this figure it can be seen that no reactant is present at the surface; hence the concentration driving force, given by $(C_{Ab}-C_{As})$, is constant at all times during the reaction of the particle. Now since it is convenient to derive the kinetic equations based on available surface, attention is focused on the unchanging exterior surface of a particle, S_{ex}. Levenspiel (14) thus arrives at the conclusion that the liquid flux though the boundary layer liquid film is proportional to the rate of disappearance of the solid reactant, i.e.

$$\frac{-1}{S_{ex}}\frac{dN_B}{dt} = \frac{-1}{4\pi R^2}\frac{dN_B}{dt} = \frac{-n_b}{4\pi R^2}\frac{dN_A}{dt}$$

$$= n_b\, k_g\,(C_{Ab} - C_{As})$$
$$= n_b\, k_g\, C_{Ab}$$
$$= \text{constant} \qquad (2.20)$$

The radius of the unreacted core in terms of fractional time for complete conversion is (Appendix 10.1)

$$\frac{t}{\tau} = 1 - \left(\frac{r_c}{R}\right)^3 \qquad (2.21)$$

This can also be written in terms of the fractional conversion X_B (Appendix 10.1) as

$$\frac{t}{\tau} = 1 - \left(\frac{r_c}{R}\right)^3 = X_B \qquad (2.22)$$

Thus the relationship between time, radius and conversion is achieved.

2.5.2 Diffusion through Ash Layer Controls

Figure 2.3 (b) illustrates the situation in which the resistance to diffusion through the ash controls the rate of reaction. Levenspiel (14) has argued that if the rate of advance of the unreacted core boundary is slow compared with the rate of reactant diffusion through the ash layer surrounding the core, then the interface is essentially stationary with respect to reactant flux at any time. The concentration gradient of reactant liquid is then given by the steady state diffusion relation

$$\frac{-dN_A}{dt} = 4\pi r^2 D_A \frac{dC_A}{dr} \qquad (2.23)$$

which in terms of the fractional conversion becomes (Appendix 10.2)

$$\frac{t}{\Gamma} = 1 - 3(1 - X_B)^{2/3} + 2(1 - X_B) \qquad (2.24)$$

2.5.3 Chemical Reaction Controls

Figure 2.1 (c) illustrates concentration gradients within a particle when chemical reaction controls. Since the progress of the reaction is unaffected by the presence of any ash layer, the quantity of material reacting is proportional to the available surface of unreacted core, the rate of disappearance of the solid is given by

$$\frac{-dN_B}{dt} = 4\pi r_c^2 \, k_s C_{Ab} \qquad (2.25)$$

The decrease in radius or increase in fractional conversion of the particle in terms of Γ is thus found to be (Appendix 10.3)

$$\frac{t}{\tau} = 1 - \frac{r_c}{R} = 1 - (1 - X_B)^{1/3} \qquad (2.26)$$

2.5.4 Combination of Resistances

The above conversion time expressions assume that a single resistance controls throughout the reaction of the particle. However, the relative importance of the liquid film, ash layer, and reaction steps will vary as conversion progresses. For example, for a constant size particle the liquid film resistance remains unchanged, the resistance to reaction increases as the surface of the unreacted core decreases, while the ash layer resistance is non-existant at the start because no ash is present, but becomes progressively more and more important as the ash layer builds up.

To account for the simultaneous action of these resistances is straight forward since they act in series and all are linear in concentration. Thus, on combining equations (2.20) , the integrated form of (2.23) and (2.25) with their individual driving forces and eliminating intermediate concentrations, it can be shown that:

$$t_{total} = t_{film} + t_{ash} + t_{reaction} \qquad (2.27)$$

Similarly, for complete conversion

$$\tau_{total} = \tau_{film} + \tau_{ash} + \tau_{reaction} \qquad (2.28)$$

2.5.5 An Alternative Derivation of the Unreacted Core Shrinking Model

Bryson (34) has considered an alternative derivation of the unreacted

$$\frac{t}{\tau} = 1 - \frac{r_c}{R} = 1 - (1 - X_B)^{1/3} \qquad (2.26)$$

2.5.4 Combination of Resistances

The above conversion time expressions assume that a single resistance controls throughout the reaction of the particle. However, the relative importance of the liquid film, ash layer, and reaction steps will vary as conversion progresses. For example, for a constant size particle the liquid film resistance remains unchanged, the resistance to reaction increases as the surface of the unreacted core decreases, while the ash layer resistance is non-existant at the start because no ash is present, but becomes progressively more and more important as the ash layer builds up.

To account for the simultaneous action of these resistances is straight forward since they act in series and all are linear in concentration. Thus, on combining equations (2.20), the integrated form of (2.23) and (2.25) with their individual driving forces and eliminating intermediate concentrations, it can be shown that:

$$t_{total} = t_{film} + t_{ash} + t_{reaction} \qquad (2.27)$$

Similarly, for complete conversion

$$\tau_{total} = \tau_{film} + \tau_{ash} + \tau_{reaction} \qquad (2.28)$$

2.5.5 An Alternative Derivation of the Unreacted Core Shrinking Model

Bryson (34) has considered an alternative derivation of the unreacted core shrinking model. In this derivation, various rate expressions are examined and it is found that

$$r_A = -ka\,\Psi \qquad (2.29)$$

(For discussion leading up to the formulation of equation (2.29) see Appendix 10.4)

The unreacted core shrinking model can also be written for non-spherical particles by defining appropriate size and shape factors. The following definitions are found to be convenient:

$$l = \text{size of unreacted core}$$
$$= (\text{volume of unreacted core})^{1/3} \qquad (2.30)$$

$$\phi = \text{shape of unreacted core}$$
$$= (\text{exposed surface area of unreacted core})/l^2 \qquad (2.31)$$

Provided all particles have the same size and shape factor:

$$a = N\phi l^2 \qquad (2.32)$$

and

$$r_A = -kN\phi l^2\psi \qquad (2.33)$$

Further

$$M = \rho_B N l^3 \qquad (2.34)$$

Eliminating l between equations (2.33) and (2.34) gives

$$r_A = -kN\phi\psi\left(\frac{M}{\rho_B N}\right)^{2/3} \qquad (2.35)$$

The rate expression now not only takes into account the effect of concentration of the liquid species, but also the variation in surface area of the reaction interface. This rate expression can also be written in a different form by substituting for N from equation (2.34) into equation (2.35)

FIG. 2. 2: The Unreacted Core Shrinking Mudel

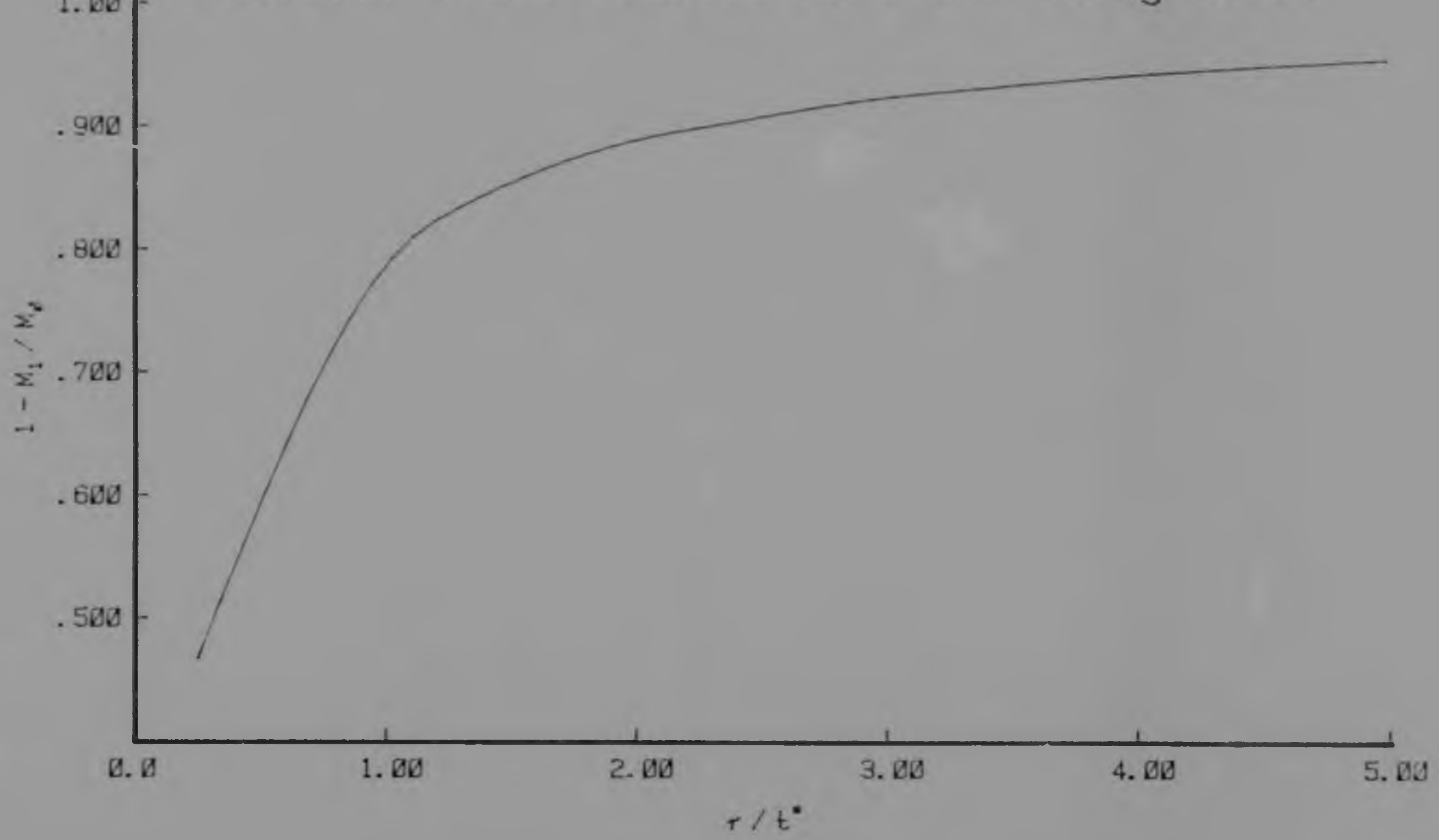

$$r_A = \frac{-k'1}{\rho_B 1} \phi \Psi \qquad (2.36)$$

The result arrived at for the unreacted core shrinking model (Appendix 10.4) is

$$1 - \frac{M_1}{M_o} = 3\frac{\tau}{t^*} - 6\left(\frac{\tau}{t^*}\right)^2 + 6\left(\frac{\tau}{t^*}\right)^3 \left(1-\exp\left(\frac{-t^*}{\tau}\right)\right) \qquad (2.37)$$

where $1 - \frac{M_1}{M_o}$ is the fractional conversion (or fractional leach efficiency) and

$$t^* = \frac{3 M_o^{1/3} (\rho_B N)^{2/3}}{kN \phi \Psi} \qquad (2.38)$$

Equation (2.37) is plotted in Figure 2.2.

Thus a test of the applicability of the unreacted core shrinking model is to plot $1 - M_1/M_o$ versus τ / t^* from experimental data and to compare with the theoretical values as shown in Figure 2.2.

2.6 The Porous Solid Model

Unlike the unreacted core shrinking model, this model assumes that the solid particles are initially porous and that the leach solution is able to diffuse easily throughout the solid particle. The solid particle is represented diagramatically in Figure 2.3.

In Figure 2.3, the black grains are the reactive component (such as the manganese in the case of leaching a reduced manganese ore). The lines represent pores or cracks. The following types of reactive mineral grain can be identified:

FIG.2.3: Representation of the Solid Particle in the Porous Solid Model.

a) grains exposed to the reagent at the surface of the particle (e.g. grain numbered 1), and

b) grains exposed to the reagent via pores or cracks (e.g. grain numbered 2).

With the reagent in a surrounding liquid, the rate of reaction between it and the reactive mineral is controlled by the rate of mass transfer of a product from the grain. However, if the particle is highly porous (i.e. the leach liquor is able to diffuse easily throughout the porous particle) then the rate of reaction is likely to be controlled by the rate at which reactant can diffuse through the liquid to the solid particle.

By using an analysis of the situation similar to that in section 2.5.5, it can be shown that (Appendix 10.5)

$$r_A = -\lambda M \tag{2.39}$$

where
$$\lambda = \frac{k\rho\varphi}{\rho_B} \tag{2.40}$$

And by applying this rate to a continuous system (Appendix 10.5)

$$1 - \frac{M_1}{M_o} = \frac{\lambda\tau}{1 + \lambda\tau} \tag{2.41}$$

Equation (2.41) is plotted in Figure 2.4.

Thus , a plot of $1 - M_1/M_o$ versus $\lambda\tau$ from experimental data will

FIG. 2.4: The Porous Solid Model

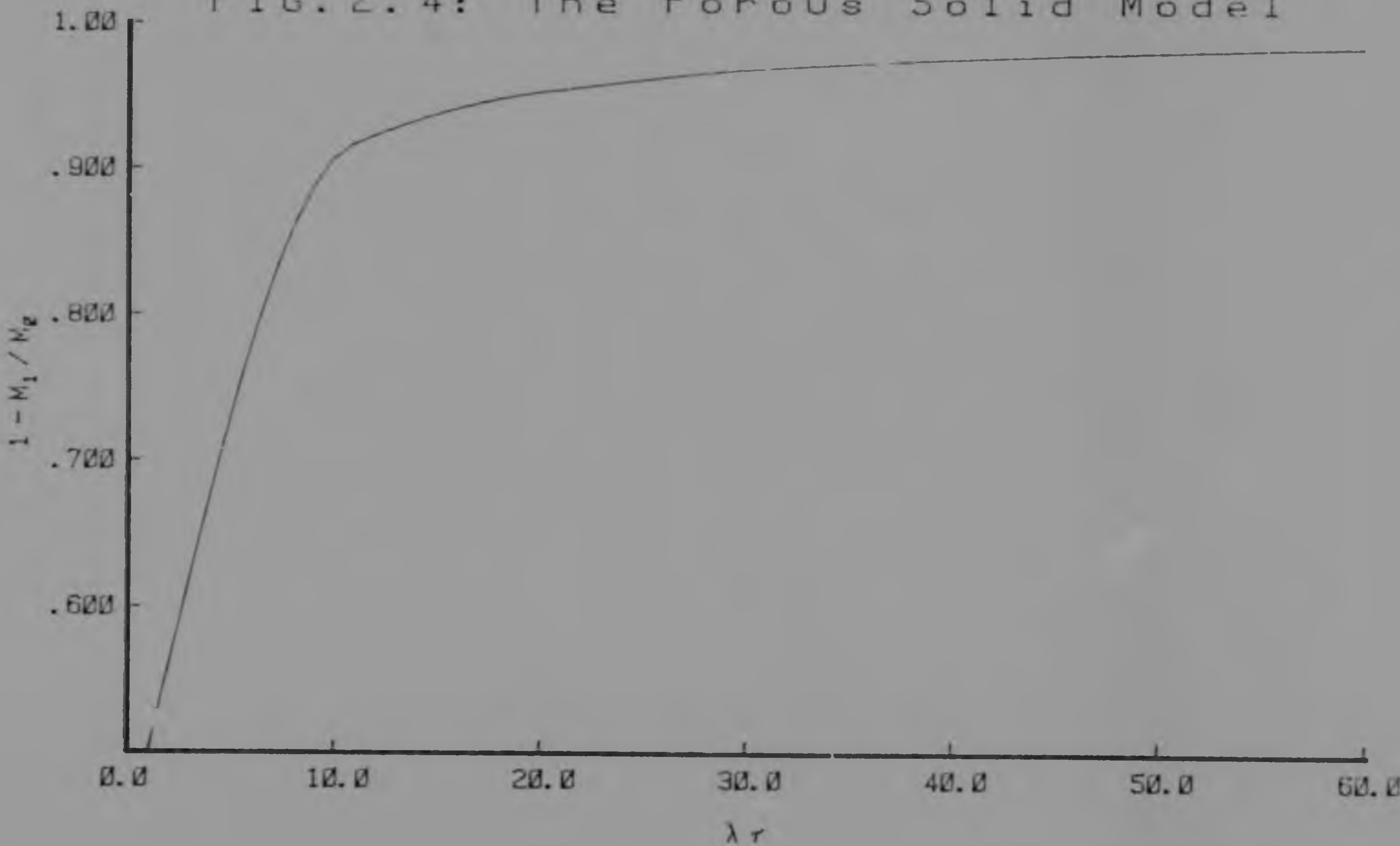

test the applicability of this model to a given system.

2.7 Calculation of the Rates of Reaction

A convenient and simple way of calculating the rates of reaction in a leaching process is via the mass balance of the system. This method gives the rates and at the same time overcomes the modelling problem. The rate determined in this way is expressed as a function of the concentration of reactant or product in either the fluid or solid phase.

The leaching apparatus used in this investigation is shown in Figure 2.5. The agitated tank is assumed to be an ideal CSTR.

The fractional leach efficiency , η, will be given by

$$\eta = \frac{W_o g_o - W_1 g_1}{W_o g_o} \qquad (2.42)$$

The rate of reaction based on the aqeous phase (Appendix 10 6)is

$$r_1 = \frac{Q_1}{V_1} \left(C_1 - \frac{Q_o}{Q_1} C_o \right) \qquad (2.43)$$

and the rate of reaction based on the solid phase (Appendix 10.6) is:

$$r_1 = \frac{W_o g_o - W_1 g_1}{V_1} \qquad (2.44)$$

Thus the rate of leaching can be calculated from a knowledge of either the solid or liquid properties.

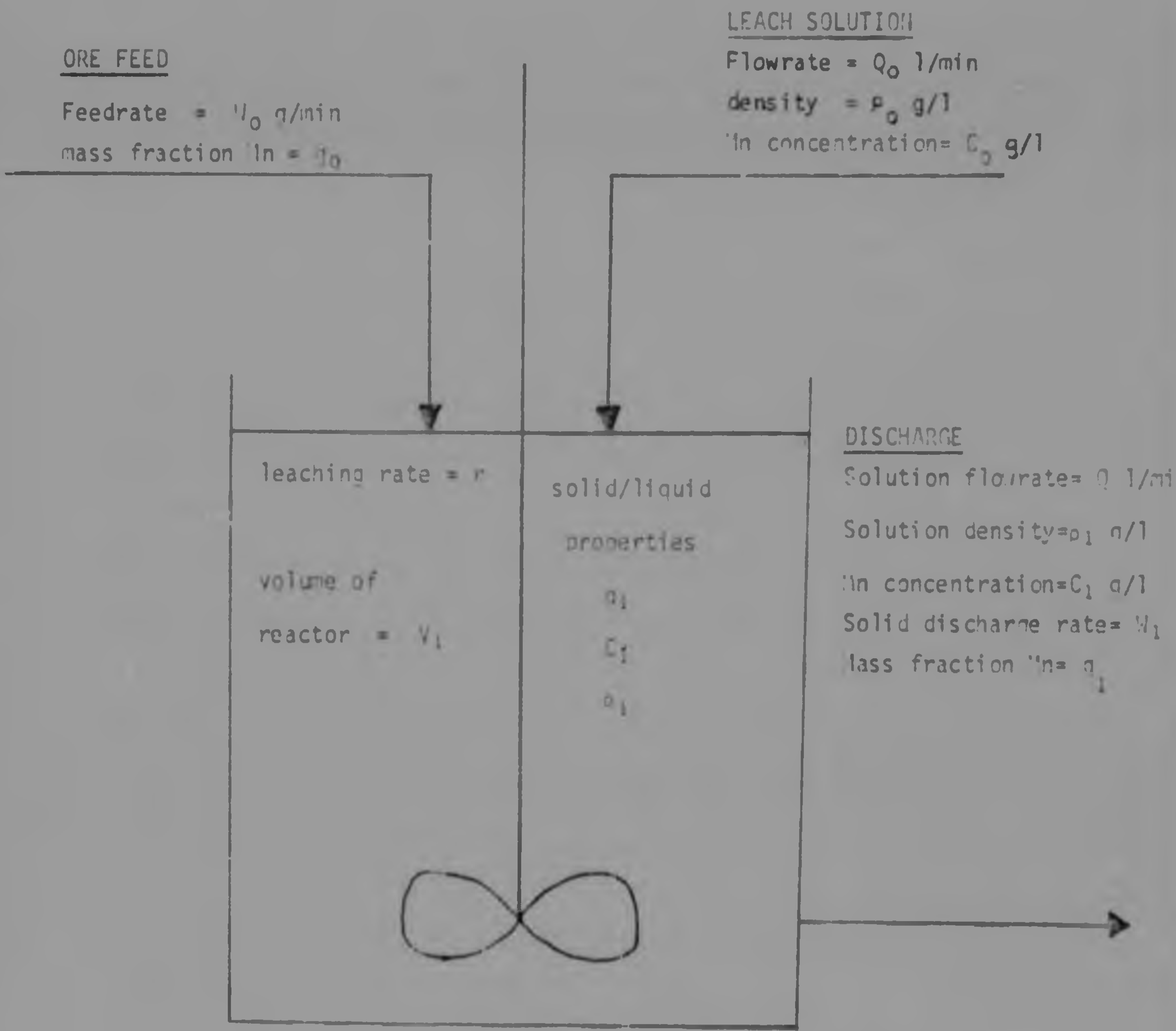

FIG.2.5: Leaching in an Agitated Vessel

3. BATCH LEACHING EXPERIMENTS

3.1 Introduction

In a batch reactor the reactants are initially charged into a container, are well mixed, and are left for a certain period to react. The resultant mixture is then discharged. This is an unsteady-state operation where composition changes with time; however, at any instant the composition throughout the reactor is uniform. Batch reactors are often utilized in kinetic studies because the reactor is simple, needs little supporting equipment and it is easy to control variables such as temperature, pressure and volume. However these kinetic studies are not easily applied to continuous systems since the composition of the fluid continually changes with time. In solid-liquid systems, all of the particles at any given time have the same characteristics. This is directly opposite to continuous systems . In continuous systems operating at steady-state the fluid characteristics are constant, whereas the particles have a residence time distribution.

During this investigation, a number of batch experiments were conducted for the following reasons;

a) To gain an idea of the approximate recovery of manganese that could be expected.

b) To test the applicability of equation (2.18) since the batch tests were performed for a time long enough to achieve equilibrium (or very nearly).

3.2 Experimental Apparatus

The experimental apparatus consisted of a large water bath with lid. The temperature of the water bath was thermostatically controlled. As many as ten glass fruit jars could be simultaneously used as leach reactors by suspending them into the water bath through holes in the water bath lid. Five of the reactors had a volume of one litre each and the other five a volume of half a litre each. Provision was made to stir the contents of each reactor, and all ten stirrers could be simultaneously rotated at a speed of about 300 r.p.m. by a single electric motor. Baffles were fitted to each reactor to increase turbulence and to prevent the settling of the leaching solids. Finally, Buchner funnels were used to separate the solids and liquid under vacuum at the completion of a run.

3.3 Procedure for a Run

In all of the experimental runs conducted, the following procedure was used:

a) The leach solution was an ammonium sulphate-manganese sulphate solution with a composition as given in Table 2.1.

b) Differing amounts of reduced manganese ore were added to each of the reactors so as to give a final pH value varying from 1,35 to 7,65 .

c) All experimental runs were performed at a temperature of $60^{0}C$.

d) All experimental runs were allowed to proceed for a period of six hours in an attempt to achieve equilibrium.

e) At the end of the run, the final pH values of each of the reactors was measured using a Metrohm 632 pH meter fitted with high-temperature Schott combination pH electrodes.

f) After the determination of pH, each of the leach slurries was filtered using Buchner funnels under vacuum.

g) After collection of the leach filtrates, the solids residues were washed with distilled water.

h) Finally, both solid residue and liquid filtrate samples were sent to The Council For Mineral Technology (MINTEK) for analysis.

3.4 Results

The results of the batch leaching tests are tabulated in Appendix 10.7. These results are plotted in Figures 3.1 and in Figures 10.2 and 10.3 (Appendix 10.7). Figure 3.1 shows the manganese in the leach filtrate as a function of pH. Figure 10.3 (Appendix 10.7) shows the percentage of manganese extracted as a function of pH.

Since all of the batch experiments were allowed to proceed for a period of six hours, it is likely that the process is at equilibrium. Thus equation (2.18), i.e.

$$C_{ms} = \frac{C_1(C_A + C_2/K_c' + C_1 + 1/K_c'K_a')}{C_2/K_c' + C_1 + 1/K_c'K_a'}$$

which represents the equilibrium manganese concentration should agree with the experimental values represented in Figure 3.1. The theoretical and experimental values are presented in Figure 3.2. The equilibrium

FIG. 3.1: Variation of the Mn Concentration with pH

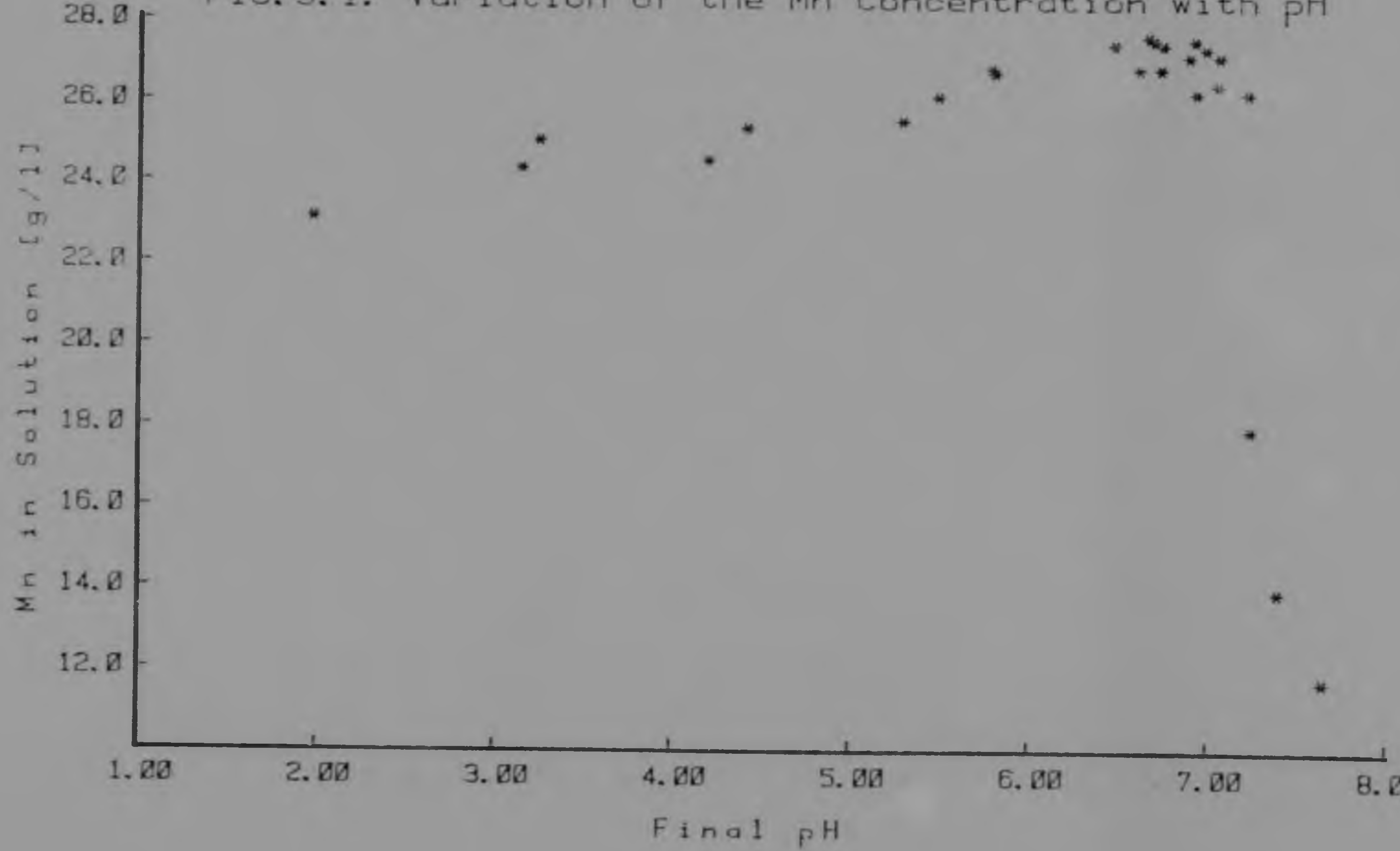

FIG.3.2: Comparison of Theoretical and Experimental Mn Equilibrium Concentrations

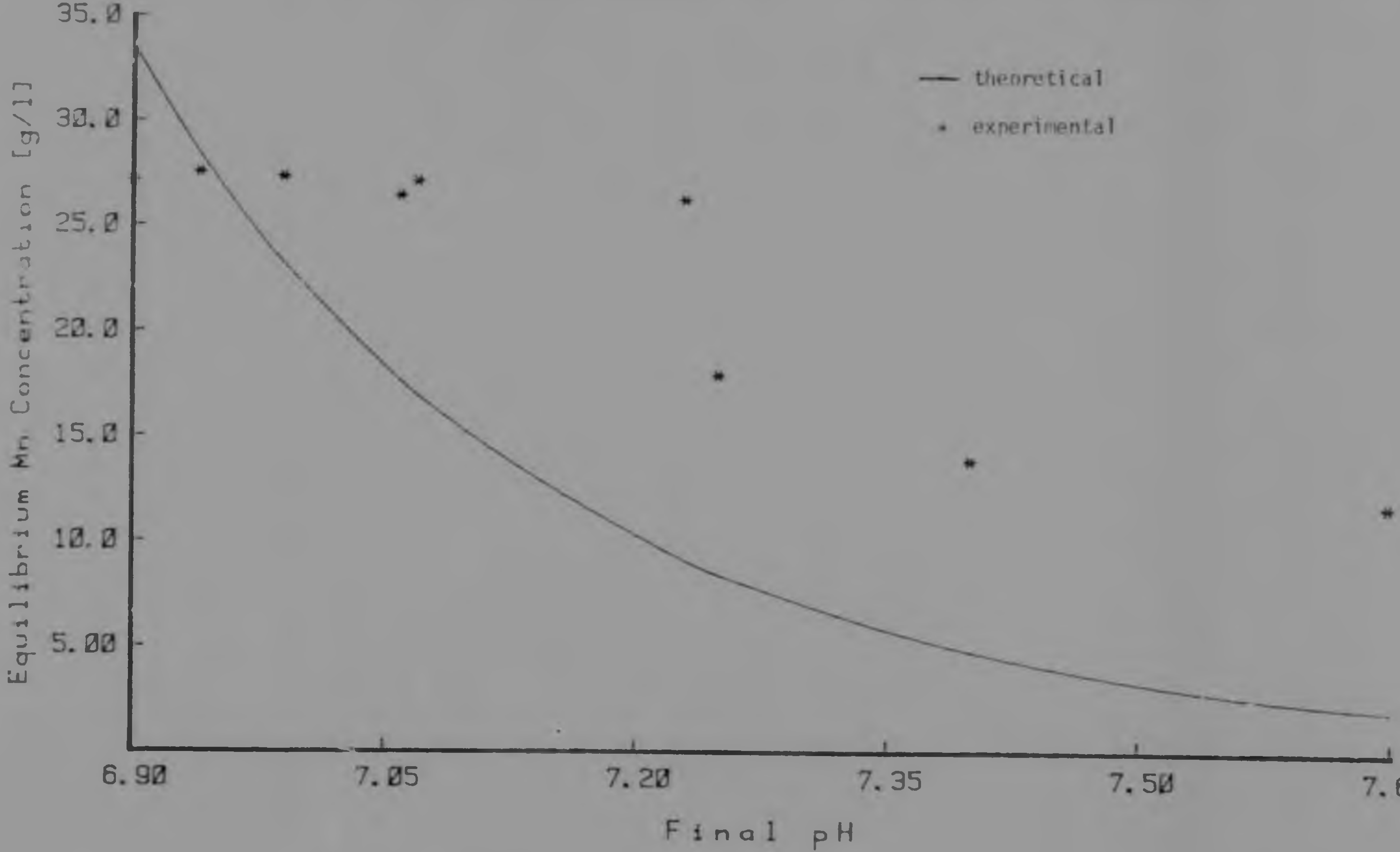

manganese concentrations can only be compared at the higher pH values since at the lower pH values, equation(2.18) predicts a theoretical manganese concentration far in excess of that physically possible. Table 10.2 (Appendix 10.7) lists the values used in plotting Figure 3.2.

This point is clarified by considering Figure 3.1. Suppose that the leaching operation was being performed at a pH of 5,1. Equation (2.18) then predicts an equilibrium manganese concentration of 3,26 X 10^5 g/l. This is clearly physically impossible. Figure 3.1 shows an equilibrium mangnaese concentration of 26g/l. Thus, in this pH range, the maximum amount of manganese possible in solution is limited by the system mass balance, and not by the equilibrium concentration. This means that two distinct regions are defined shown in Figure 3.3. The dissolution of manganese below the curve AB is limited by the system mass balance whereas the dissolution of manganese below the curve BC is controlled by the equilibrium manganese concentration predicted by equation (2.18). The intersection of these two regions occurs at a pH value of about 7,1.

3.5 Discussion

As can be seen from Figure 3.2, the experimental and theoretical values do not agree very well. This could be due to a number of reasons:

a) The manganese ore is not fully reduced, thus a smaller amount of manganese is soluble and available for leaching than would be the case if the ore was fully reduced.

b) The composition of the solution used in this investigation may have a slightly different composition to that tested by Rodriques (7).

FIG.3.3: Maximum values of Manganese possible in solution.

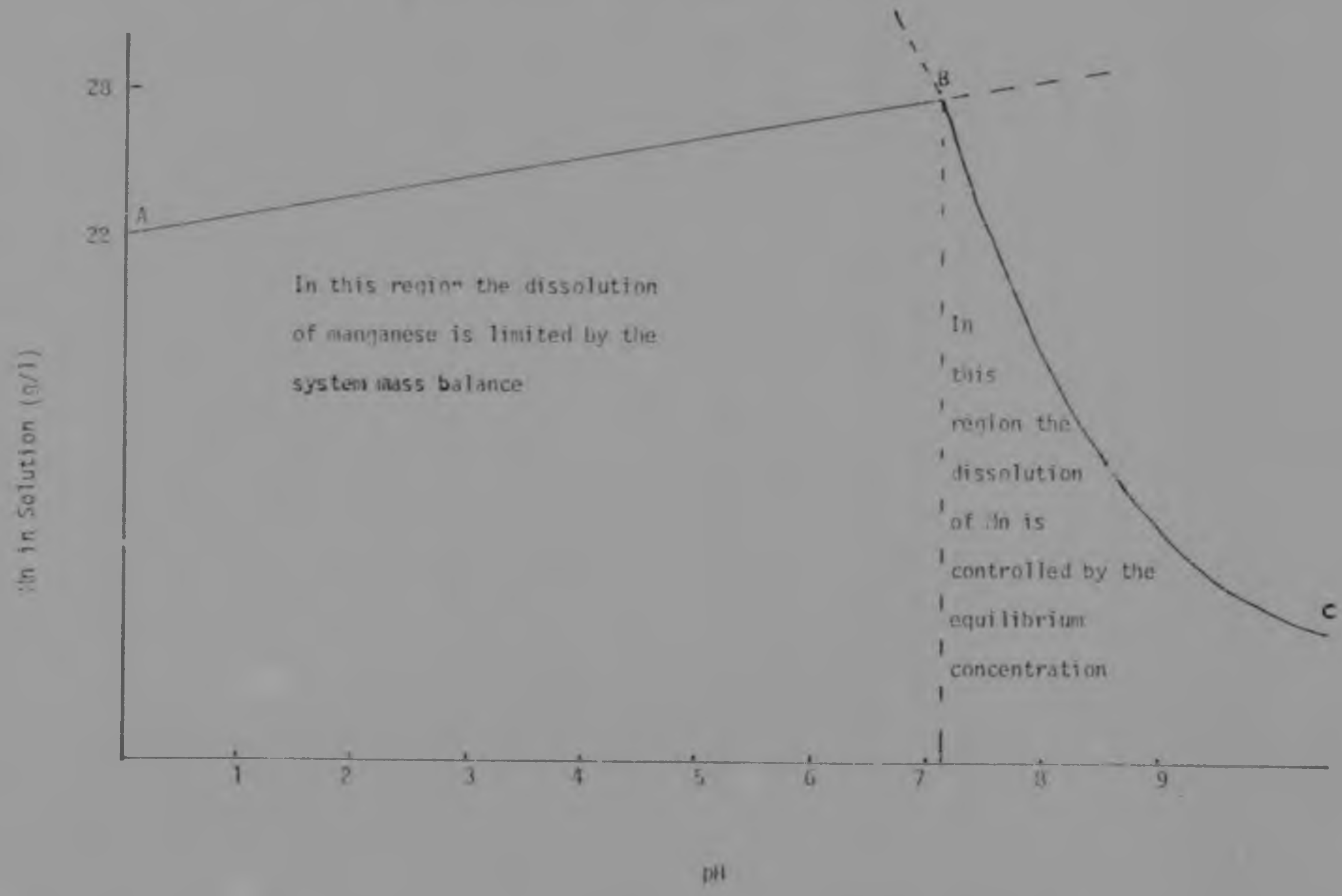

c) The anolyte used as a leaching liquid in this investigation is artifically made up and it is likely to have different characteristics to an anolyte which is returned from electrolytic cells on a manganese production plant.

d) The system reactions may not yet have reached equilibrium.

e) The manganese ore may be reoxidizing during the experiment, but this is unlikely as no air was provided to the batch reactors to improve agitation.

f) The theoretical manganese equilibrium concentrations as modelled by Rodrigues (7) were modelled in the temperature range $295<T<330$. The batch experiments were performed at $T=333$.

In view of the above, it was decided to modify equation (2.7) slightly in order to achieve a better fit between theoretical and experimental results. According to Rodrigues (7), this equation is the one most susceptible to error, since it is the equilibrium ratio of the reaction

$$Mn^{2+} + 2H_2O = Mn(OH)_2(s) + 2H^+ \qquad (2.1)$$

in which he assumes that the surface of any MnO remaining is completely hydrolysed, i.e. in the form $Mn(OH)_2$.

Thus, it is found that if equation (2.7), i.e.

$$K_s' = \exp(-65{,}17 + 0{,}1025T)$$

is changed to

$$K_s' = \exp(-66{,}00 + 0{,}1025T) \qquad (3.1)$$

a better agreement results between measured and theoretical manganese equilibrium concentrations. This is shown in Figure 3.4.

3.6 Conclusions

From these elementary batch experiments, it appears that the optimum operating range for continuous experiments is in the pH range 6,0 to 6,8 since this allows for a high recovery of manganese as well as for a high throughput of reduced manganese ore.

FIG.3.4.: Comparison of Modified Theoretical and Experimental Mn Equilibrium Concentrations.

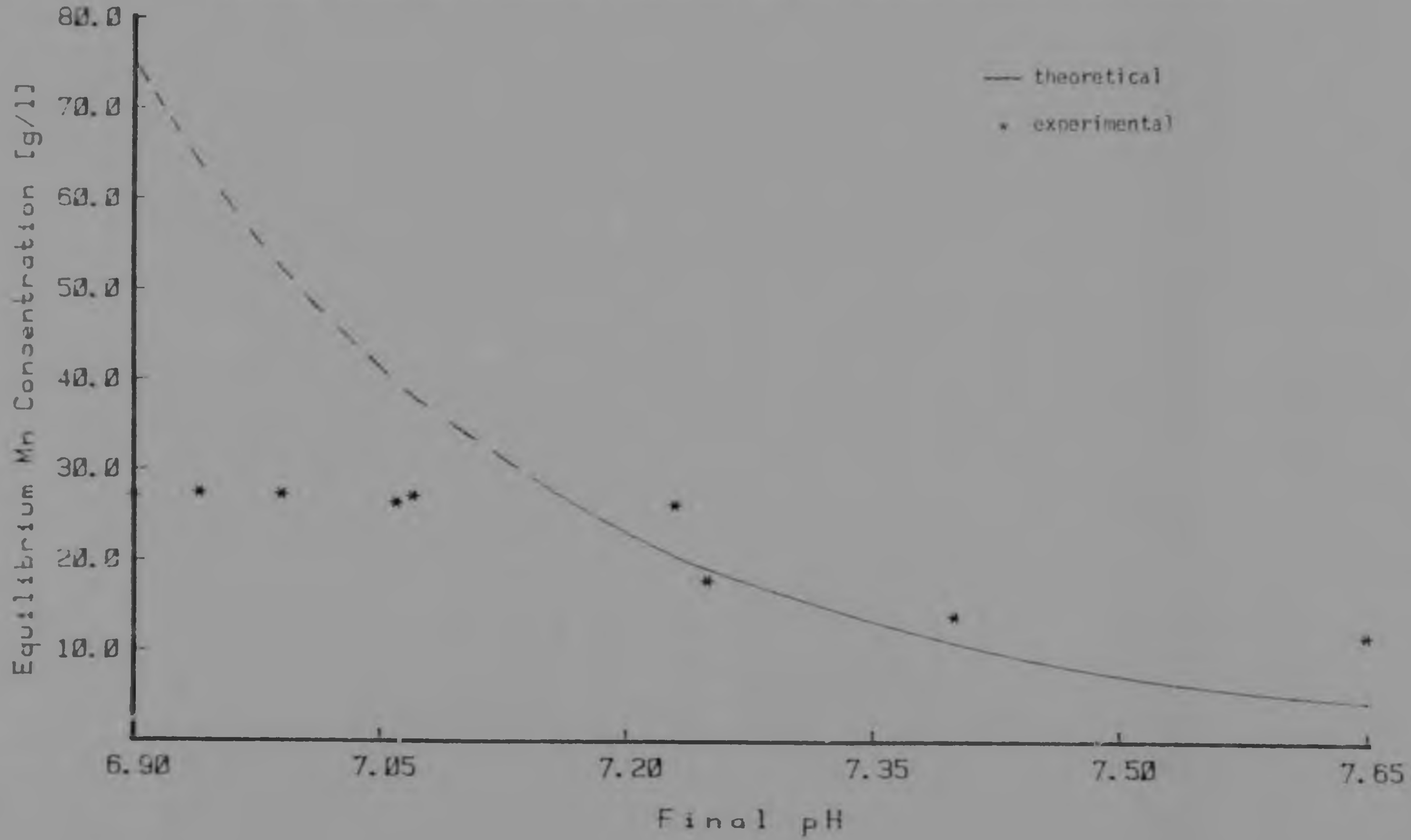

4. CONTINUOUS LEACHING EXPERIMENTS

4.1 Experimental Apparatus

The general layout of the experimental apparatus is shown in Figure 4.1. The apparatus consisted of the following items:

a) An anolyte storage vessel with a capacity of 450 liters.

b) The anolyte solution was heated by four teflon heating pads to maintain the anolyte at 50°C (the pads used are manufactured by Heatflon®, U.S.A.). The pads were thermostatically controlled.

c) The height of the storage vessel was twelve metres above that of the leaching vessel. This was done to create a pseudo constant head tank making it easier to control the anolyte flowrates at a constant level.

d) The piping between the anolyte storage vessel and the leaching vessel was well insulated. A heating tape was also attached to the piping to keep the anolyte solution hot. (The tape used was an isopad isotape type ITW/SS - 33/13m with a maximum temperature of 170°C).

e) The anolyte flowrate was controlled by means of a conventional globe valve, the flowrate being measured by means of a rotameter (type metric 7S, Rotameter MFG Co., England).

f) An ore feeder consisting of an adjustable funnel in which the ore is held. The ore is fed by a vibrating channel, the frequency of which can be controlled .(The ore feeder is manufactured by Fritsch laborette, type 24.002).

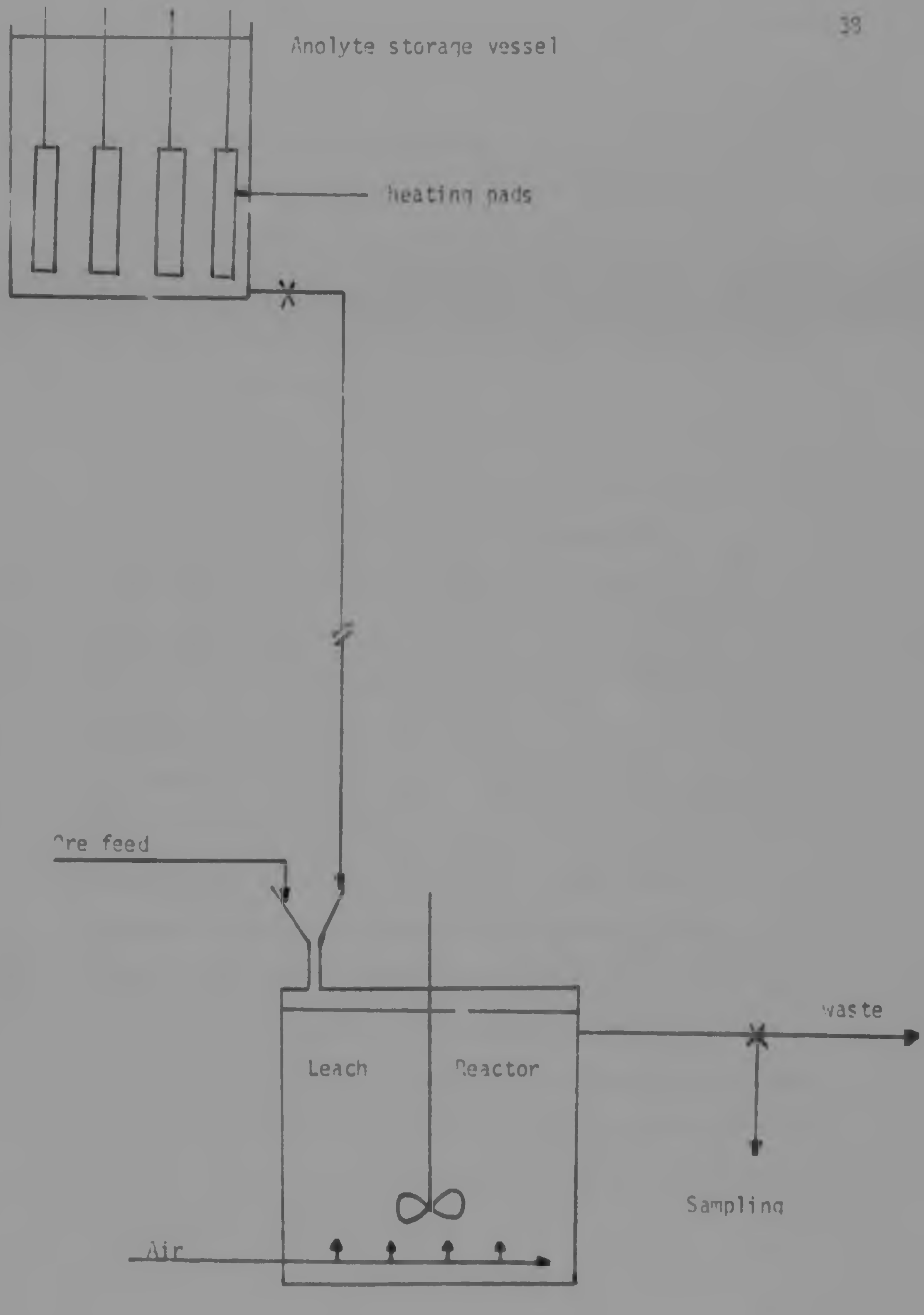

FIG.4.1: Layout of the Experimental Apparatus

g) Both the ore and anolyte solution are fed into a funnel in such a way as to completely wet the ore before entering the leach reactor. This prevents the ore from floating on top of the leach solution in the reactor.

h) The leach reactor itself had the following characteristics:

i) A volume of fourteen litres.

ii) Agitation by means of a mechanical impeller connected to an electric motor (Multifix Record variable speed motor). The speed of rotation of the impeller was about 300 r.p.m.

iii) Further agitation by the introduction of compressed air through the bottom of the reactor.

iv) Three baffles to increase turbulence and to prevent the settling of leaching solids.

v) The outlet of the reactor was an overflow. The overflow was covered by a section of pipe (see Figure 4.2) to prevent any bypassing of solids (i.e.to prevent any solids from floating on top of the leach solution directly to the outlet).

vi) Provision was made to sample the outlet (once the system had achieved steady state) over a given period by allowing the solution to flow directly into a Buchner funnel under vacuum. This allowed the immediate separation of the solid and liquid phases.During periods when no sampling was performed, the leach solution was discarded.

vii) The leach reactor was assumed to be an ideal CSTR.

4.2 Procedure for a Run

The procedure for an experimental run was as follows:

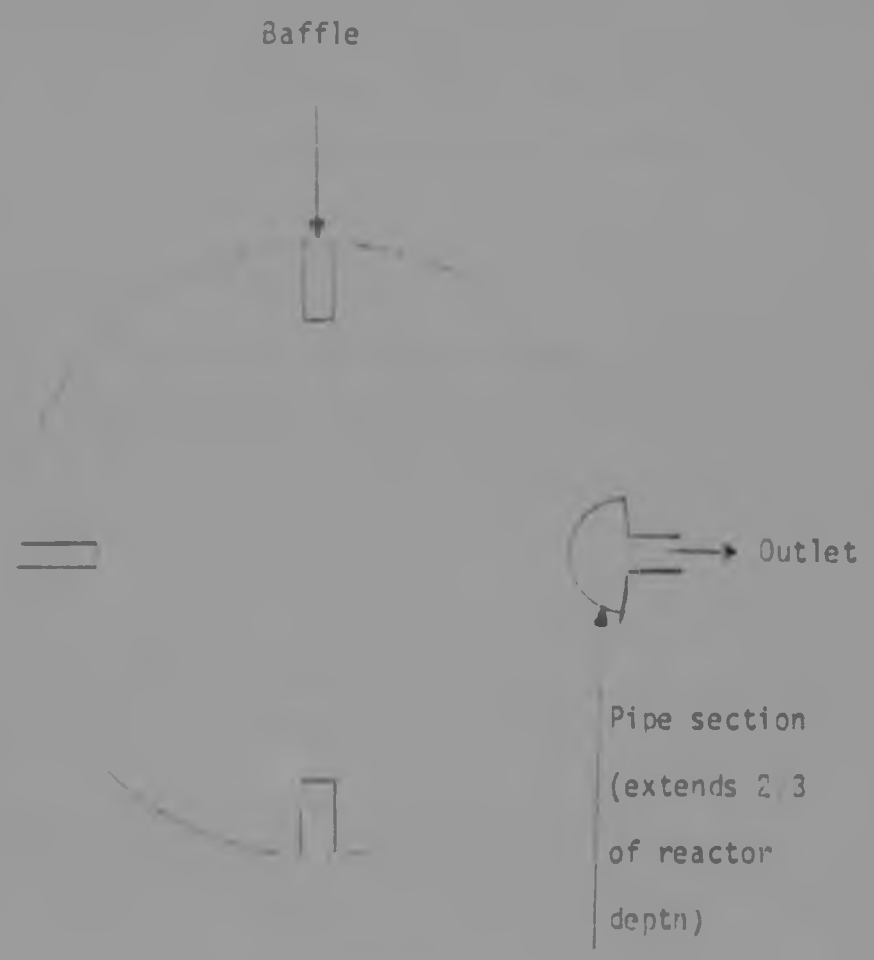

FIG.4.2: Top view of the Leach Reactor

a) The desired ore flowrate was set and the anolyte solution flowrate varied to obtain results at different pH values.

b) The pH and temperature of the outlet stream was measured by a Metronm 632pH meter fitted with high temperature Schott combination pH electrodes. The temperature was measured by means of a thermometer (as was the inlet anolyte solution).

c) Once steady state was realised, the outlet was sampled. The sample was immediately filtered to prevent the further leaching of solids.

d) After collection of the leach filtrate, the solid residue was washed with distilled water and then dried in an oven.

e) The liquid filtrate and solid residue were then sent to MINTEK for analysis.

The calibration curves for the ore feeder and rotameter are included in Appendix 10.9.

5. EXPERIMENTAL RESULTS

5.1. Leaching of Manganese

Three different experimental runs were conducted. In each of the runs, the ore feedrate was set at a certain value and the anolyte flowrate was then varied to give results at different pH values. These results are presented in Appendix 10.10 (Tables 10.6 - 10.8). During each experiment, the following were measured:

a) Inlet anolyte flowrate (Q_0).

b) Inlet solid flowrate (I_0) - constant for any particular set of runs.

c) Inlet concentration of manganese in the anolyte (C_0) - constant for all experimental runs.

d) Mass fraction of manganese in the ore feed (g_0) - constant for all experimental runs.

e) Outlet solution flowrate (Q_1).

f) Outlet solid discharge rate (I_1).

g) Outlet concentration of manganese in the solution (C_1).

h) Outlet mass fraction of manganese in the solid (g_1).

Knowing the above information, it is possible to calculate both the rate of leaching and the fractional leach efficiency.

The leaching rates at different pH values are calculated from either equation (2.43) i.e.

$$r_1 = \frac{Q_1}{V_1} \left(C_1 - \frac{Q_0}{Q_1} C_0 \right)$$

or equation (2.44), i.e.

$$r_1 = \frac{W_0 g_0 - W_1 g_1}{V_1}$$

In this case, the leaching rates were calculated from equation (2.44) since analyses of solid phases are generally more accurate than the analyses of liquid phases. The rates of reaction as a function of pH are tabulated in Tables 10.9 - 10.11 (Appendix 10.10) and a typical run is presented graphically in Figure 5.1. (The rest of the results are presented in Figures 10.6 - 10.8 in Appendix 10.10)

The fractional leach efficiency can be calculated from equation (2.42), i.e.

$$\eta = \frac{W_0 g_0 - W_1 g_1}{W_0 g_0}$$

These values are tabulated in Tables 10.9 - 10.11 (Appendix 10.10) and a typical set of results are presented in Figure 5.2. (The rest of the results are presented in Figures 10.9 - 10.11 in Appendix 10.10)

An example of how the leaching rate and the fractional leach efficiency are calculated is also included in Appendix 10.10.

For completeness of the experimental results, particle size determinations of the solid residues at some pH values were also conducted. These values are given in Appendix 10.10.

FIG. 5. 1: Leaching Rates-Run 1

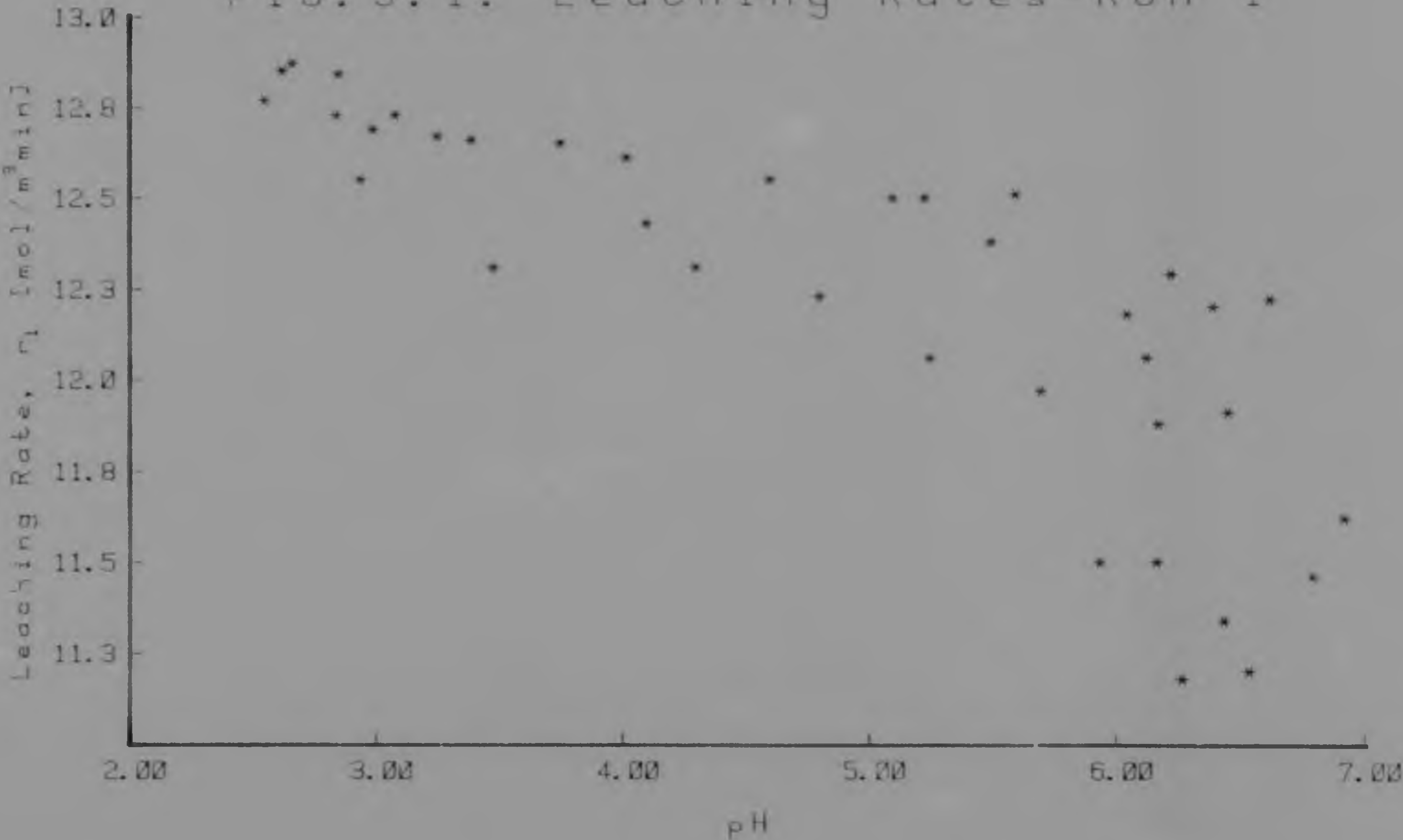

FIG.5.2: Fractional Leach Efficiency - Run 1.

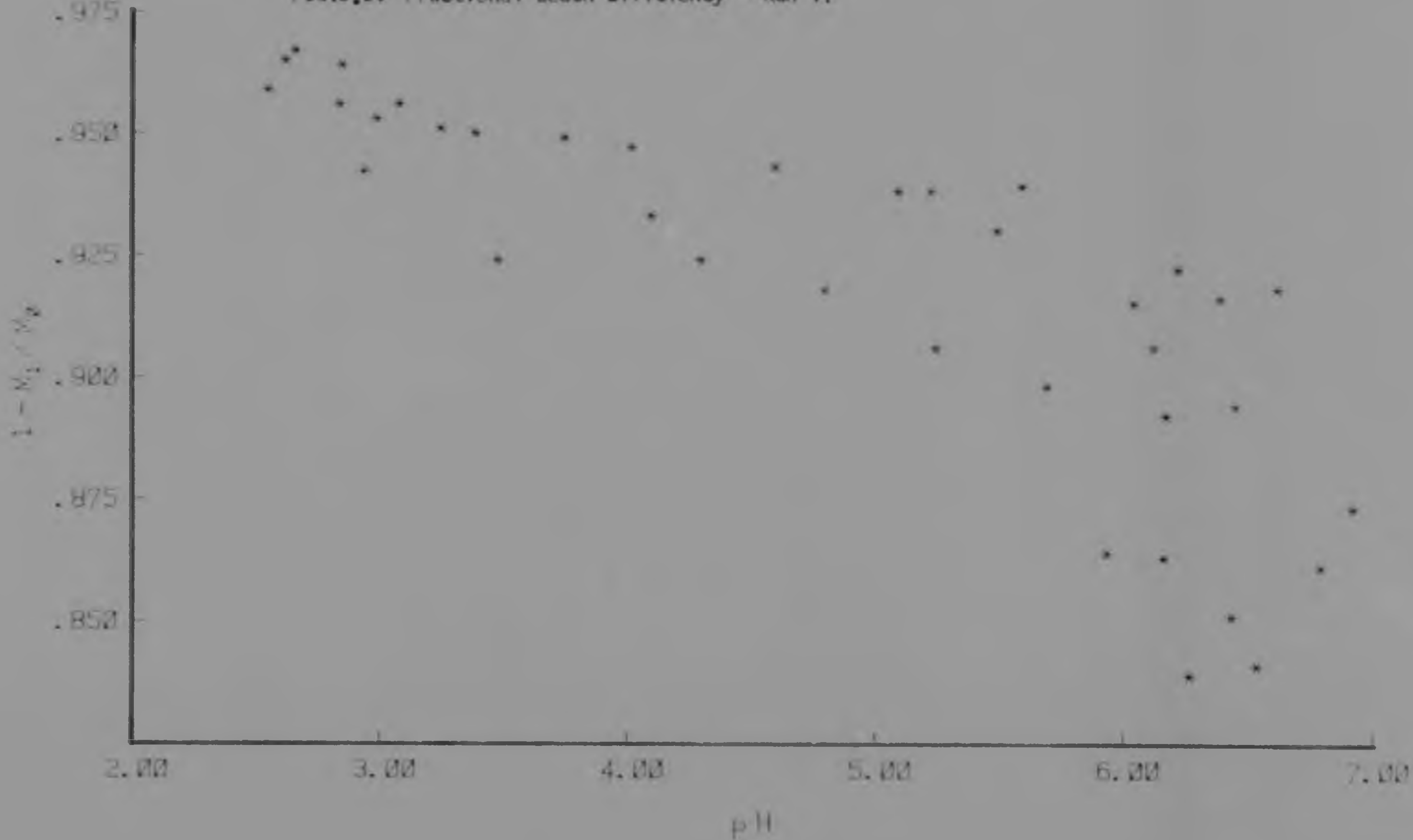

FIG.5.2: Fractional Leach Efficiency - Run 1.

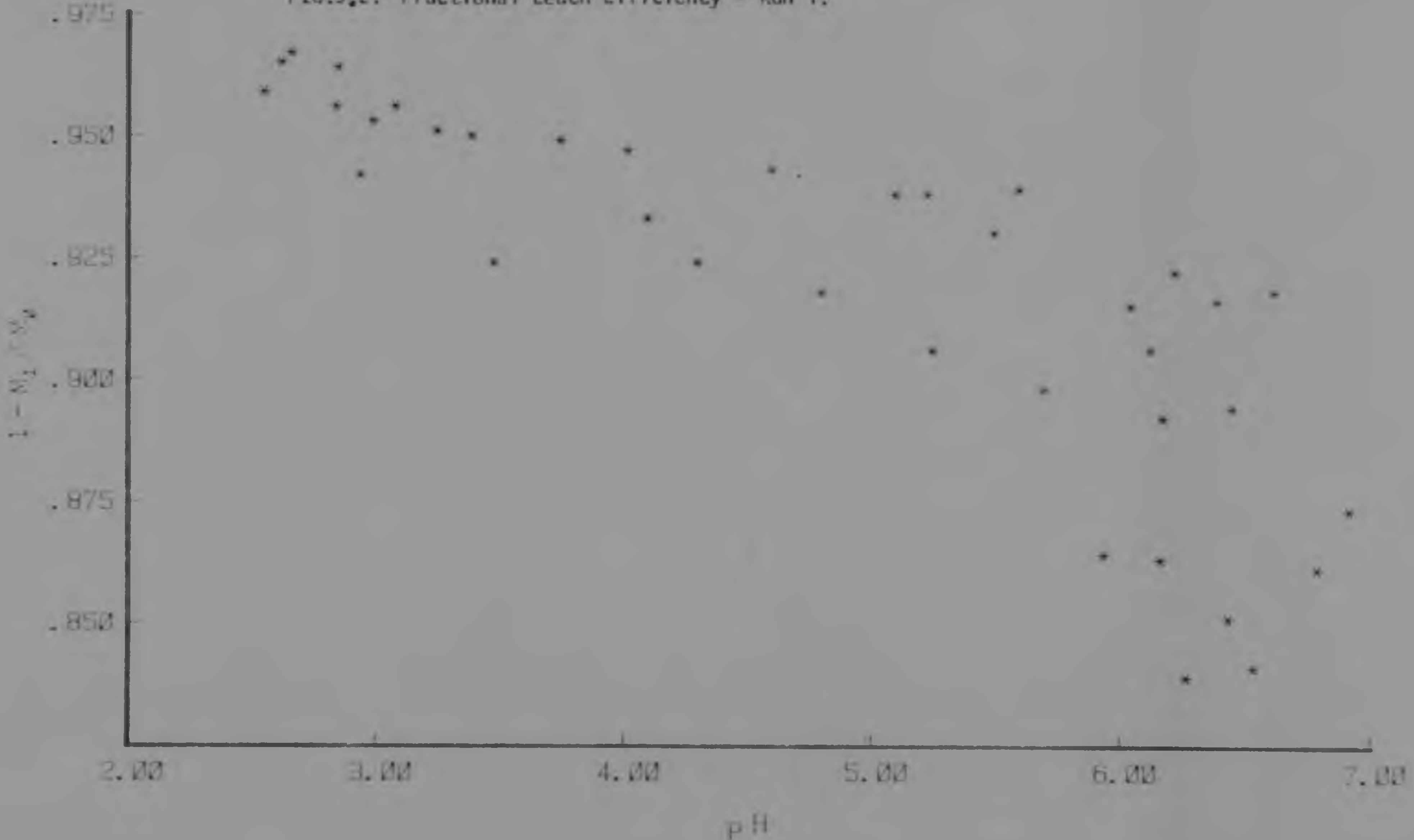

5.2 Leaching of the Minor Elements

During this investigation, it was decided to analyse for some of the more important minor elements at the same time as analysing for the manganese. These elements are iron, silicon, zinc, cobalt and nickel.

The above elements, if present in large quantities, have a deleterious effect on the current efficiency during the manganese electrowinning process. Although the leach solution is purified before electrowinning, it is important to attempt to keep the levels of impurities low during the leach process. Leaching at pH values of between 5,2 and 6,2 minimizes the dissolution of iron and any iron (II) in solution at this stage must be oxidized with air to levels of less than 50mg/l (50ppm). The precipitation of iron in the leaching section plays an important part in the purification of the solution since some chromium and copper and most of the arsenic, molybdenum, and silica are co-precipitated with the iron.

All metals more noble than manganese, if present in quantities above certain critical limits, will decrease the current efficiency at which manganese can be plated. Since the only metals less noble than manganese are aluminium and the alkali and alkaline earth metals, practically all the other metals will have a deleterious effect on the current efficiency. Good current efficiencies are therefore largely a function of electrolyte purity. The maximum levels of some impurities that can be tolerated in the cell feed solution without affecting the current efficiency are given in Table 5.1(3)

Table 5.1

Maximum Levels of Impurities in Cell Feed Solution

	ppm
Iron(ferrous)	15
Silicon	10
Zinc	10
Cobalt	0,3
Nickel	1

It has been proved (3) that a combination of impurities often has a greater negative effect than any one impurity alone. This is especially the case with cobalt, which on its own has the greatest negative effect of all the impurities listed.

Although Table 5.1 lists the maximum impurity levels after purification of the leach solution, it does give a good idea of the levels to be aimed at during the leacning process.

The results for the leaching of the minor elements are presented in Tables 10.20 - 10.22 (Appendix 10.14), and a typical result is shown in Figure 5.3. The complete set of results are presented in Appendix 10.14, Figures 10.23 - 10.37.

FIG.5.3: Leaching of Iron - Run 1

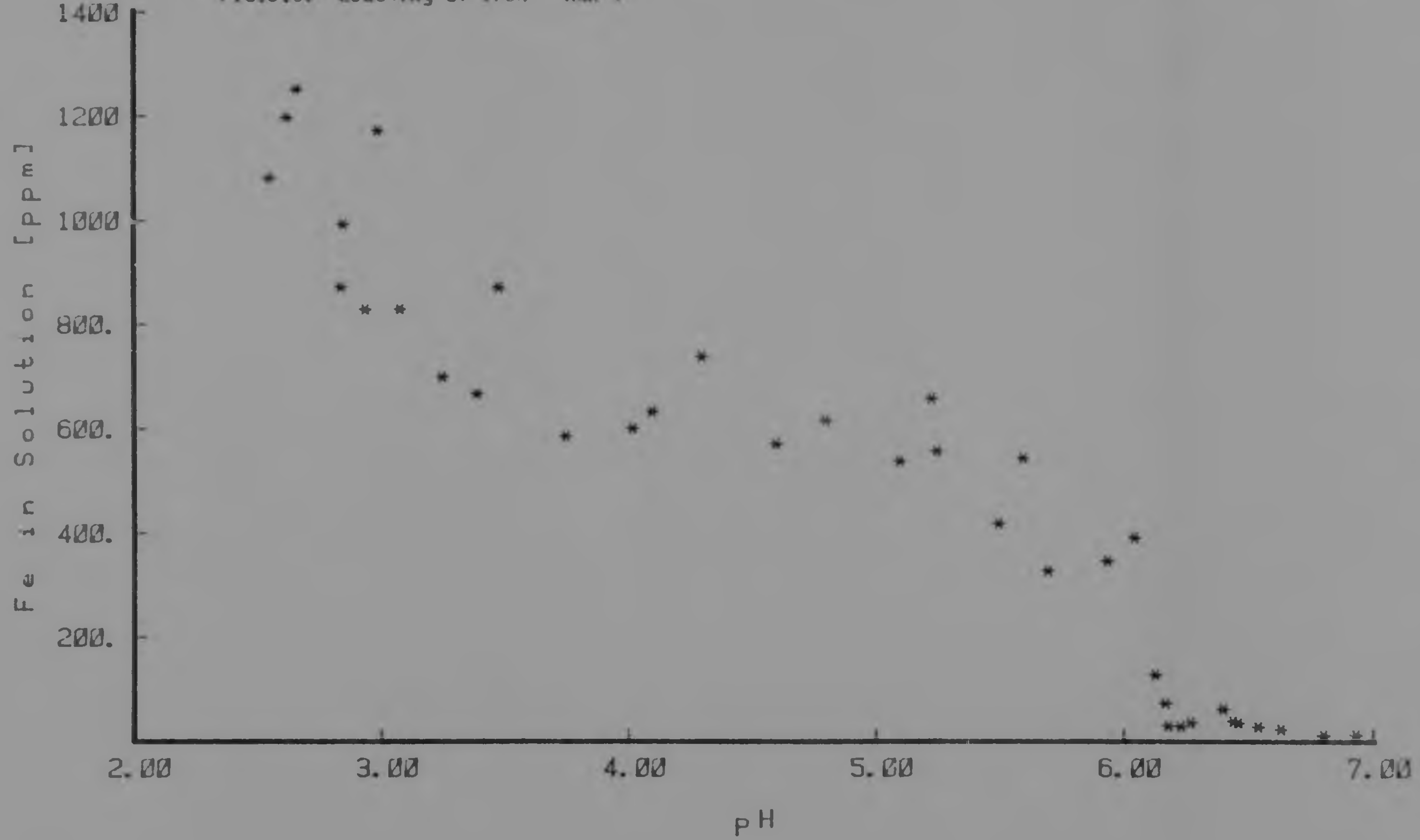

No attempt has been made to model these results since very little data concerning the equilibrium concentrations of these elements at different pH values are known. Instead, the concentration of each element in solution as a function of pH is given.

6. MATHEMATICAL MODELLING

The two theoretical fluid-solid models presented earlier, i.e. the unreacted core shrinking model and the porous solid model can be viewed as two extreme cases. In the former, the solid particle is assumed to be non-porous, with reaction occurring only at a discrete interface between solid and liquid. In the latter, the solid is assumed porous, with the reaction between solid and fluid proceeding homogenously throughout the solid. Thus, both of these models will be tested and should neither of them agree with experimental data, a model between these two should model the real situation.

Both of these models are tested with the rate of reaction being mass transfer controlled. Sherman (6) discusses the reduction of manganese ore and concludes that if the ore is properly reduced, the available manganese is readily leachable. Thus, it is unlikely that the reaction will be chemically controlled. The rate of reaction is likely to be controlled by the rate at which the fluid (anolyte) is able to diffuse to the site of reaction. Of the two diffusion processes (i.e. fluid film diffusion and ash layer diffusion), the fluid film diffusion model is tested first , since the data needed is readily available from the experimental results.

6.1 Applicability of the Unreacted Core Shrinking Model

Since this model is the most widely used model in describing fluid-solid systems, it is compared with the experimental data first.

From equation (2.36)

$$r_m = \frac{-kM}{\rho_B l} \phi\psi$$

For a mass transfer controlled reaction,

$$\psi = C_{ms} - C_m \qquad (6.1)$$

Substituting (6.1) into (2.36) gives

$$-r_m = \frac{k\phi}{\rho_B} \frac{M}{l} (C_{ms} - C_m) \qquad (6.2)$$

The rates of reaction (r_m) have already been calculated (Appendix 10.10) If the fluid properties are kept constant and $k\phi$ is assumed to be independant of conversion (this is true if all particles are assumed to be of the same shape and that k is essentially constant for each set of runs), then a plot of $-r_m$ vs $M/l \times (C_{ms} - C_m)$ will yield $k\phi/\rho_B$ from the slope of the plot.

Now , from equation (2.38) i.e.

$$t^* = \frac{3M_o^{1/3} (\rho_B N)^{2/3}}{kN\phi\psi}$$

and substituting for ψ from equation (6.1) and N from equation (2.34) gives

$$t^* = 3 \frac{\rho_B}{k\phi} \left(\frac{M_o}{M}\right)^{1/3} \frac{1}{(C_{ms} - C_m)} \qquad (6.3)$$

Thus , t* can be calculated.

The residence time , τ , of the leach reactor is calculated from

$$\tau = \frac{V_1}{Q_1} \qquad (6.4)$$

Thus , τ/t^* can be calculated, and since the fractional leach efficiency (η or $1-M_1/M_0$) is known (Appendix 10.10), a plot of τ/t^* versus $1-M_1/M_0$ for the experimental values can be compared with the theoretical plot of Figure 2.2. The comparisons are presented in Tables 10.13 - 10.15 (Appendix 10.11) and a typical result is presented in Figure 6.1. (The complete set of results are presented in Figures 10.14 - 10.16, Appendix 10.11). An example of how t^* is calculated from experimental data is given in Appendix 10.11.

6.2 Applicability of the Porous Solid Model.

In the reduction of manganese ore, the manganese particles give off oxygen molecules. Since some of the manganese is contained within the solid particle, this means that the oxygen must diffuse out of the particle. As it does so, the oxygen leaves behind pores or cracks in the solid particle. Thus the fluid is able to enter the matrix of the solid particle and react homogenously with the solid.

From equation (2.39)

$$-r_m = \lambda M$$

and substituting for λ from equation (2.40)

$$-r_m = \frac{k\rho}{\rho_B} M v \qquad (6.5)$$

For a mass transfer controlled reaction, from equation (6.1)

FIG.6.1: Comparison of Theoretical and Experimental Values of the Unreacted Core Shrinking Model - Run 1

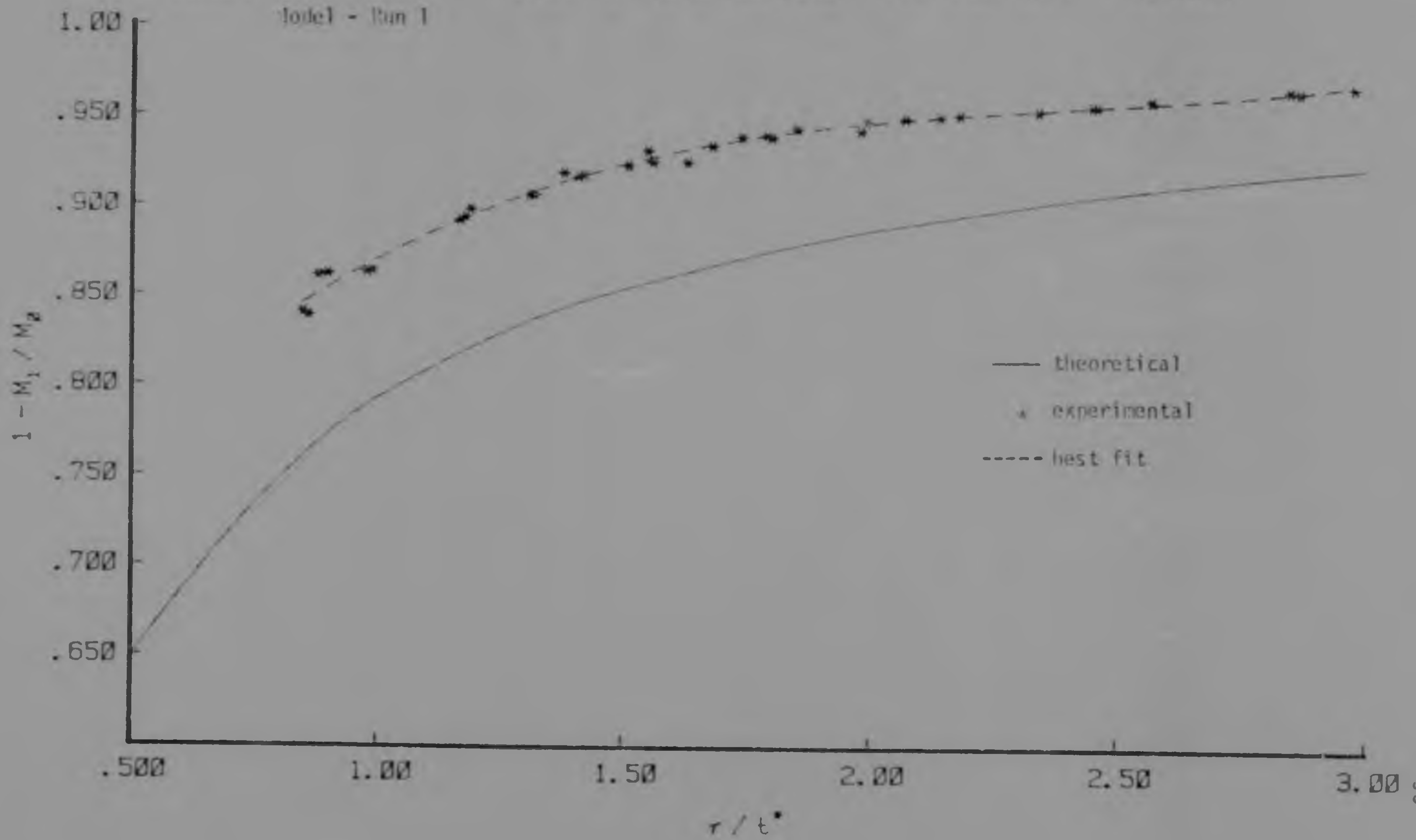

$$\Psi = C_{ms} - C_m$$

and the rate becomes

$$-r_m = \frac{kp}{\rho_B} M(C_{ms} - C_m) \qquad (6.6)$$

If k is again assumed to be essentially constant for a set of experimental runs, then a plot of $-r_m$ versus $M(C_{ms} - C_m)$ will yield a straight line of slope kp/ρ_B.

From equation (2.40) i.e.

$$\lambda = \frac{kp}{\rho_B} (C_{ms} - C_m)$$

it is then possible to calculate the value of λ for each experiment.

To test the applicability of this model, the fractional leach efficiency $(1-I/I_0)$ can be plotted against $\lambda\tau$ and the experimental results compared with the theoretical values predicted in Figure 2.4. These comparisons are tabulated in Tables 10.16 - 10.18 (Appendix 10.12) and a typical result is plotted in Figure 6.2. (The complete set of results are presented in Figures 10.17 - 10.19, Appendix 10.12). An example of the calculation of λ is given in Appendix 10.12.

FIG.6.2: Comparison of Theoretical and Experimental Values of the Porous Solid Model-Run 1

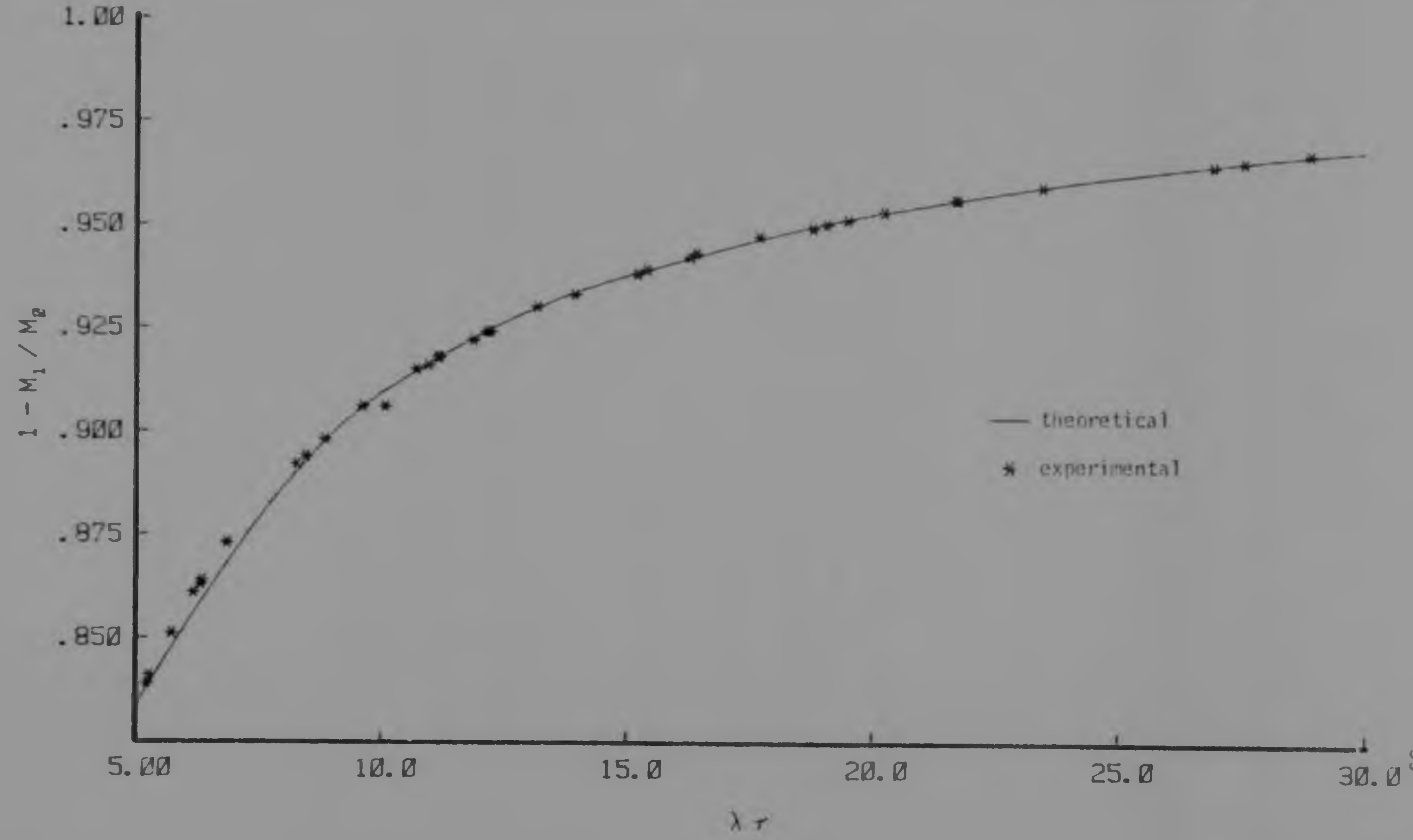

7. DISCUSSION

7.1 As can be seen from Figure 5.1, the rates of reaction decrease with an increase in the pH value for any of the experimental runs.

7.2 From Figure 5.4, it is noted that the fractional leach efficiency also decreases with an increase in pH for any experimental run.

Both of the above observations agree with the batch leaching results although the fractional leach efficiencies in the continuous runs are slightly higher than those found in the batch experiments. At a pH of below 5,5 a large amount of iron will dissolve, forming a bulky precipitate which is difficult to filter and wash. On the other hand, if the pH goes above 6,5 , the leaching rate becomes very slow. If the pH goes above 7,0 the reduced manganese ore reacts with the ammonium sulphate liberating ammonia gas which precipitates manganese hydroxide from the leach solution. The manganese hydroxide thus precipitated will react with air in the solution to form insoluble manganese dioxide which will be lost in the leach residue.

7.3 It is also noted that for each of the experimental runs, different leaching rates at similar pH values are found. This is due to the form of the rate expression as given in equation (2.35), i.e.

$$r_A = -k'' a \Psi \left(\frac{1}{D''}\right)^{2/3}$$

or equation (2.36), i.e.

$$r_A = \frac{-kM}{\rho_B l} \text{ [illegible]}$$

Thus, the leaching rate is dependant on the system since for each run, the ore feedrate is different. This means that M varies (the greater the ore flowrate, the bigger the value of M). k may also change from run to run, due to the different number of particles, N, in the reactor for different ore flowrates. For a particular pH value, the value of the equilibrium manganese concentration, C_{ms}, is the same, but the value of C_m is bigger for higher ore feedrates since there is more manganese available for leaching. ρ and l remain essentially unchanged for each run, assuming that the particles all have the same shape and size (at a particular pH value). Larger leaching rates are thus expected when the ore feedrate is bigger. This is more easily seen from equation (2.44), i.e.

$$r_l = \frac{W_o g_o - W_l g_l}{V_l}$$

For a bigger ore feedrate, $W_o g_o - W_l g_l$ is bigger since $W_l g_l$ does not change as much as $W_o g_o$. This observation is confirmed in Figures 10.6 - 10.8 (Appendix 10.10). Thus, the leaching rates in this investigation are only directly applicable to systems which have the same characteristics.

7.4 From Figure 6.1 and Figures 10.14 - 10.16 (Appendix 10.11), it is noted that the experimental values agree fairly well with the unreacted core shrinking model with mass transfer controlling. The average percentage difference between experimental and theoretical values is 10,4. However, the leach recoveries experimentally obtained are always greater than those predicted by the model for a particular value of τ/t^*.

Figure 6.4 and Figures 10.17 - 10.19 (Appendix 10.12) indicate that the porous solid model with mass transfer control provides a far better agreement between experimental and theoretical observations. Here, the average percentage difference is only 0,1.

This observation agrees with that of Sherman (6) in discussion of the reduction of this manganese ore. During the reducing process, the ore is reduced from manganese (IV) to manganese (II) In order for this to occur, the manganese particles have to liberate oxygen molecules, each manganese atom liberating two oxygen atoms. Since at least some of the manganese is contained within the ore particle, the liberated oxygen leaves behind pores or cracks in the particle, thus forming a porous solid particle. The liquid reactants are then easily able to diffuse throughout the solid particle and to react homogenously with the particle. It is also obvious that the rate of reaction will then be controlled by the rate at which liquid reactant diffuses to the solid particle since the particle is not limited by diffusion in the ash layer. Further, the reduced manganese is readily leachable at pH values below 7 making chemical reaction an unlikely controlling process.

7.5 In the calculation of t^* for the unreacted core shrinking model or the calculation of λ in the porous solid particle model, the leaching rate is plotted against some function of M and C_m to obtain unknown constants from the slope of this plot.(See Appendices 10.11 and 10.12). The form of this plot should be as shown in Figure 7.1. However, for each of the experimental runs, the plot resembles that shown in Figure 7.2. This is due to the fact that r, M and C_m are related via a mass balance (Appendix 10.13) of the form:

$$r = \frac{W_o Q_o}{V_1} - \frac{M}{\tau} \qquad (7.1)$$

Thus a plot of r versus M/τ will give a straight line having a slope of -1 and intercept $\frac{W_o Q_o}{V_1}$.

This is in actual fact the case (see Figures 10.20 - 10.22, Appendix 10.13). The theoretical and experimental values for the slope and intercept are given in Table 10.19. As can be seen, the values agree well.

It can then be concluded from the above that the correct method of performing continuous experiments is to run a set of experiments at a constant W_o/Q_o ratio. This will generate a set of experimental reaction rates at the same pH value, resulting in a plot similar to Figure 7.1. The method used here,i.e., setting an ore feedrate (W_o) and varying the anolyte flowrate (Q_o) generates data as shown in Figure 7.2 (and corresponding to point B in Figure 7.1). By running experiments with W_o/Q_o constant, the remaining points between point A and point B in Figure 7.1 will be generated.

FIG.7.1: Theoretical Leaching Rates

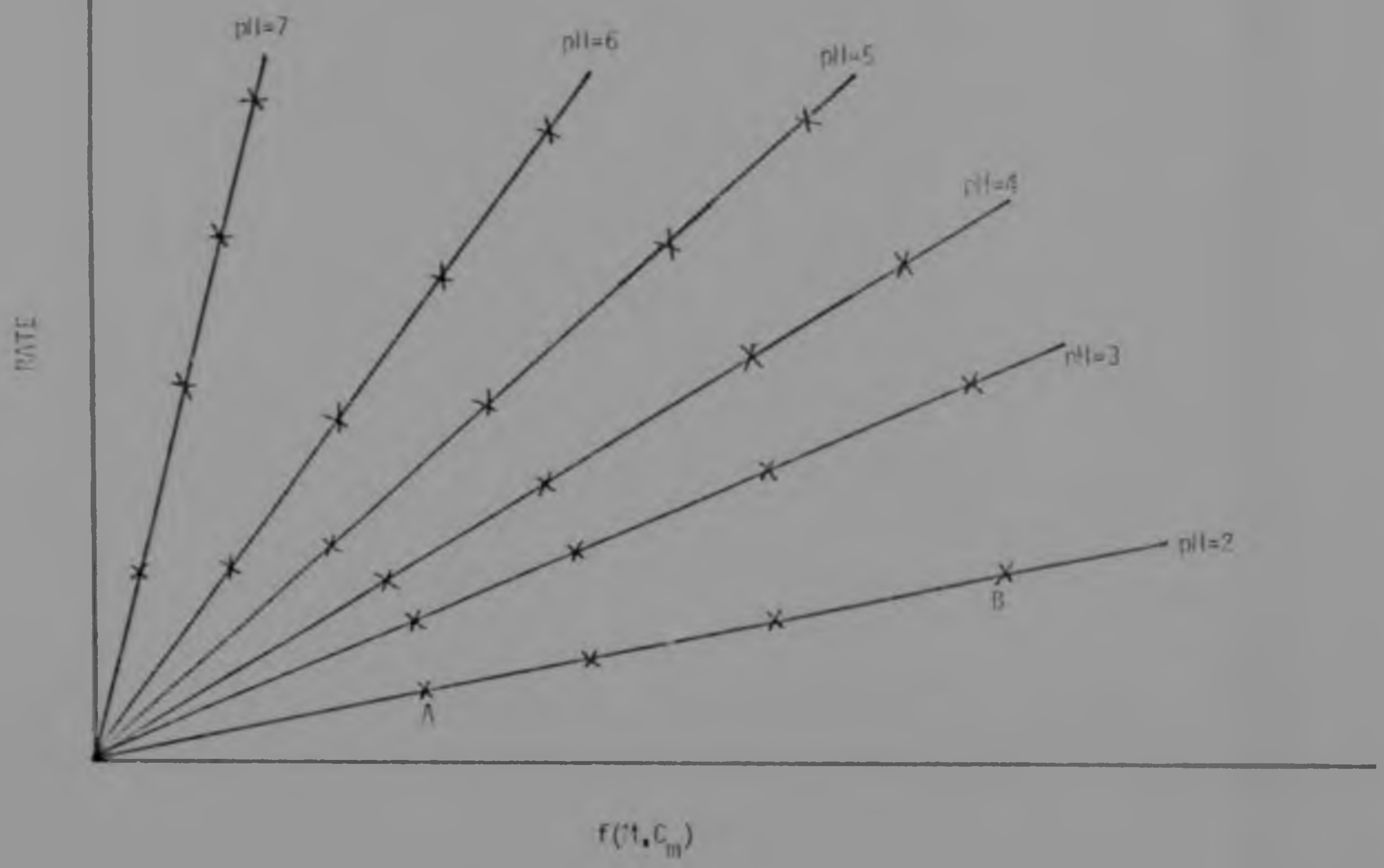

FIG 7.2: Experimental Leaching Rates

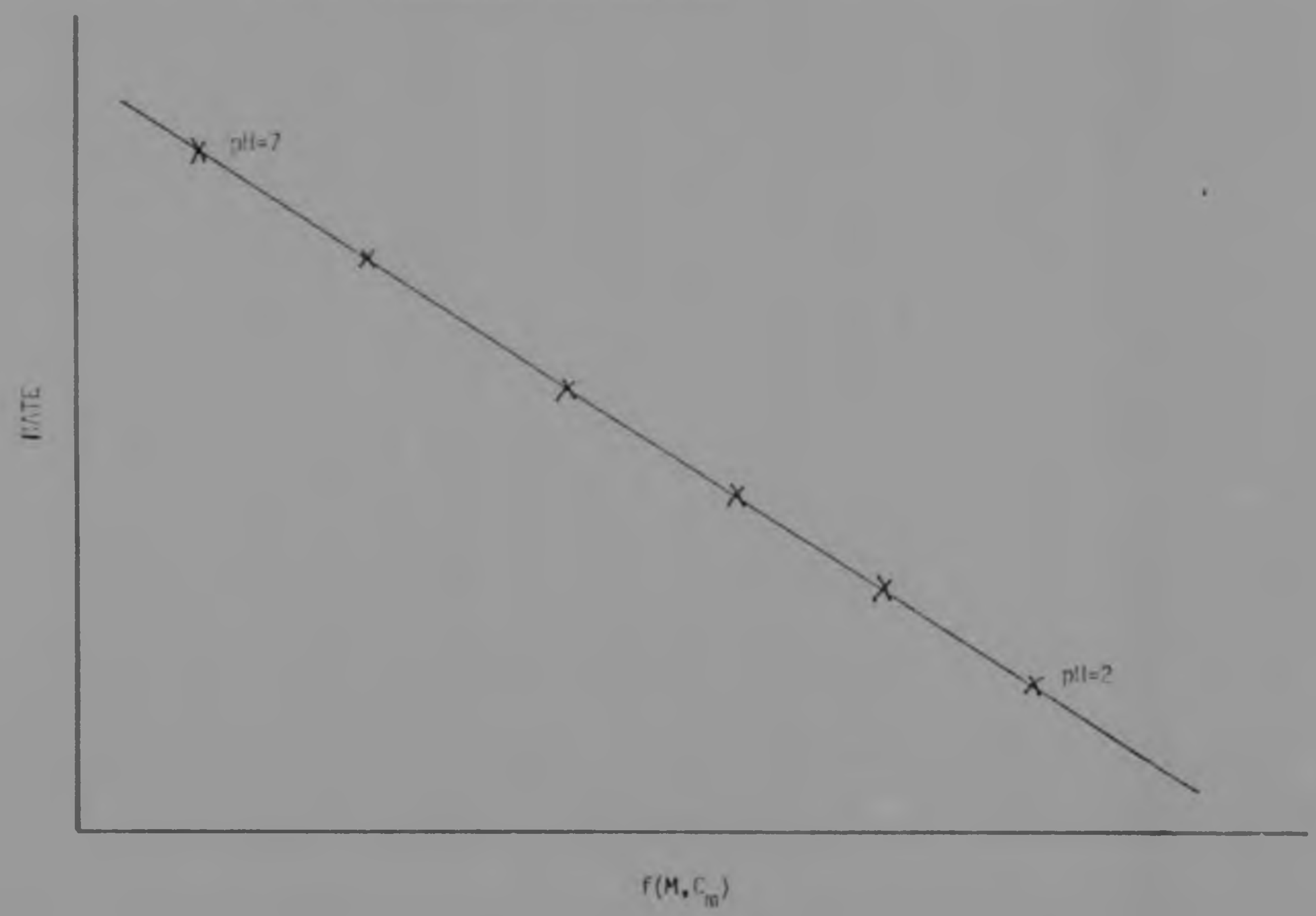

7.6 From figures 10.12 and 10.13 (Appendix 10.10) it can be seen that the mean particle size initially increases with pH to a pH value of about 5 and then the particle decreases in size. This means that at the lower pH values, the particles are almost completely reacted, with the smaller particle sizes reacting completely. Thus, at a particular equivalent spherical diameter, there is a smaller amount of particles of that size at the lower pH values than at the higher pH values. This trend occurs up to a pH value of about 5 corresponding to the situation in which a large amount of iron dissolves into the leach solution. As the pH goes above 5, the leaching rates become slower resulting in the incomplete reaction of the particle. Thus, at any particular equivalent spherical diameter, the cumulative mass percent should be greater, which it is. As the pH goes above 7, the reduced manganese ore forms manganese dioxide which precipitates from the leach solution. In fact, the mean particle diameter at this pH is almost the same as that of the feed.

7.7 From the above discussion, it can be concluded that the Porous Solid Model gives an excellent fit between theoretical and observed data. This model is described by the following equations:

$$r_A = -\lambda M \qquad (2.39)$$

and

$$1 - \frac{M_i}{M_0} = \frac{\lambda\tau}{1+\lambda\tau} \qquad (2.41)$$

From the equations above it would appear that any leach recovery between 0 and 100 per cent is possible. This is not the case, since the value of M cannot be smaller than some value, M^* say. This is due to the observation that some of the manganese in the ore is unleachable, regardless of the residence time or volume of the leach reactor. (This is confirmed in the batch experiments, where complete recovery was unobtainable in spite of a lengthy residence time).

Thus, the above equations which describe the leaching process are subject to the following limitation:

$$r_A = -\lambda M \quad , M > M^*$$

where the value of M^* is given by equation (10.45)(Appendix 10.13), i.e.

$$M^* = \frac{M_0 Q_0}{Q_1} + \frac{Q_0}{Q_1} C_0 - C_{ms}$$

When designing a leach system, the above limitation must always be considered.

7.8 An example of the design of a leaching vessel is given below. For the process considered in this investigation, the leach reaction is

$$MnO + H_2SO_4 = MnSO_4 + H_2O$$

The process is shown in Figure 7.3. All the symbols have their usual meaning and F refers to the hydrogen ion concentration.

Assume that $q_0, Q_0, F_1, C_0, F_0, \rho_0$ and ρ_1 are known. Then from consideration of electrical neutrality,

$$C_1 = C_0 + \tfrac{1}{2}(F_0 - F_1) \qquad (7.2)$$

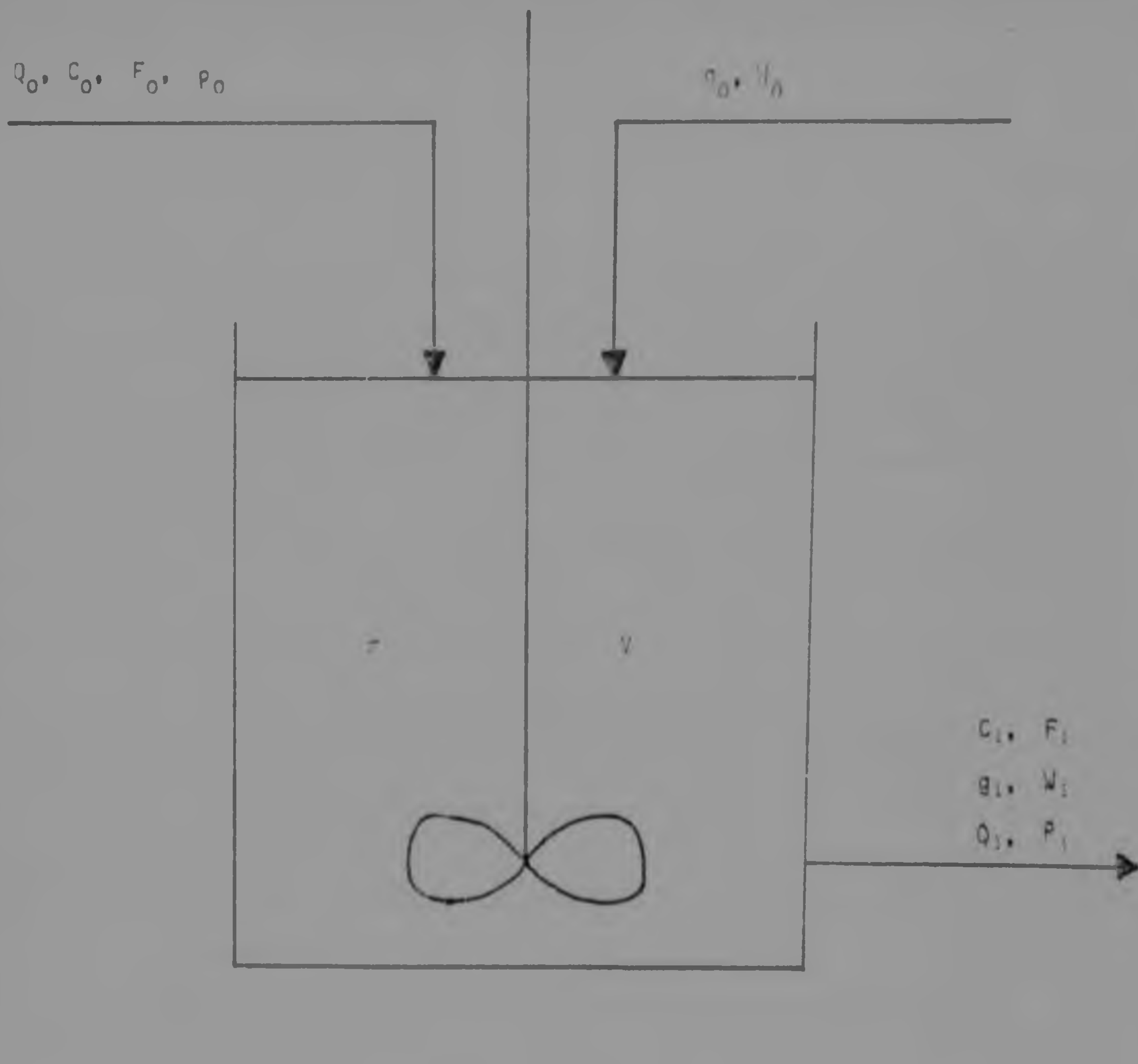

Fig.7.3: Leaching of Mn oxide

The overall mass balance is given by equation (10.35)

$$W_o + \rho_o Q_o = W_1 + \rho_1 Q_1$$

The overall manganese mass balance is given by equation (10.36)

$$W_o g_o + C_o Q_o = W_1 g_1 + C_1 Q_1$$

and the aqueous phase mass balance for manganese is given by equation (10.37)

$$C_o Q_o = C_1 Q_1 - r_1 V_1$$

An inert mass balance will then be

$$(1 - g_o) W_o = (1 - g_1) W_1 \qquad (7.3)$$

Thus, the following equations describe the system and can be used in design:

$$W_1 = W_o \left(\frac{1-g_o}{1-g_1} \right) \qquad (7.3)$$

$$C_1 = C_o + \tfrac{1}{2}(F_o - F_1) \qquad (7.2)$$

$$Q_1 = \frac{\rho_o}{\rho_1} Q_o + \frac{W_o}{\rho_1} \left(1 - \frac{1-g_o}{1-g_1} \right) \qquad (7.4)$$

$$\frac{Q_1}{V_1} = \frac{r}{C_1 - Q_o/Q_1\, C_o} \qquad (10.37)$$

and W_o can be solved by substituting (7.3), (7.2) and (7.4) into (10.36).

<u>Example:</u> Suppose that data for the leaching of manganese is given as follows:

leach efficiency=90%

pH = 6,4 (therefore $F_1 = 10^{-6,4}$)

Q_o = 1000 l/hr

If the same type of anolyte and ore is used as was used during this investigation, then the following is also known:

$$C_0 = 12,24 \text{ g/l } (0,22 \text{ mol/l})$$

$$F_0 = 0,64 \text{ mol/l}$$

$$g_0 = 0,54$$

ρ_0 and ρ_1 are assumed to be the same as that of water, i.e.

$$\rho_0 = \rho_1 = 1000 \text{g/l}$$

now,
$$1 - \frac{M_1}{M_0} = \frac{g_0 - g_1}{g_0(1-g_1)} =$$

therefore
$$\frac{0,54 - g_1}{0,54 - 0,54 g_1} = 0,9$$

$$\underline{g_1 = 0,11}$$

$$C_1 = C_0 + \tfrac{1}{2}(F_0 - F_1)$$

$$= 0,22 + \tfrac{1}{2}(0,64 - 10^{-0,4})$$

$$C_1 = 0,54 \text{ mol/l}$$

or
$$\underline{C_1 = 29,7 \text{ g/l}}$$

From equation (7.3),

$$W_1 = W_0\left(\frac{1-g_0}{1-g_1}\right)$$

$$W_1 = 0,52\, W_0$$

and from equation (7.4)

$$Q_1 = \frac{(1000)(1000)}{1000} + \frac{W_0}{1000}(1-0,52)$$

$$Q_1 = 1000 + 4,83 \times 10^{-4} W_0$$

and from the overall manganese mass balance,

$$W_0 g_0 = W_1 g_1 + C_1 Q_1 - C_0 Q_0$$

and substituting for W_1 and Q_1 in terms of W_o gives

$$W_o(0,54) = 0,52W_o(0,11) + 29,7(1000 + 4,38 \times 10^{-4} W_o)$$
$$-(12,24)(1000)$$

$W_o(0,54 - 0,06 - 0,01) = 29700 - 12240$

$W_o \quad = \quad 37149$ g/hr

thus

$Q_1 \quad = \quad 1018$ l/hr

and

$W_1 \quad = \quad 19317$ g/hr

From the equations describing the Porous Solid Model,

$-r \quad = \quad \lambda M$

From Table 10.16 (Appendix 10.12), the value of λ at a pH of 6,4 is

$\lambda \quad = \quad 0,35 \text{ min}^{-1}$

and

$$M = \frac{W_1 q_1}{Q_1}$$

$$M = \frac{(19317)(0,11)}{(1018)}$$

$M \quad = \quad 2,09$ g/l

At this point, the value of M must be checked to ensure that it is greater than the value of M*, as discussed in section 7.7. M* is calculated from equation (10.45), i.e.

$$M^* = \frac{W_o q_o}{Q_1} + \frac{Q_o}{Q_1} C_o - C_{ms}$$

Thus $M^* = 1{,}73$ g/l ($C_{ms} = 30$ g/l)

Since $M > M^*$, the Porous Solid Model equations may be used.

$$-r = \lambda M$$

$$-r = 0{,}73 \text{ g/l min} \quad (43{,}8 \text{ g/l hr})$$

and the volume of the leaching vessel is calculated from the aqueous phase manganese balance

$$V_1 = \frac{C_o Q_o - C_1 Q_1}{-r}$$

$$\underline{V_1 = 411 \text{ l}}$$

8. CONCLUSIONS

8.1 Having established a leaching model, it is now possible to predict the rate of leaching for a given system which could lead to a better operating procedure. Alternatively, it is possible to design new systems and be able to predict the volume of the leach reactor for a given conversion or outlet concentration.

8.2 Various phenomena that have been observed during this investigation have led to a better understanding of the leaching process and have agreed with other limited observations in the literature.

8.3 Perhaps the best method of confirming the results of this investigation will be to perform a set of experiments at constant W_0/Q_0 ratios as discussed in section 7.5.

8.4 The leaching model which best fits the experimental results is the Porous Solid Model. This model is described in section 7.7 and an example of its' use given in section 7.8

9. REFERENCES

1. Allen, L.N. "Recovery of Manganese from Low-Grade Ores" Chem.Eng.Progress, 50, (Jan 1954). pp.9-13

2. Harris, M. "The History, Production and Uses of Electrolytic Manganese." Metallurgie, XVII (4), (1977). pp.121-127

3. Harris, M., Meyer, D.M. and Auerswald, K. "The Production of Electrolytic Manganese in South Africa." J.S.Afr. Inst. Min. Metall., 77(7), (1977). pp.137-142

4. Auerswald, K. "The Production of Electrolytic Manganese from South African Ore" Delta Manganese internal publication, (1972).

5. Dean, R.S. "Electrolytic Manganese and its' alloys" Ronald Press, New York, (1965). Chap.1.

6. Sherman, L. "Gaseous Reduction Characteristics of Hotazel Ore Fines in a Batch Rotating Tube Reactor." M.Sc. (Eng.) Dissertation, University of the Witwatersrand, Johannesburg, (1981).

7. Rodrigues, J.C.P. "Modelling the Performance of Manganese Electrowinning Cells." M.Sc (Eng.) Dissertation, University of the Witwatersrand, Johannesburg, (1982).

8. Warren,I.H. "Introduction to Hydrometallurgy" in Vacation School-Hydrometallurgy, S.Afr. Inst.Min. Metall., Johannesburg, South Africa,(1976).

9. Peters,E. "Theory of Leaching" in Vacation School-Hydrometallurgy, S.Afr.Inst.Min.Metall., Johannesburg, South Africa, (1976).

10. Bryson,A.W. and Rodrigues,J.C.P. "Modelling the Performance of Manganese Electrowinning Cells" To be presented at the 3rd International Symposium on Hydrometallurgy,Atlanta,Georgia.1983.

11. Lele.A.S.,Chowdury,P.J. and Seshadri,V. "Studies on Leaching Behaviour of Pre-reduced Manganese Ore" Trans.Indian .Inst. Met.,2,(1980) pp.170-172.

12. Nwoka,V.O. "Leaching of Manganese Pyrolusite Ore and Electrodeposition of Manganese from Purified Leach Solution" Chem.Age India, 31(3),(1977) pp.262-265.

13. Yagi,S. and Kunii,D. "Studies on Combustion of Carbon Particles in Flames and Fluidized Beds". Proc.5th.Int . Symp.Combustion,(1955)pp.231-244.

14. Levenspiel,O. Chemical Reaction Engineering . 2nd ed., John Wiley, New York,(1972).

15. Smith,J.M. Chemical Engineering Kinetics. 2nd ed., McGraw-Hill, New York, (1970).

16. Wen,C .Y. "Noncatalytic Heterogeneous Solid Fluid Reaction Models." Ind.Eng.Chem.,60(9), (1968).pp.34-54.

17. Roach,G.I.D. and Prosser,A.P. "Prediction of rates of chemical processes for treatment of low-grade materials: theory and tests for mass-transfer controlled reactions." IMM Trans, 87, (1978).pp.C129-C138.

18. Petersen,E.E. "Reaction of Porous Solids." A.I.Ch.E. Journal. 3(4),(1957).pp. 443-448.

19. Hashimoto,K. and Silveston, P.L. "Gasification I: Isothermal kinetic control model for solids with a pore size distribution." A.I.Ch.E.Journal,19(2). pp.259-268.

20. Hashimoto,K. and Silveston, P.L. "Gasification II: Extension to diffusion control." A.I.Ch.E.Journal,19(2). pp.268-277.

21. Hashimoto,K. and Silveston,P.L. "Approximation of rate expressions involving pore size distributions." A.I.Ch.E. Journal, 19(2). pp 368-369.

22. Wen,C.Y. and Wei,L.Y. "Simultaneous non-catalytic solid-fluid reactions." A.I.Ch.E. Journal,16(5),(1970). pp.848-856.

23. Brittan, M.I. "Variable Activation Energy Model for Leaching Kinetics" Int. J. Min. Proc.,2,(1975) pp.321-331.

24. Bowen,J.H. and Cheng, C.K."A diffuse interface model for fluid-solid reaction" Chem.Eng.Sci.,24,(1969). pp.1829-1831.

25. Loveday,B.K. "A model for the leaching of non-porous particles" J.S.Afr.Inst.Min. Metall., 76(2),(1975).pp.16-19.

26. Cunningham,R.E.and Calvelo,A."Kinetic expressions for reaction rate in non-catalytic solid-gas systems" Ind. Eng.Chem. Fund. ,9(3), (1970). pp.505-507.

27. Bowen,J.H. "Misinterpretation of Shrinking Core Data in Chemical Reactions" Can.J.Chem.Eng., 49,(1971).pp.882-884.

28. Liddell,R.C. and Bautista, R.G."Modelling the Chemical Equilibria in Solid-Liquid Reactions-Application to Leaching of Ores" Amer.Chem.Society,38,(1980).pp.741-755.

29. Novosad,Z. and Rehakova,M. "Fractional conversion of dispersed phase in multistage solid-liquid reactors" Inst.Chem.Proc.Fund.,49.pp31-39.

30. Park,J.Y. and Levenspiel,O."The Crackling Core Model for the Reaction of Solid Particles" Chem.Eng.Sci.,

30,(1975).pp.1207-1214.

31. Kramers,H. and Westerterp,K.R. Elements of Chemical Reactor Design and Operation. Netherlands University Press,Amsterdam, (1962).

32. Froment,G.F.and Bischoff,K.B.Chemical Reactor Analysis and Design. John Wiley, New York, (1979).

33. Verbaan,B. "A Kinetic Study of the Dissolution of Natural and Synthetic Sphalerite in Aqeous Sulphuric Acid and in Acidic Ferric Sulphate Media". P.hD.Thesis, University of Natal, Durban,(1977).

34. Bryson,A.W. "Leach Reactors". in A Refresher Course in Reactor Design for Chemical and Hydrometallurgical Processes, University of the Witwatersrand, (1981).

35. Bond,G.C. Heterogenous Catalysis Principles and Applications. Clarendon Press, Oxford, (1974).

36. Coulson,J.M. and Richardson,J.F. Chemical Engineering Vol. III 2nd ed.,Pergamon Press, Oxford,(1979).

37. Perry,R.H. and Chilton,C.H. Chemical Engineers Handbook. 5th ed., McGraw-Hill,Tokyo,(1973).

38. Weast,R.C. CRC Handbook of Chemistry and Physics. CRC

Press, Florida,(1980).

39. Treybal,R.E. Mass Transfer Operations. 2nd ed., McGraw-Hill, Tokyo,(1968).

40. Denbigh,K. The Principles of Chemical Equilibrium. 3rd ed., Cambridge University Press, Cambridge,(1978).

41. Gerald,C.F. Applied Numerical Analysis . 2nd ed., Addison-Wesley, Massachusetts,(1978).

42. Pecsok,R.L. et. al. Modern Methods of Chemical Analysis. 2nd ed., John Wiley, New York, (1976).

43. Weber,A.P. "The Design of Commercial Continuous-Reactor Systems". Chem.Eng.Progress., (Jan.1953).pp.26-34.

44. Jones,R.W. "A General Graphical Analysis of Continuous Reactions in Series of Agitated Vessels". Chem. Eng. Progress,(Jan.1951).pp.46-48.

45. Musiker,R. "Style Guide for Theses and Dissertations". Occasional Publications, University of the Witwatersrand, Johannesburg,(1980).

10. APPENDICES

10.1 Solution of Unreacted Core Shrinking Model when Diffusion through Liquid Film Controls

The differential equation describing the system is

$$\frac{-dN_B}{dt} = -\frac{n_b}{4\pi R^2}\frac{dN_A}{dt} = n_b k_g C_{Ab} \qquad (2.20)$$

The amount of solid reactant within the shrinking core is

$$N_B = \rho_B V$$
$$= \frac{4}{3}\pi r_c^3 \rho_B \qquad (10.1)$$

The decrease in volume or radius of unreacted core accompanying the disappearance of dN_B moles of solid reactant or $n_b dN_A$ moles of liquid reactant is then given by

$$-dN_B = -n_b dN_A = -\rho_B dV = -\rho_B d(\tfrac{4}{3}\pi r_c^3)$$
$$= -4\pi \rho_B r_c^2 \, dr_c \qquad (10.2)$$

Substituting (10.2) into (2.20) gives the rate of reaction in terms of the shrinking radius of unreacted core, or

$$-\frac{1}{S_{ex}}\frac{dN_B}{dt} = -\frac{\rho_B r_c^2}{R^2}\frac{dr_c}{dt} = bk_g C_{Ab} \qquad (10.3)$$

Rearranging and integrating, we find how the unreacted core shrinks with time. Thus,

$$-\frac{\rho_B}{R^2}\int_R^{r_c} r_c^2 \, dr_c = bk_g C_{Ab}\int_0^t dt$$

or

$$t = \frac{\rho_B R}{3n_b k_g C_{Ab}} \left(1 - \left(\frac{r_c}{R}\right)^3 \right) \qquad (10.4)$$

Let the time for complete reaction of a particle be τ .

Then by taking $r_c = 0$ in equation (10.4)

$$\tau = \frac{\rho_B R}{3n_b k_g C_{Ab}} \qquad (10.5)$$

The radius of unreacted core in terms of fractional time for complete conversion is obtained by combining equations (10.4) and (10.5), or

$$\frac{t}{\tau} = 1 - \left(\frac{r_c}{R}\right)^3 \qquad (2.21)$$

This can be written in terms of fractional time for conversion by noting that

$$1 - X_B = \left(\frac{\text{volume of unreacted core}}{\text{total volume of particle}}\right)$$

$$= \frac{\frac{4}{3}\pi r_c^3}{\frac{4}{3}\pi R^3} = \left(\frac{r_c}{R}\right)^3 \qquad (10.6)$$

Therefore

$$\frac{t}{\tau} = 1 - \left(\frac{r_c}{R}\right)^3 = X_B \qquad (2.22)$$

10.2 Solution of the Unreacted Core Shrinking Model when Diffusion through the Ash Layer Controls

The differential equation describing diffusion in the ash layer is

$$-\frac{dN_A}{dt} = 4\pi r^2 D_A \frac{dC_A}{dr} \qquad (2.23)$$

Integrating across the ash layer from R to r_c

$$-\frac{dN_A}{dt}\int_R^{r_c}\frac{dr}{r^2} = 4\pi D_A\int_{C_{Ab}}^{0} dC_A$$

Or $$-\frac{dN_A}{dt}\left(\frac{1}{r_c} - \frac{1}{R}\right) = 4\pi D_A C_{Ab} \qquad (10.7)$$

This expression represents the conditions of a reacting particle at any time. Next, let the size of the unreacted core change with time. For a given size of unreacted core, dN_A/dt is constant; however, as the core shrinks the ash layer becomes thicker, lowering the rate of diffusion of A. Consequently, integration of equation (10.7) with respect to time and other variables should give the required relationship. But equation (10.7) contains three variables, t, N_A, and r_c, one of which must be eliminated or written in terms of the other variables. As with film diffusion, N_A can be written in terms of r_c. This relationship is given by equation (10.2); hence replacing in equation (10.7), seperating variables and integrating, we obtain

$$-\rho_B \int_R^{r_c} \left(\frac{1}{r_c} - \frac{1}{R}\right) r_c^2 dr_c = n_b D_A C_{Ab} \int_0^t dt$$

or

$$t = \frac{\rho_B R^2}{6 n_b D_A C_{Ab}} \left(1 - 3 \left(\frac{r_c}{R}\right)^2 + 2\left(\frac{r_c}{R}\right)^3\right) \quad (10.8)$$

For complete conversion of a particle, $r_c = 0$, and the time required is

$$\tau = \frac{\rho_B R^2}{6 n_b D_A C_{Ab}} \quad (10.9)$$

The progression of reaction in terms of the time required for complete conversion is found by dividing equation (10.8) by equation (10.9),

$$\frac{t}{\tau} = 1 - 3\left(\frac{r_c}{R}\right)^2 + 2\left(\frac{r_c}{R}\right)^3 \quad (10.10)$$

which in terms of fractional conversion becomes

$$\frac{t}{\tau} = 1 - 3(1 - X_B)^{2/3} + 2(1 - X_B) \quad (2.24)$$

10.3 Solution of the Unreacted Core Shrinking Model when Chemical Reaction Controls

The differential equation describing this process is given by

$$-\frac{dN_B}{dt} = 4\pi\, r_c^2\, k_s\, C_{Ab} \qquad (2.25)$$

Writing N_B in terms of the shrinking radius, as given in equation (10.2) gives

$$-\frac{1}{4\pi r_c^2}\rho_B 4\pi r_c^2 \frac{dr_c}{dt} = -\rho_B \frac{dr_c}{dt} = n_b\, k_s\, C_{Ab} \qquad (10.11)$$

which on integration becomes

$$-\rho_B \int_R^{r_c} dr_c = n_b\, k_s\, C_{Ab} \int_0^t dt$$

or

$$t = \frac{\rho_B}{n_b\, k_s\, C_{Ab}} (R - r_c) \qquad (10.12)$$

The time required for complete conversion is given when $r_c = 0$, or

$$\tau = \frac{\rho_B R}{n_b\, k_s\, C_{Ab}} \qquad (10.13)$$

The decrease in radius or increase in fractional conversion of the particle in terms of τ is found by combining equations (10.12) and (10.13) to give

$$\frac{t}{\tau} = 1 - \frac{r_c}{R} = 1 - (1 - X_B)^{1/3} \qquad (2.26)$$

10.4 Transport Phenomena in the Liquid Near the Solid Surface

In most cases of practical interest (such as leaching), the flow characteristics of the liquid in the neighbourhood of a solid surface are very complicated. By using the stagnant film model, however, a simple expression can be obtained for the mass transfer rate in terms of the overall concentration driving force. The film model is shown diagramatically in Figure 10.1. The rate of mass transfer of A from the surface is

$$r_A = -D_A a \left.\frac{dC_A}{dx}\right|_{x=0}$$

$$\text{or} \quad r_A = -D_A a(C_{Ab} - C_{As}) / \delta$$

$$= -k_m a(C_{Ab} - C_{As}) \qquad (10.14)$$

10.4.1 Adsorption on Solid Surfaces

Experimental evidence suggests that two types of adsorption mechanism occur, namely physical adsorption and chemisorption. The first type is non-specific and the forces attracting the liquid to the solid surface are relatively weak. The second type is specific and the adsorbed molecules of the liquid phase are held to the solid surface by valence forces of the same type as those occurring between atoms in molecules.

It is widely accepted th chemisorption plays a major role in determining the kinetics of reactions in both catalytic and non-catalytic systems. The Langmuir model (35) is commonly used to interpret kinetic measurements for both types of adsorption processes,

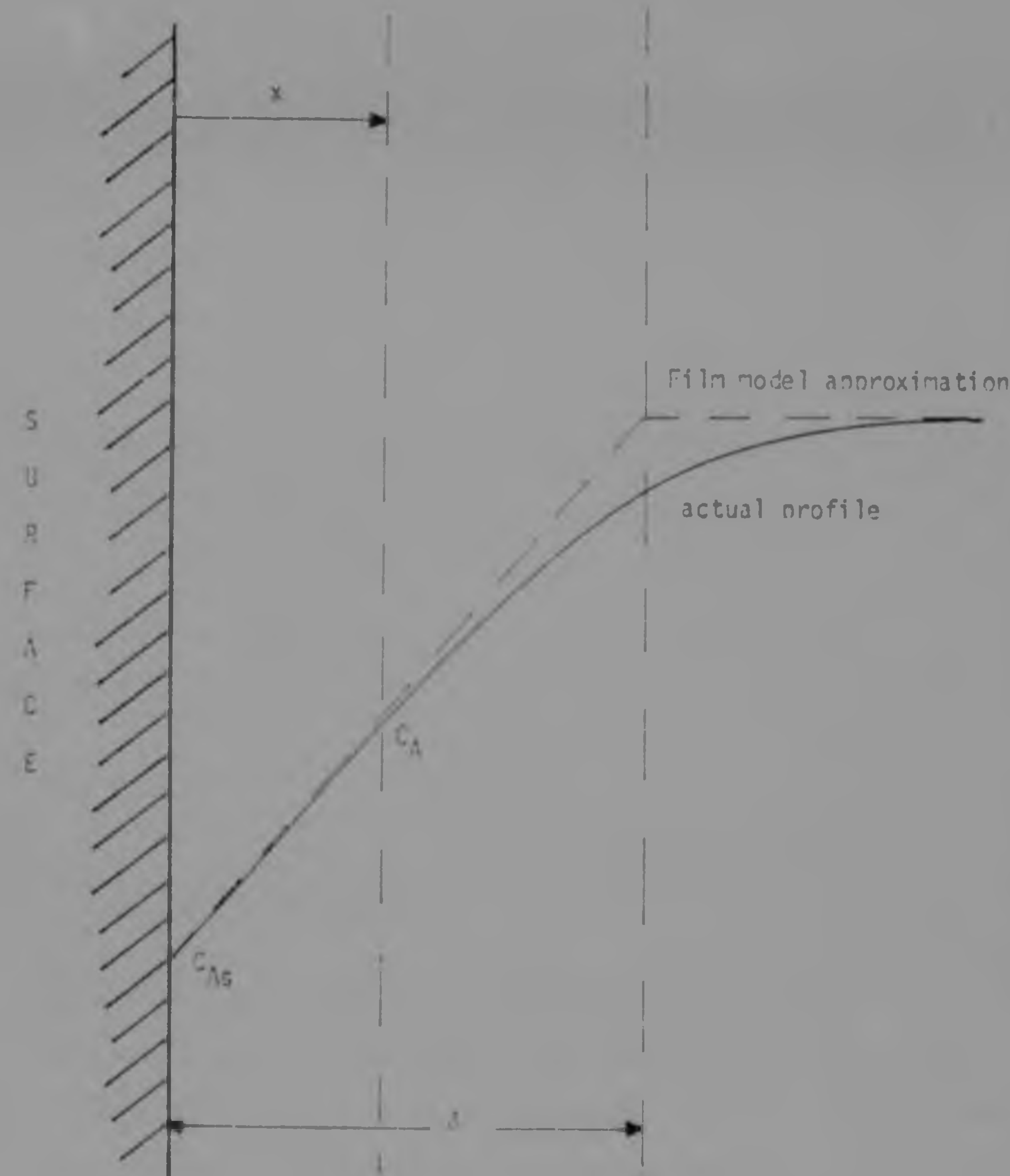

FIG.10.1: The Film Model

although Langmuir originally derived it for physical adsorption under fairly restricted conditions. According to the model, the rate of adsorption of a single component A has the form

$$r_{Ap} = ka\, C_{As}\,(1 - \theta) \tag{10.15}$$

The rate of desorption is similarly given by

$$r_{Ad} = k'a\theta \tag{10.16}$$

At equilibrium with no reaction taking place, $r_{Ap} = r_{Ad}$ and thus

$$\theta = \frac{kC_{As}}{k' + kC_{As}}$$

$$= \frac{kC_{As}}{1 + KC_{As}} \tag{10.17}$$

where $K = k/k'$

10.4.2 Particulate Systems

Most solid-liquid reactors are designed such that the solid appears in a particulate form. This results in large surface to volume ratios for the solid and correspondingly high reaction rates. In particulate systems where the solid phase is modified by reaction , a commonly used model to simulate this effect is the unreacted core shrinking model, shown diagrammatically in Figure ?.1.

Examining the rate expressions given by equations (10.14),(10.15)

(10.16):

$$r_A = -ka\Psi \qquad (2.29)$$

By defining appropriate size and shape factors for the solid particles, and provided all the particles have the same factors,

$$r_A = -kN\phi\Psi \left(\frac{M}{\rho_B N}\right)^{2/3} \qquad (2.35)$$

or $$r_A = -\frac{kN}{\rho_B N}\phi\Psi \qquad (2.36)$$

Although batch leaching is not commonly used on an industrial scale, it is often convenient as a tool for studying kinetics. Consider the same reaction discussed in section 2.4, i.e.

$$A(l) + n_b B(s) = n_c C(l) + n_p P(s) \qquad (2.19)$$

A differential mass balance gives

$$\frac{dM}{dt} = r_A \qquad (10.18)$$

Using the unreacted core shrinking model given by equation (2.35)

$$\frac{dM}{dt} = -kN\phi\Psi\left(\frac{M}{\rho_B N}\right)^{\frac{2}{3}} \qquad (10.19)$$

If M_o is the initial value of M,

$$\int_{M_o}^{M} \frac{dM}{M^{2/3}} = -\int_0^t \frac{kN\phi\Psi}{(\rho_B N)^{2/3}}\, dt \qquad (10.20)$$

Defining $t^* = \dfrac{3M_0^{1/3}(\rho_B N)^{\frac{2}{3}}}{kN\,\phi\Psi}$ (2.38)

and integrating the left-hand side of equation (10.20)

$$M^{1/3} - M_0^{1/3} = -M_0^{1/3}\int_0^t \frac{dt}{t^*}$$

or $$M = M_0\left(1 - \int_0^t \frac{dt}{t^*}\right)^3 \qquad (10.21)$$

If the fluid properties are kept constant (i.e. constant Ψ) and $k\phi$ is independant of conversion, then equation (10.21) may be integrated to give

$$M = M_0(1 - t/t^*)^3, \text{ for } t \leq t^*$$

and $$M = 0 \text{ for } t > t^* \qquad (10.22)$$

In a CSTR, such as a continuous leach reactor, the concentration of each fluid species is uniform throughout the reactor. Provided $k\phi$ is constant, t^* may be assumed to be independant of the residence time of the particle. If Ep(t)dt is the fraction of particles leaving the reactor which have resided for times between t and t + dt, then a mass balance for B in the solid phase at the reactor outlet will be

$$M_1 = \int_0^\infty (M)_{batch}\, Ep(t)dt \qquad (10.23)$$

Substituting equation (10.22) for (M) batch

$$M_1 = \int_0^{t^*} M_0(1 - t/t^*)^3\, Ep(t)dt \qquad (10.24)$$

For a CSTR

$$Ep(t) = {}^{1}/_{\tau} \exp(-t/\tau) \tag{10.25}$$

Therefore

$$\frac{M_1}{M_o} = \int_0^{t^*} \left(1 - 3\frac{t}{t^*} + 3\left(\frac{t}{t^*}\right)^2 - \left(\frac{t}{t^*}\right)^3\right)\frac{1}{\tau} \exp\left(\frac{-t}{\tau}\right) dt$$

$$= 1 - 3\frac{\tau}{t^*} + 6\left(\frac{\tau}{t^*}\right)^2 - 6\left(\frac{\tau}{t^*}\right)^3 \left(1 - \exp\left(\frac{-t^*}{\tau}\right)\right)$$

$$\text{or } 1 - \frac{M_1}{M_o} = 3\frac{\tau}{t^*} - 6\left(\frac{\tau}{t^*}\right)^2 + 6\left(\frac{\tau}{t^*}\right)^3 \left(1 - \exp\left(\frac{-t^*}{\tau}\right)\right) \tag{2.37}$$

10.5 The Porous Solid Model

Consider very porous particles all of an initial size l having a mineral content $z_0=1$. For the system under consideration ϕ and ψ are constant.

Since the particle is initially all mineral, the available surface area for reaction is proportional to the volume of the particle, or

$$a \propto v$$

i.e. $a = \rho v$ (10.26)

This situation is an approximation to a system in which the solid particles are very porous. This is because, in this derivation, the mineral content and the gangue occurring in each particle are treated as discrete particles themselves.

If the reaction were to occur in a batch reactor, the differential mass balance on solid reactant B would be

Rate of accumulation of B/ unit volume + rate of leaching of B = 0

or $$\frac{d(Nv\sigma_B)}{dt} + k l a \psi = 0 \qquad (10.27)$$

Substituting for a from equation (10.26) into equation (10.27) gives:

$$\frac{d(N\sigma_B v)}{dt} = -k\rho v l \psi$$

$$\text{or} \quad \frac{dv}{dt} = -\frac{k\rho}{\rho_B}\, v \qquad (10.28)$$

$$\text{defining } \lambda = \frac{k\rho}{\rho_B} \qquad (2.40)$$

$$\text{gives } \frac{dv}{dt} = -\lambda v \qquad (10.29)$$

Equation (10.29) can be integrated between the initial value of v, v_0 (at time $t=0$) and v (at a time $t = t$) i.e.

$$\int_{v_0}^{v} \frac{dv}{v} = -\lambda \int_{0}^{t} dt$$

$$\text{or} \quad \frac{v}{v_0} = \exp(-\lambda t) \qquad (10.30)$$

Now, since the volume of the particle is directly related to the mass of solid reactant by

$$M = \rho_B\, v \qquad (10.31)$$

equation (10.30) may also be expressed as

$$\frac{M}{M_0} = \exp(-\lambda t) \qquad (10.31)$$

Equation (10.31) can be differentiated with respect to time to give

$$\frac{d(M/M_0)}{dt} = -\lambda \exp(-\lambda t) \qquad (11.32)$$

Substituting equation (10.31) into (10.32) gives

$$\frac{d(M/M_0)}{dt} = - \lambda \left(\frac{M}{M_0}\right)$$

$$\text{or} \quad \frac{dM}{dt} = r_A = -\lambda M \qquad (2.39)$$

The above equation represents the rate of reaction.

In a CSTR the concentration of each fluid species is uniform throughout the reactor. Provided kϕ is constant, λ may be assumed to be independant of the residence time of the particle. If Ep(t)dt is the fraction of particles leaving the reactor which have resided for times between t and t + dt, then the mass balance for B at the reactor outlet is given by equation (10.23), i.e.

$$M_1 = \int_0^\infty (M)_{batch}\, Ep(t)dt$$

Substituting for $(M)_{batch}$ from equation (10.31) and for Ep(t)dt from equation (10.25) gives

$$M_1 = \int_0^\infty M_0 \exp(-\lambda t) \frac{1}{\tau} \exp\left(\frac{-t}{\tau}\right) dt$$

$$\text{or} \quad \frac{M_1}{M_0} = \int_0^\infty \frac{1}{\tau} \exp\left(-t\left(\lambda + \frac{1}{\tau}\right)\right)dt \qquad (10.33)$$

which may be integrated to give

$$\frac{M_1}{M_0} = \frac{1}{1 + \lambda\tau} \qquad (10.34)$$

or, in terms of the fractional leach efficiency

$$1 - \frac{M_1}{M_0} = \frac{\lambda\tau}{1+\lambda\tau} \qquad (2.41)$$

10.6 Calculation of Rates of Reaction from the System Mass Balances

Referring to Figure 2.5 , the overall mass balance is

$$W_0 + \rho_0 Q_0 = W_1 + \rho_1 Q_1 \qquad (10.35)$$

The mass balance for manganese is

$$W_0 g_0 + C_0 Q_0 = W_1 g_1 + C_1 Q_1 \qquad (10.36)$$

The aqeous phase mass balance for manganese is

manganese in = manganese out - rate of manganese leaching

or $$C_0 Q_0 = C_1 Q_1 - r_1 V_1 \qquad (10.37)$$

which gives $$r_1 = \frac{Q_1}{V_1}\left(C_1 - \frac{Q_0}{Q_1} C_0 \right) \qquad (2.43)$$

The solid phase mass balance for manganese is

manganese in = manganese out + rate of manganese leaching

or $$W_0 g_0 = W_1 g_1 + r_1 V_1 \qquad (10.38)$$

which gives $$r_1 = \frac{W_0 g_0 - W_1 g_1}{V_1} \qquad (2.44)$$

10.7 Batch Leaching Experimental Results

The results of the batch leaching experiments are presented in Table 10.1 below.

Table 10.1

Batch leaching results

Final pH	Mn in solution (g/l)	Mn in solid (%)	% Mn recovered
1,35	18,1	5,3	84,06
1,98	23,1	21,4	88,36
3,15	24,3	15,[illegible]	81,28
3,25	25,0	16,1	86,03
4,20	24,5	12,0	80,01
4,42	25,3	13,9	85,12
5,29	25,5	11,1	83,[illegible]
5,49	26,1	14,8	87,26
5,79	26,8	11,7	88,69
5,81	26,7	11,7	84,10
6,48	27,4	11,0	86,62
6,62	26,8	11,0	83,88
6,67	27,6	11,3	83,57
6,70	27,5	13,8	84,11
6,74	26,3	14,0	79,24
6,75	27,4	13,6	82,14
6,90	27,1	14,6	78,57

Table 10.1 continued

Final pH	Mn in solution (g/l)	Mn in solid (%)	% Mn recovered
6,93	27,5	12,6	81,76
6,94	26,2	17,3	80,32
6,99	27,3	15,3	79,48
7,06	26,4	16,3	72,83
7,07	27,1	15,9	77,55
7,23	26,2	19,8	70,29
7,25	17,9	25,7	24,45
7,40	13,9	23,8	8,32
7,65	11,7	24,8	0,61

These results are plotted in Figures 10.2 and 10.3 below.

Table 10.2

Comparison of Theoretical and Experimental Mn Equilibrium Concentrations

Final pH	Mn equilibrium concentration(g/l)	
	Theoretical	Experimental
6,90	33,5	27,[illegible]
6,94	28,4	27,5
6,99	23,2	27,3
7,06	17,6	26,4
7,07	16,9	27,1

FIG.10.2: Variation of the Mn Concentration with pH

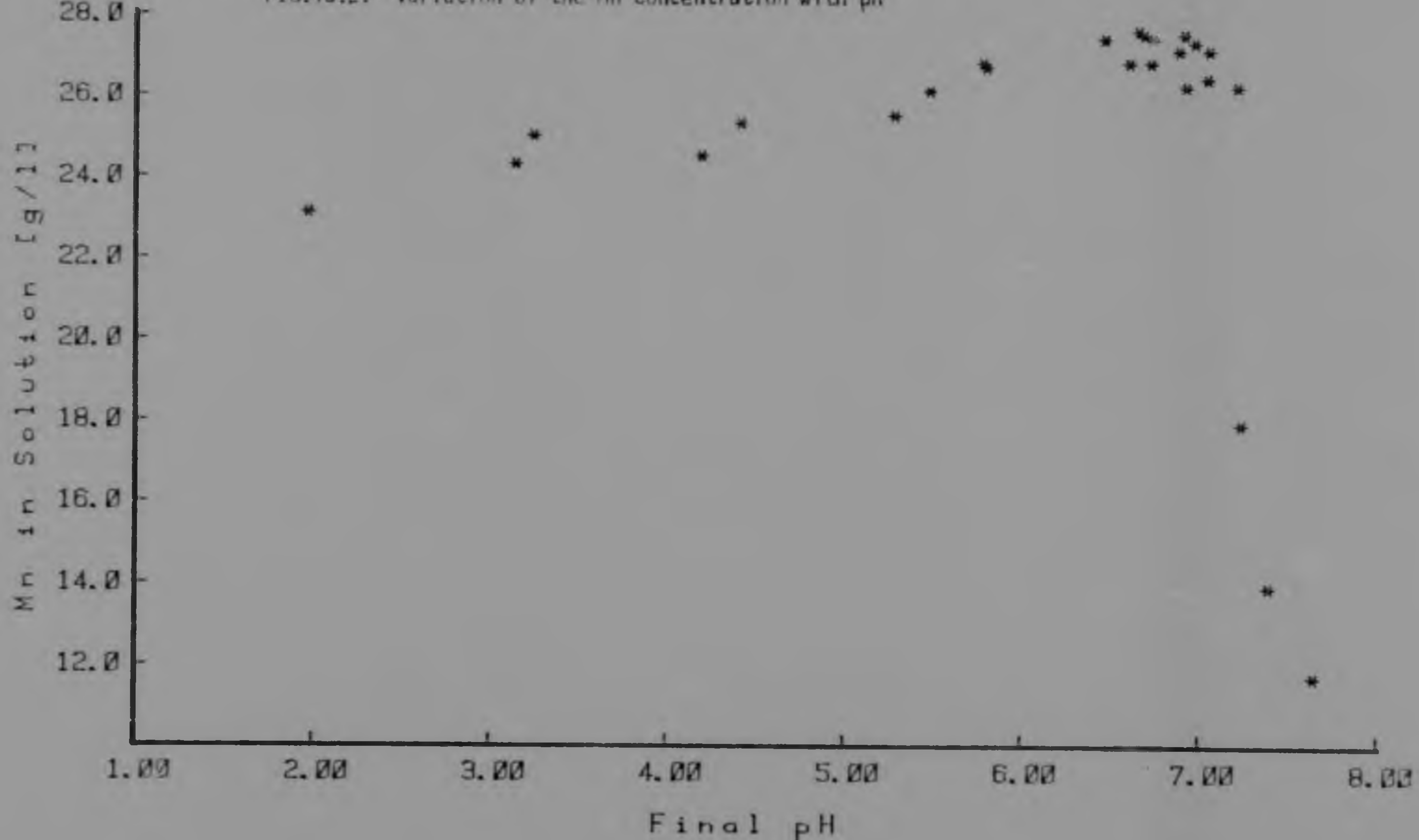

FIG.10.3: Variation of the Mn Extracted with pH

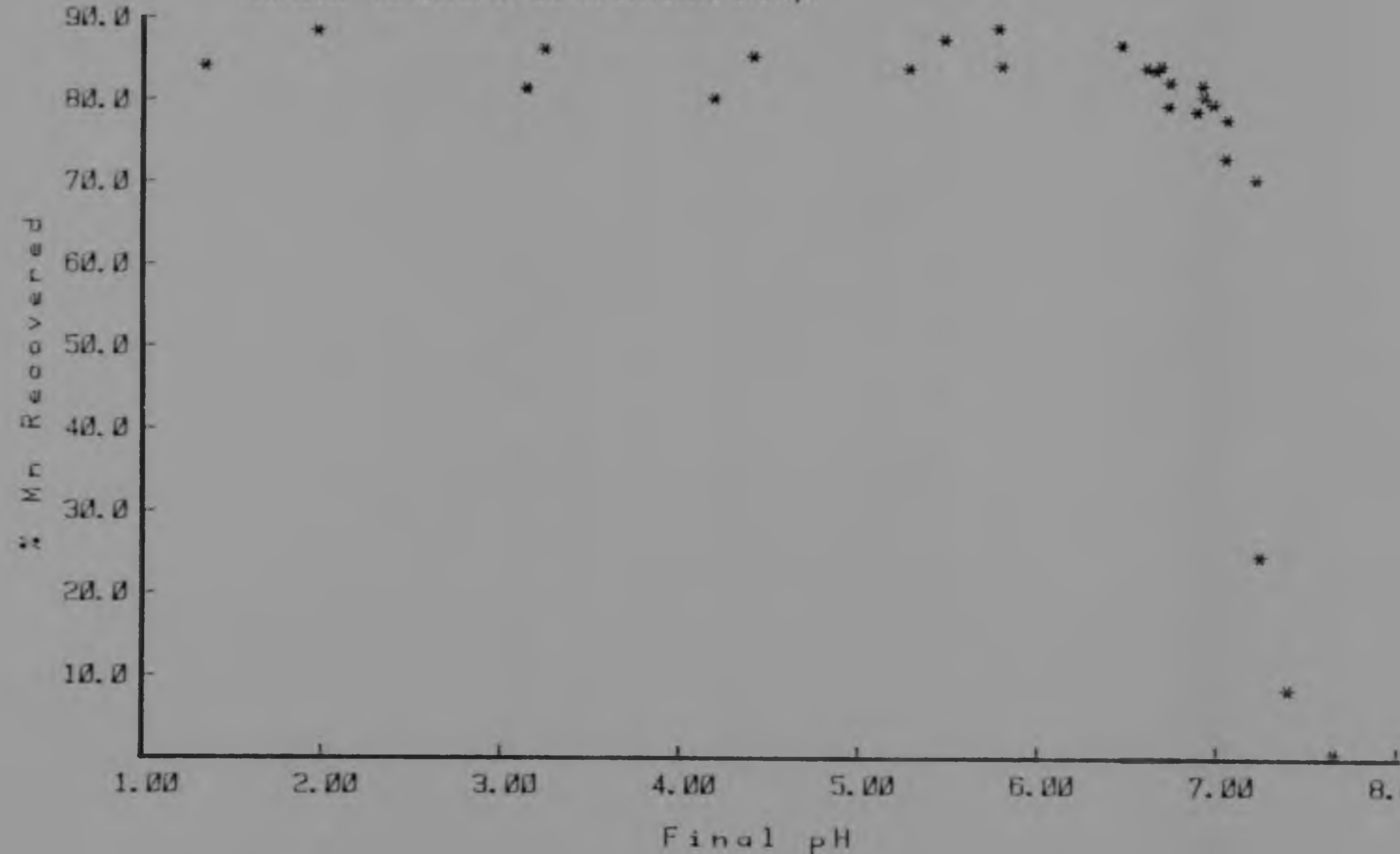

Table 10.2 continued

Final pH	Mn equilibrium concentration(g/l)	
	Theoretical	Experimental
7,23	9,1	26,2
7,25	8,4	17,9
7,40	4,8	13,9
7,65	2,0	11,7

An example of how the theoretical manganese equilibrium concentration is calculated is given in Appendix 10.3

Table 10.3

Comparison of modified theoretical and experimental Mn equilibrium concentration

Final pH	Mn equilibrium concentration (g/l)	
	Theoretical	Experimental
6,90	75,3	27,1
6,94	64,0	27,5
6,99	52,3	27,3
7,06	39,6	26,4
7,07	38,1	27,1
7,23	20,5	26,2
7,25	19,1	17,9
7,40	10,9	13,9
7,65	4,5	11,7

10.8 Calculation of the Theoretical Mn Equilibrium Concentration

Example: Final pH of batch test is 6,90

Since all batch tests were performed at $60^{\circ}C$ (333K), substitute T = 333 in equations (2.7), (2.8) and (2.9) to give:

$$K'_s = 3,316 \times 10^{-14}$$

$$K'_c = 2,302 \times 10^{-8}$$

$$K'_a = 1,799 \times 10^{8}$$

now

$$C = 10^{-pH}$$

$$= 10^{-6,90}$$

$$= 1,259 \times 10^{-7} \text{ mol/l}$$

From equation (2.12)

$$C = \frac{C^{2}}{K'_s}$$

$$= 0,478 \text{ mol/l}$$

And from equation (2.18), substituting in the values of C, C_A, K'_s, K'_c and K'_a gives:

$$C_{mB} = \frac{0,478(1,7 + 5,469 + 0,478 + 0,241)}{5,469 + 0,478 + 0,241}$$

$$= 0,609 \text{ mol/l}$$

therefore

$$C_{mB} = 0,609 \times 54,938$$

$$= 33,5 \text{ g/l}$$

(54,938 is the atomic weight of manganese)

All other equilibrium manganese concentrations were calculated similarly.

10.9 Calibration Curves for the Ore Feeder and Rotameter.

10.9.1. Rotameter Calibration

The calibration was conducted by setting the rotameter to a specified setting and measuring the volume of liquid over a time period. The results are given in Table 10.4.

Table 10.4

Rotameter Calibration Values

Rotameter Setting (cm)	Anolyte Flowrate (l/min at 50°C)
0	0
4	0,22
6	0,27
9	0,37
12	0,45
15	0,54
18	0,64
21	0,76
24	0,88
27	0,97
30	1,10

These values are represented diagramatically in Figure 10.4.

FIG 10.4: Rotameter Calibration Curve

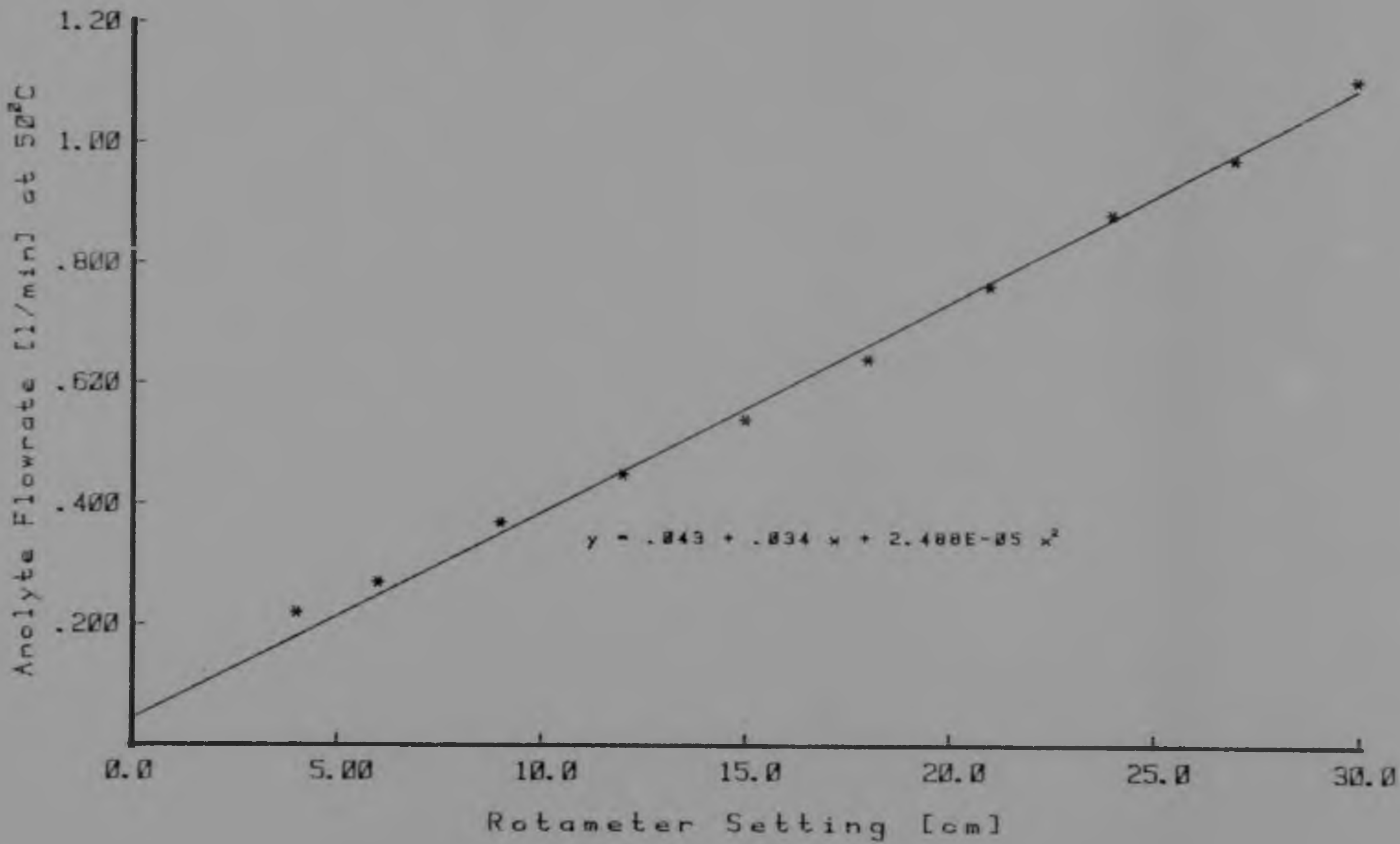

10.9.2 Ore Feeder Calibration

The ore feeder calibration was performed in a similar way to the roatmeter calibration. The results are given in Table 10.5 and are plotted in Figure 10.5.

Table 10.5

Ore Feeder Calibration Values

Ore Feeder Setting	Ore Flowrate (g/min.)
4	19,0
4,5	29,0
5	33,8

FIG.10.5: Ore Feeder Calibration Curve

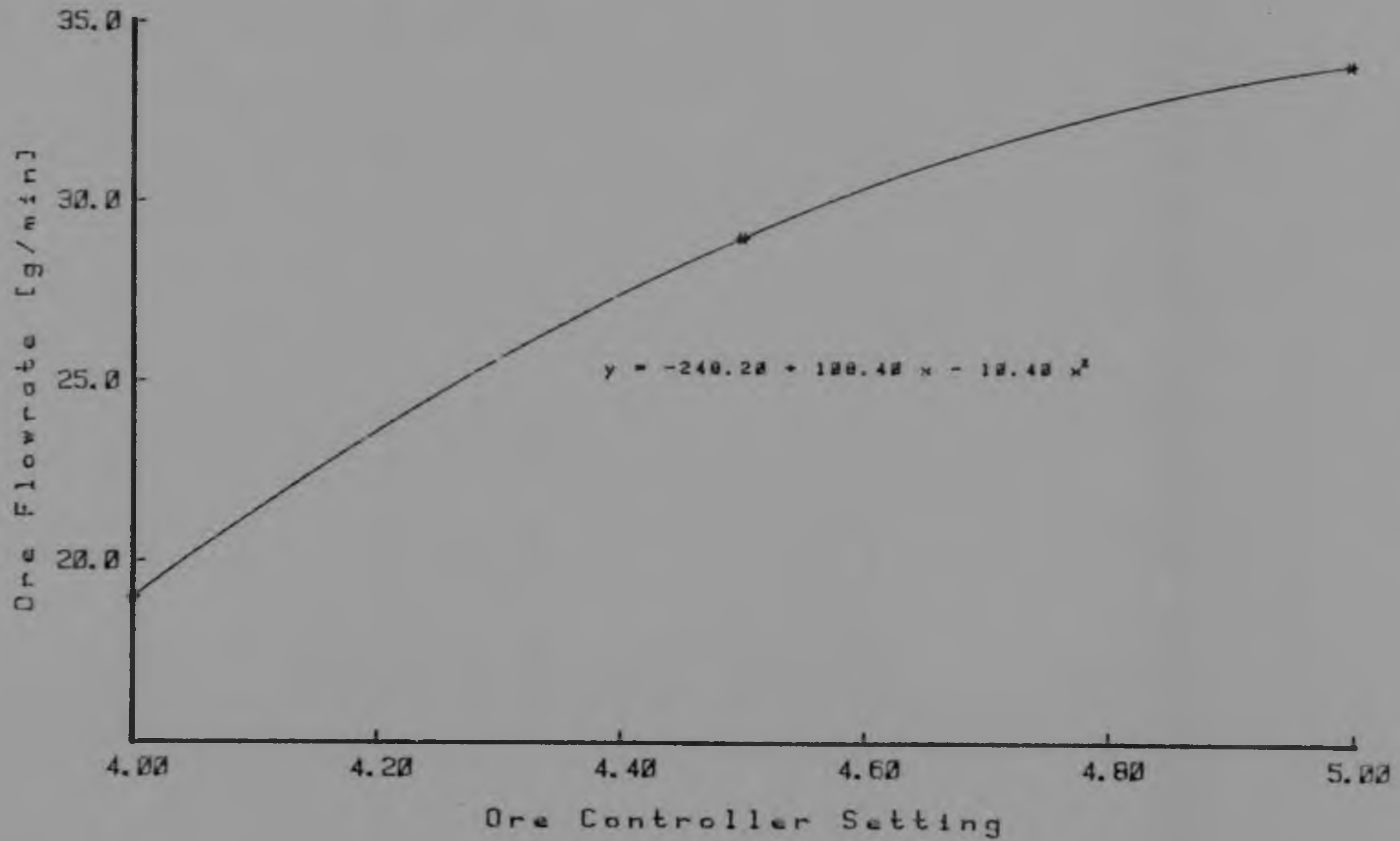

10.10 Continuous Leaching Results

The results of the continuous leaching experiments (for each of the runs) are presented below in Tables 10.6 - 10.8

Table 10.6

Continuous Leaching Results- Run 1

Conditions W_o = 18,97 g/min

C_o = 12,24 g/l

g_o = 0,54

pH	Mn in solution (g/l) C_1	Mn in solid (fraction) g_1	Inlet solution flowrate (l/min) Q_o	Solid discharge rate (g/min) W_1	Outlet solution flowrate (l/min) Q_1
2,55	27,0	0,146	0,5239	2,87	0,6014
2,62	26,7	0,124	0,5204	2,89	0,6088
2,66	27,8	0,118	0,5135	2,90	0,5823
2,84	28,0	0,200	0,5031	2,25	0,5697
2,85	28,9	0,135	0,5031	2,71	0,5545
2,94	26,7	0,160	0,4892	3,70	0,5858
2,99	28,7	0,125	0,4823	3,36	0,5458
3,08	28,9	0,149	0,4754	3,03	0,5402
3,25	25,7	0,168	0,4650	2,98	0,6006
3,39	25,8	0,173	0,4546	2,95	0,5929
3,48	28,2	0.164	0,4442	4,72	0,5286
3,75	25,2	0,167	0,4235	3,10	0,5916

Table 10.6 continued

pH	Mn in solution (g/l) C_1	Mn in solid (fraction) g_1	Inlet solution flowrate (l/min) Q_0	Solid discharge rate (g/min) W_1	Outlet solution flowrate (l/min) Q_1
4,02	26,0	0,164	0,4062	3,35	0,5642
4,10	26,4	0,154	0,3820	4,45	0,5392
4,30	28,0	0,160	0,3683	4,86	0,4835
4,60	26,1	0,173	0,3614	3,40	0,5394
4,80	26,2	0,208	0,3545	4,04	0,5245
5,10	25,9	0,183	0,3476	3,45	0,5354
5,23	29,3	0,160	0,3407	3,95	0,4704
5,25	26,7	0,196	0,3407	4,90	0,5049
5,50	25,5	0,190	0,3333	3,30	0,5337
5,60	28,5	0,160	0,3372	3,90	0,4824
5,70	25,6	0,208	0,3372	5,00	0,5208
5,94	29,2	0,193	0,3306	7,25	0,4415
6,05	30,3	0,186	0,3235	4,70	0,4399
6,13	30,0	0,202	0,3200	4,77	0,4398
6,17	29,5	0,212	0,3166	6,60	0,4312
6,18	28,9	0,207	0,3166	5,33	0,4503
6,23	30,7	0,189	0,3097	4,21	0,4313
6,27	30,2	0,214	0,3063	7,70	0,4088
6,40	29,2	0,168	0,3132	5,10	0,4527
6,44	29,5	0,229	0,2960	6,65	0,4184

Table 10.6 continued

pH	Mn in solution (g/l) C_1	Mn in solid (fraction) g_1	Inlet solution flowrate (l/min) Q_0	Solid discharge rate (g/min) W_1	Outlet solution flowrate (l/min) Q_1
6,46	29,8	0,203	0,2926	5,33	0,4276
6,54	30,0	0,216	0,2926	7,56	0,4064
6,63	29,2	0,155	0,2719	5,44	0,4359
6,80	28	0,255	0,2273	5,60	0,4098
6,93	30,1	0,264	0,1794	4,94	0,3699

Table 10.7

Continuous Leaching Results - Run 2.

Conditions: $W_0 = 29 g/min$

$C_0 = 12,24 g/l$

$g_0 = 0,54$

pH	Mn in solution (g/l) C_1	Mn in solid (fraction) g_1	Inlet solution flowrate (l/min) Q_0	Solid discharge rate (g/min) W_1	Outlet solution flowrate (l/min) Q_1
7,05	27,6	0,277	0,3407	12,80	0,5900
7,10	25,6	0,239	0,3372	11,10	0,6665
7,20	28,6	0,287	0,3372	12,21	0,5694

Table 10.7 continued

pH	Zn in solution (g/l) C_1	Zn in solid (fraction) g_1	Inlet solution flowrate (l/min) Q_o	Solid discharge rate (g/min) W_1	Outlet solution flowrate (l/min) Q_1
7,26	26,1	0,236	0,3338	11,20	0,6553
7,31	29,9	0,301	0,3304	11,80	0,5402
7,35	25,9	0,240	0,3304	12,70	0,6431
7,40	29,7	0,309	0,3235	14,15	0,5134
7,42	26,0	0,240	0,3235	12,00	0,6438
7,50	26,9	0,328	0,3166	19,40	0,4397
7,70	22,4	0,305	0,3097	21,83	0,5712

Table 10.8

Continuous Leaching Results - Run 3

Conditions: W_o = 33,8g/min

C_o = 12,24g/l

g_o = 0,54

pH	Zn in solution (g/l) C_1	Zn in solid (fraction) g_1	Inlet solution flowrate (l/min) Q_o	Solid discharge rate (g/min) W_1	Outlet solution flowrate (l/min) Q_1
2,01	23,5	0,119	0,6631	2,67	1,1085
2,50	23,7	0,148	0,6456	2,87	1,0857

Table 10.8 continued

pH	Mn in solution (g/l) C_1	Mn in solid (fraction) q_1	Inlet solution flowrate (l/min) Q_0	Solid discharge rate (g/min) W_1	Outlet solution flowrate (l/min) Q_1
2,88	26,1	0,184	0,6282	2,83	0,9740
2,93	25,6	0,148	0,6100	4,47	0,9792
3,20	24,5	0,168	0,5934	4,07	1,0135
3,22	26,3	0,198	0,5934	6,68	0,9027
3,27	27,6	0,145	0,5899	6,50	0,8888
3,35	33,8	0,147	0,5864	6,59	0,7238
3,50	25,8	0,189	0,5829	5,55	0,9433
4,02	25,3	0,190	0,5760	5,33	0,9600
4,10	25,9	0,184	0,5690	5,17	0,9369
4,40	25,9	0,194	0,5655	5,90	0,9278
4,97	25,6	0,171	0,5586	4,47	0,9502
5,42	26,6	0,198	0,5551	6,11	0,8961
5,60	25,3	0,206	0,5517	5,83	0,9408
5,87	25,3	0,216	0,5308	6,91	0,9193
5,90	27,1	0,219	0,5239	6,28	0,8591
5,92	34,6	0,216	0,5239	8,98	0,6568
6,05	31,8	0,221	0,4546	10,55	0,6562
6,13	26,0	0,216	0,4407	11,33	0,8154
6,17	35,0	0,200	0,4200	6,50	0,6312
6,20	29,4	0,233	0,3355	8,11	0,7242
6,25	35,1	0,201	0,3320	8,00	0,6074

Table 10.8 continued

pH	Mn in solution (g/l) C_1	Mn in solid (fraction) g_1	Inlet solution flowrate (l/min) Q_0	Solid discharge rate (g/min) W_1	Outlet solution flowrate (l/min) Q_1
6,30	27,1	0,235	0,3820	6,37	0,7821
6,36	33,9	0,222	0,3759	8,49	0,6195
6,40	27,8	0,255	0,3751	8,05	0,7479
6,42	27,9	0,246	0,3751	10,50	0,7262
6,50	35,3	0,206	0,3717	6,44	0,6084
6,53	28,1	0,255	0,3717	6,88	0,7490
6,57	35,0	0,237	0,3717	9,00	0,5899
6,63	29,3	0,234	0,3632	5,00	0,7368
6,83	34,5	0,263	0,3648	10,61	0,5776
6,91	27,2	0,273	0,3614	10,57	0,7275
6,97	31,7	0,276	0,3510	12,30	0,5999
7,00	29,2	0,273	0,3372	5,40	0,7159
7,32	29,8	0,296	0,3269	17,76	0,5704
7,35	31,5	0,301	0,3166	13,55	0,5730

In all of the above tables, the outlet solution flowrate is calculated from equation (10.36), i.e.

$$W_0 g_0 + C_0 Q_0 = W_1 g_1 + C_1 Q_1$$

and was compared to the measured value of Q_1. In most cases the theoretical and experimental values agree well.

From the data above, it is now possible to calculate the leaching rates (at different pH values) from equation(2.43),i.e.

$$r_1 = \frac{Q_1}{V^1}\left(C_1 - \frac{Q_0}{Q_1}C_0\right)$$

or from equation (2.44) i.e.

$$r_1 = \frac{W_0 g_0 - W_1 g_1}{V_1}$$

The leaching rates were calculated from the latter equation since analyses based on the solid phase are generally more reliable than those based on the liquid phase.

The fractional leach efficiency, η , can be calculated from equation (2.42),i.e.

$$\eta = \frac{W_0 g_0 - W_1 g_1}{W_0 g_0}$$

Example: From Table 10.6, at pH = 2,55

W_0 = 18,97 g/min

C_0 = 12,24 g/l

g_0 = 0,54

C_1 = 27,0 g/l

g_1 = 0,146

Q_0 = 0,5239 l/min

W_1 = 2,87 g/min

Q_1 = 0,6014 l/min

therefore $r = \dfrac{W_0 g_0 - W_1 g_1}{V_1}$

$$= \frac{(18,97)(0,54) - (2,87)(0,146)}{14}$$

$$= 0,70177 \text{ g/l min}$$

(V_1 = volume of reactor = 14 liters)

therefore $r_1 = 0,70177 \times 1000 \times \dfrac{1}{54,933}$

(54,938 is the atomic weight of Mn)

therefore $\underline{r_1 = 12,77 \text{ mol/m}^3\text{min}}$

and $\eta = \dfrac{W_0 g_0 - W_1 g_1}{W_0 g_0}$

$$= \frac{(18,97)(0,54) - (2,37)(0,146)}{(18,97)(0,54)}$$

$$\underline{\eta = 0,959.}$$

Similarly, the leaching rates and fractional leach efficiencies were calculated for the other experimental runs and are tabulated in Tables 10.9 - 10.11

Table 10.9

Leaching Rates and Fractional Leach Efficiency - Run 1

pH	Rate (mol/m^3 min)	η
2,55	12,77	0,959

Table 10.9 continued

pH	Rate (mol/m^3min)	η
2,62	12,85	0,965
2,66	12,87	0,967
2,84	12,73	0,956
2,85	12,84	0,964
2,94	12,55	0,942
2,99	12,69	0,953
3,08	12,73	0,956
3,25	12,67	0,951
3,39	12,66	0,950
3,48	12,31	0,924
3,75	12,65	0,949
4,02	12,61	0,947
4,10	12,43	0,933
4,30	12,31	0,924
4,60	12,55	0,943
4,80	12,23	0,918
5,10	12,50	0,938
5,23	12,50	0,938
5,25	12,06	0,906
5,50	12,38	0,930
5,60	12,51	0,939
5,70	11,97	0,898
5,94	11,50	0,864

Table 10.9 continued

pH	Rate(mol/m^{3}min)	n
6,05	12,18	0,915
6,13	12,06	0,906
6,17	11,50	0,863
6,18	11,88	0,892
6,23	12,29	0,922
6,27	11,18	0,839
6,40	12,20	0,916
6,44	11,34	0,851
6,46	11,91	0,894
6,54	11,20	0,841
6,63	12,22	0,918
6,80	11,46	0,861
6,93	11,62	0,873

Table 10.10

Leaching Rates and Fractional Leach Efficiency - Run 2

pH	Rate(mol/m^{3}min)	n
7,05	15,75	0,774
7,10	16,82	0,826
7,20	15,81	0,776
7,26	16,92	0,831
7,31	15,71	0,773
7,35	16,40	0,805

Table 10.10 continued

pH	Rate(mol/m^3min)	η
7,40	14,68	0,721
7,42	16,62	0,816
7,50	12,09	0,594
7,70	11,70	0,575

Table 10.11

Leaching Rates and Fractional Leach Efficiency - Run 3

pH	Rate(mol/m^3min)	η
2,01	23,32	0,983
2,50	23,18	0,977
2,38	23,05	0,971
2,93	22,87	0,964
3,20	22,84	0,963
3,22	22,01	0,928
3,27	22,51	0,948
3,35	22,48	0,947
3,50	22,37	0,943
4,02	22,41	0,944
4,10	22,49	0,948
4,40	22,24	0,937
4,97	22,74	0,958

Table 10.11 continued

pH	Rate(mol/m^3min)	n
5,42	22,16	0,934
5,60	22,17	0,934
5,87	21,97	0,918
5,90	21,94	0,925
5,92	21,21	0,894
6,05	20,70	0,872
6,13	20,55	0,866
6,17	22,04	0,929
6,20	21,55	0,903
6,25	21,64	0,912
6,30	21,78	0,918
6,36	21,28	0,897
6,40	21,06	0,888
6,42	20,37	0,858
6,50	22,01	0,927
6,53	21,45	0,904
6,57	20,93	0,882
6,68	22,21	0,936
6,83	20,10	0,847
6,91	19,98	0,842
6,97	19,14	0,806
7,00	21,81	0,919
7,32	16,90	0,712
7,35	18,43	0,777

The results of Table 10.11 are plotted in Figures 10.6 - 10.11

For the sake of completeness of experimental results, particle size distributions at various pH values were done as well. The distributions are listed below in Table 10.12.

Table 10.12

Particle Size Distributions

Equivalent spherical diameter (μm)	Cumulative mass percent						
	Feed	pH=2,5	pH=3	pH=4	pH=5	pH=6	pH=7
2,8	4,03	4,00	2,03	0,97	1,53	2,97	4,60
3,9	10,77	8,00	4,90	3,07	2,43	6,37	11,23
5,5	20,87	17,60	11,40	7,77	6,73	13,20	22,10
7,8	27,73	24,00	14,67	9,83	8,97	18,67	31,13
11	34,83	30,57	19,33	11,50	11,57	25,13	40,03
16	46,90	44,87	30,27	22,10	21,30	33,90	50,80
22	56,87	52,60	35,60	30,67	27,93	40,30	55,50
31	64,10	63,10	46,80	41,97	40,00	49,60	64,57
44	78,37	72,00	58,57	54,97	53,97	60,80	73,83
62	90,20	86,93	78,73	76,10	73,83	75,50	85,90
88	90,20	95,17	90,73	89,97	88,13	88,10	92,97
125	99,57	100,00	100,00	100,00	100,00	100,00	100,00
mean d	29,40	30,33	40,40	43,67	45,40	40,23	29,53

The particle size distributions were determined using a Leeds and Northrup Microtrac X-ray analyser.

Figure 10.12 shows the variation of particle size distribution as a function of pH and Figure 10.13 shows the variation of the mean particle size as a function of pH.

FIG.10 6: Leaching Rates - Run1

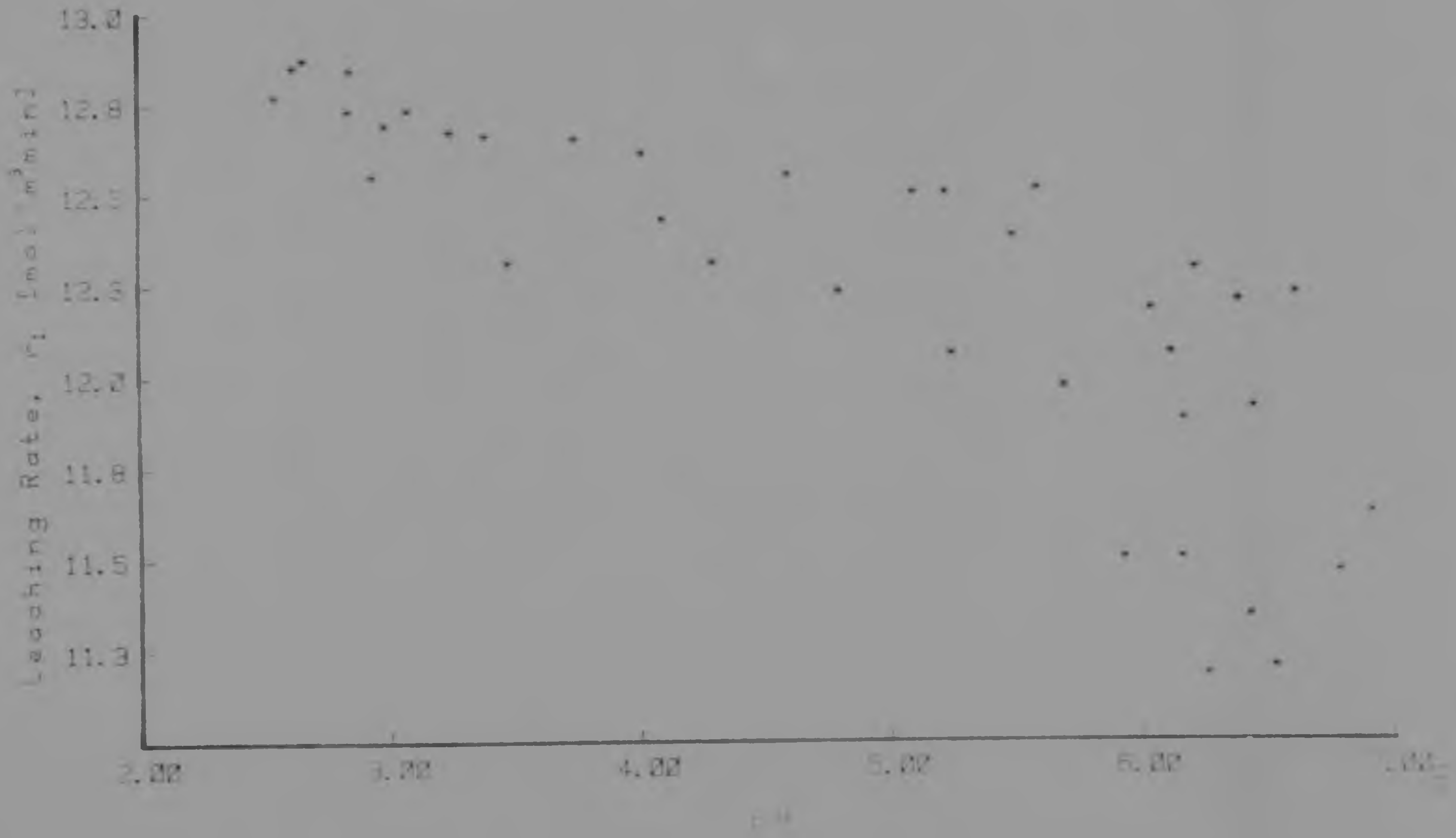

FIG.10.7: Leaching Rates - Run 2.

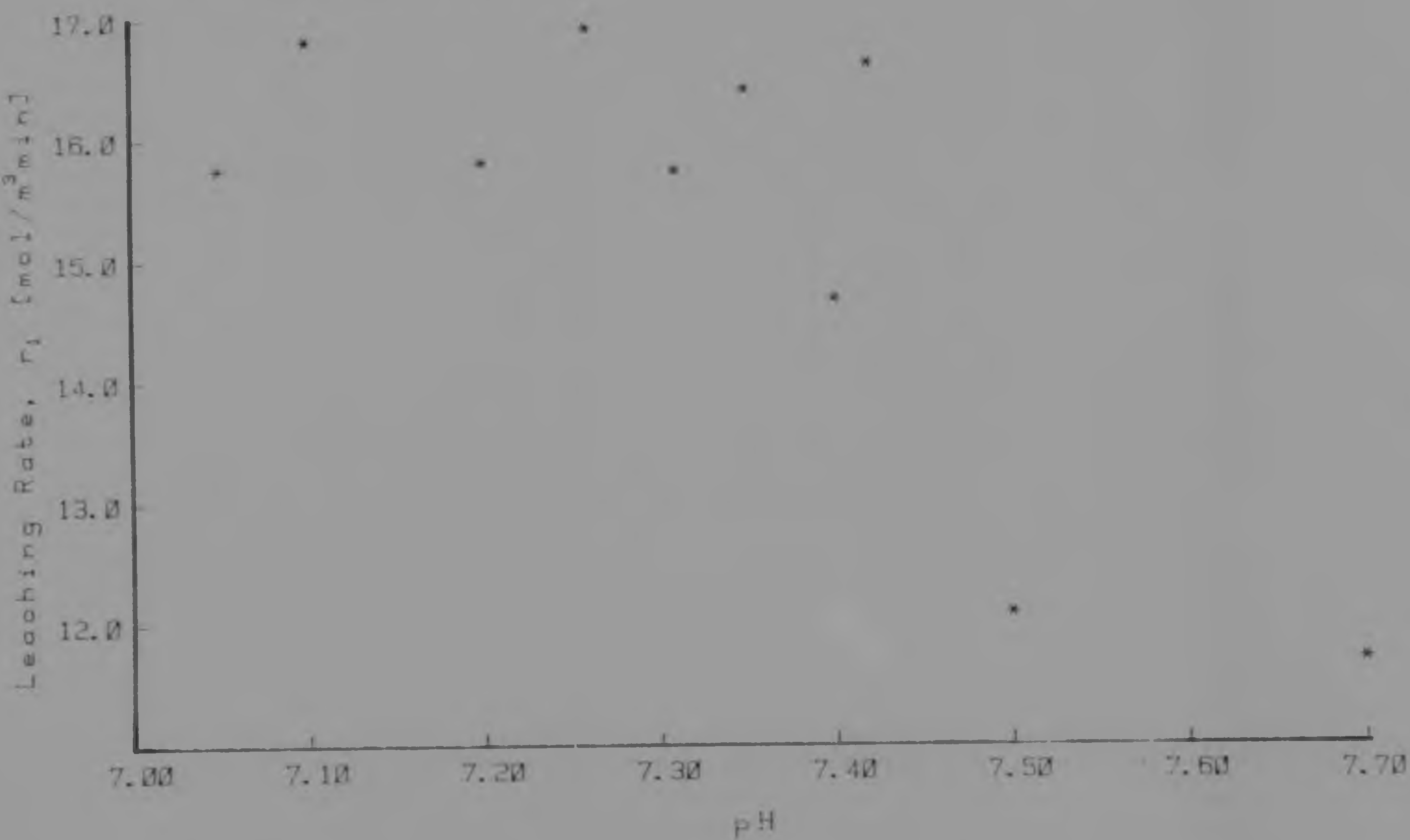

FIG.10.8: Leaching Rates - Run 3.

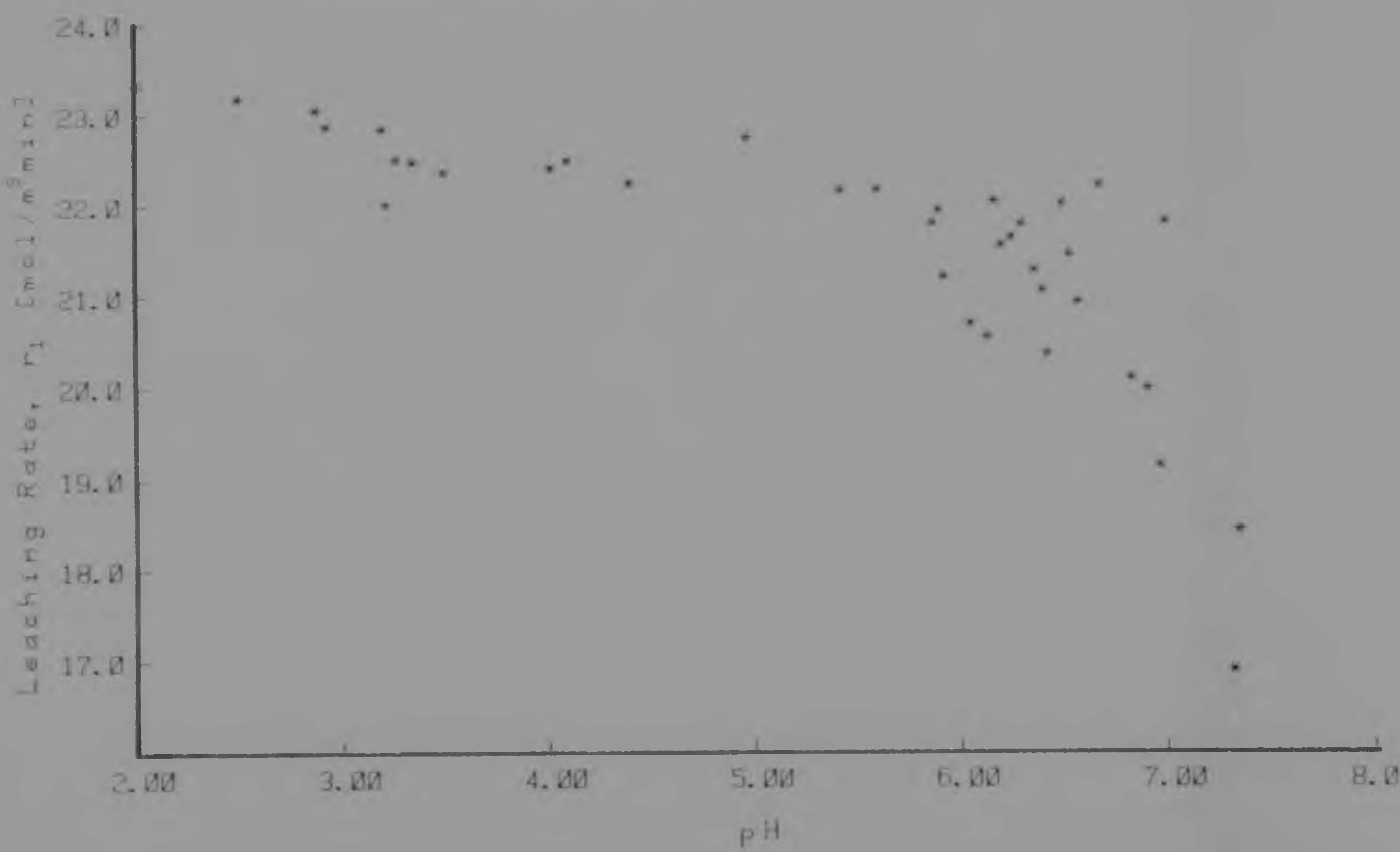

FIG.10.9: Fractional Leach Efficiency - Run 1

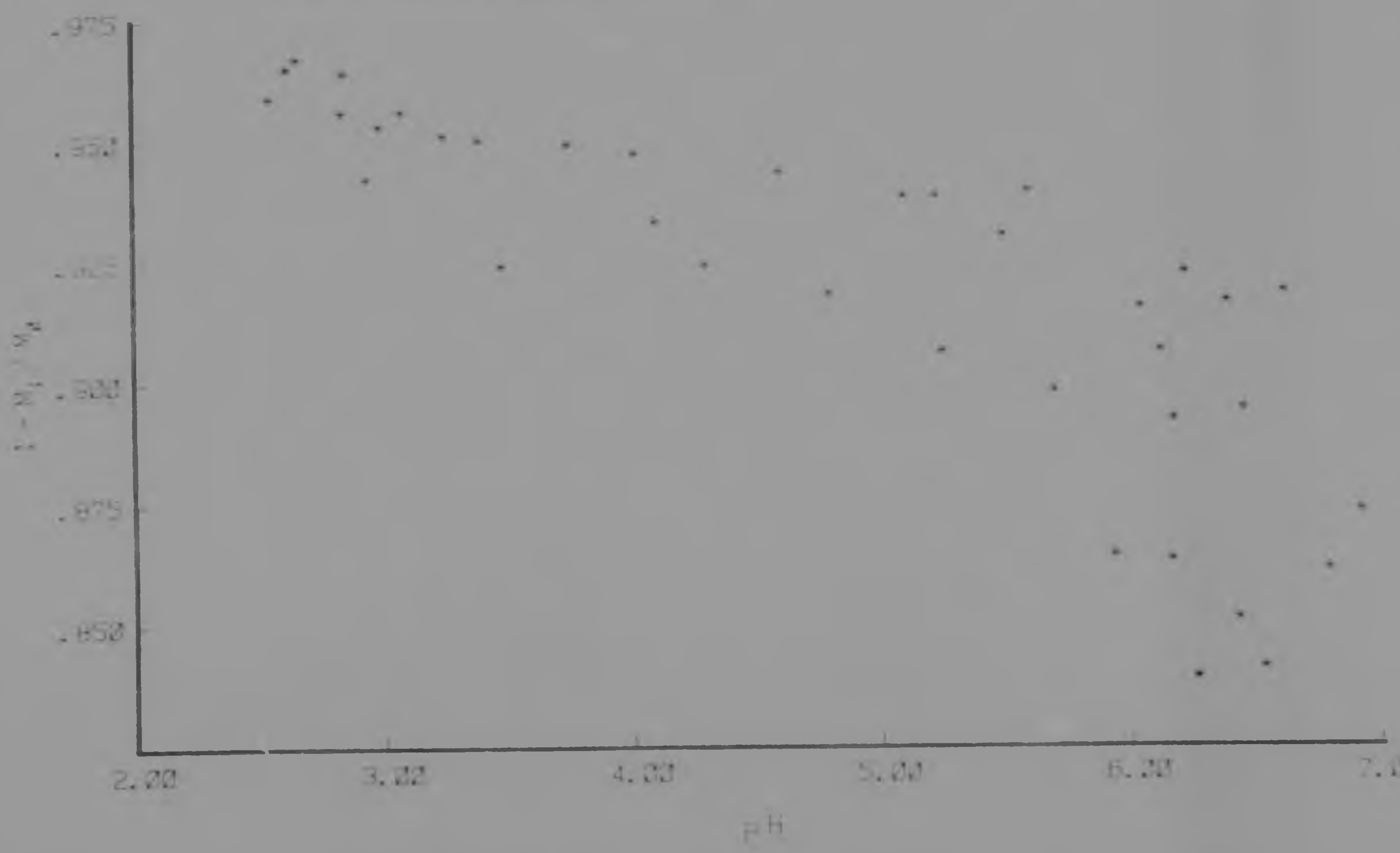

FIG.10.10: Fractional Leach Efficiency - Run 2

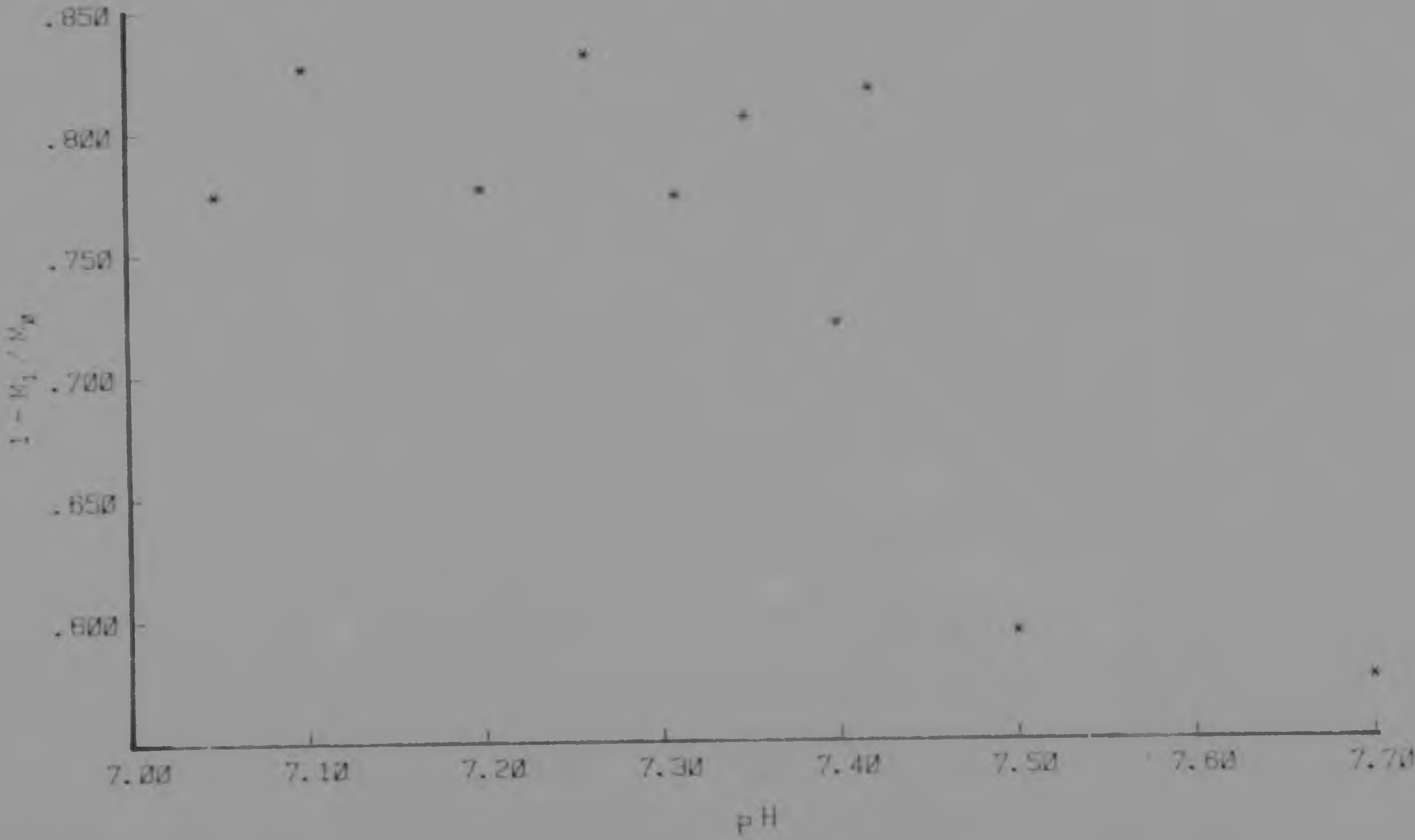

FIG.10.11: Fractional Leach Efficiency - Run 3.

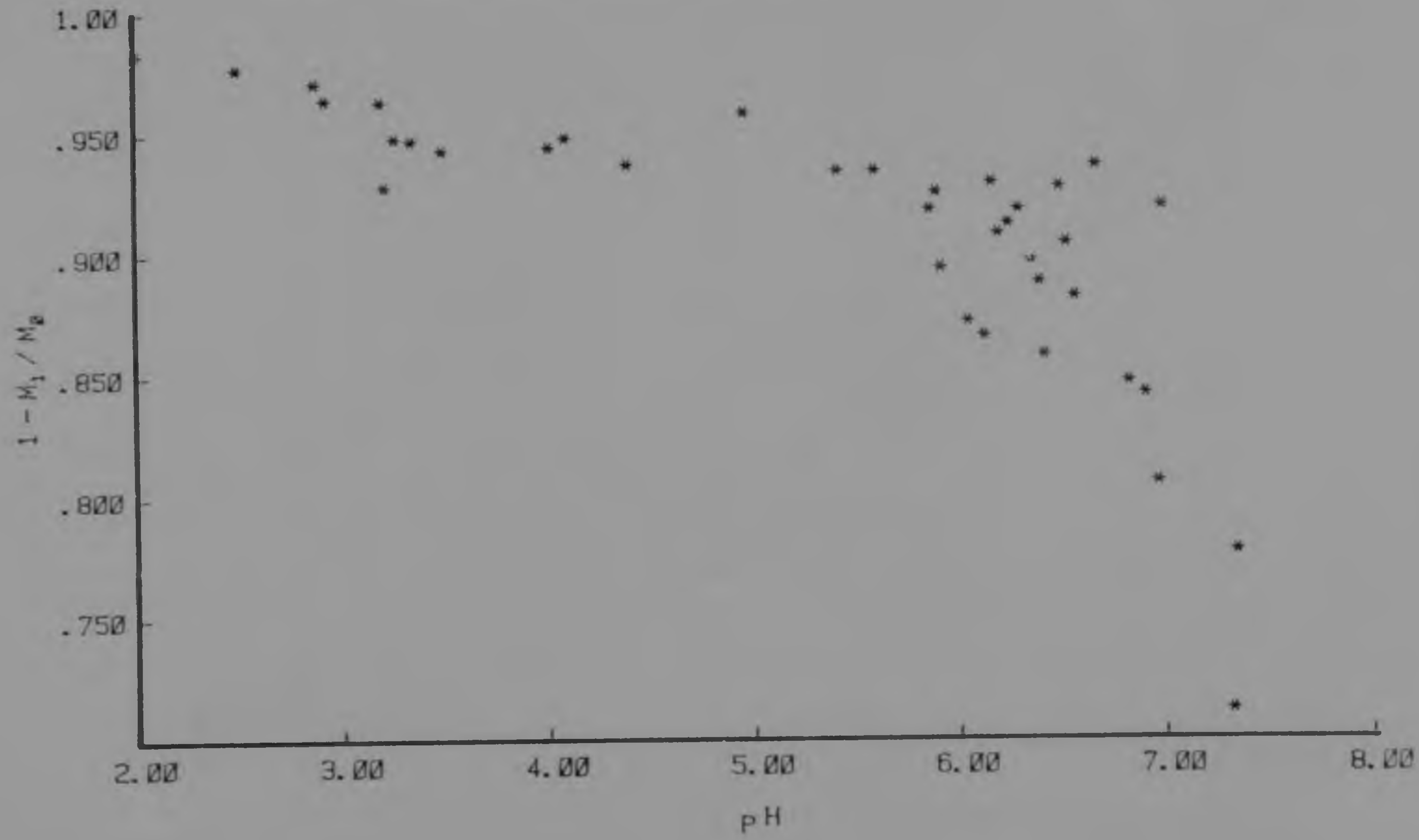

FIG.10.12: Particle Size Distributions

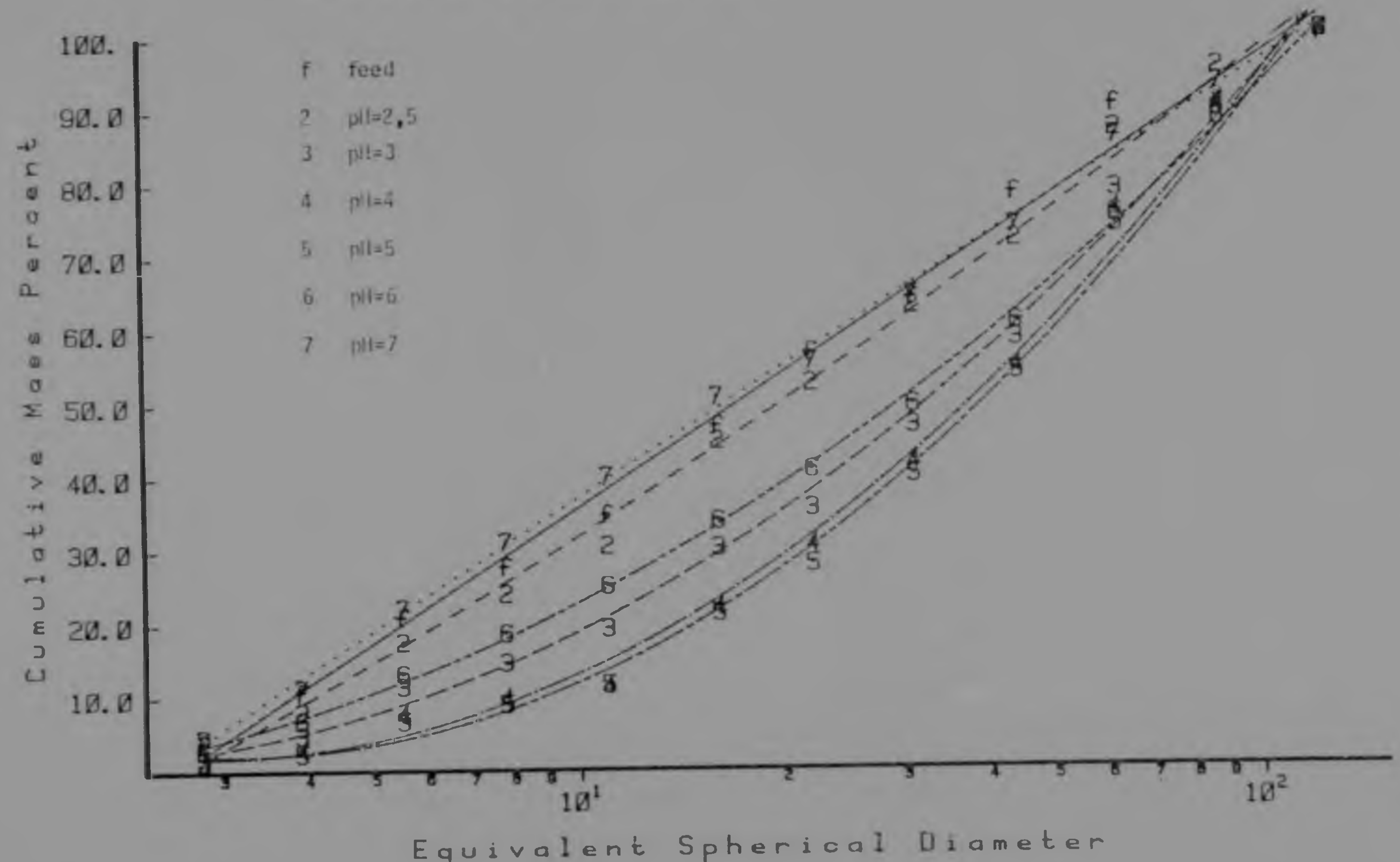

FIG.10.13: Variation of Mean Particle Size

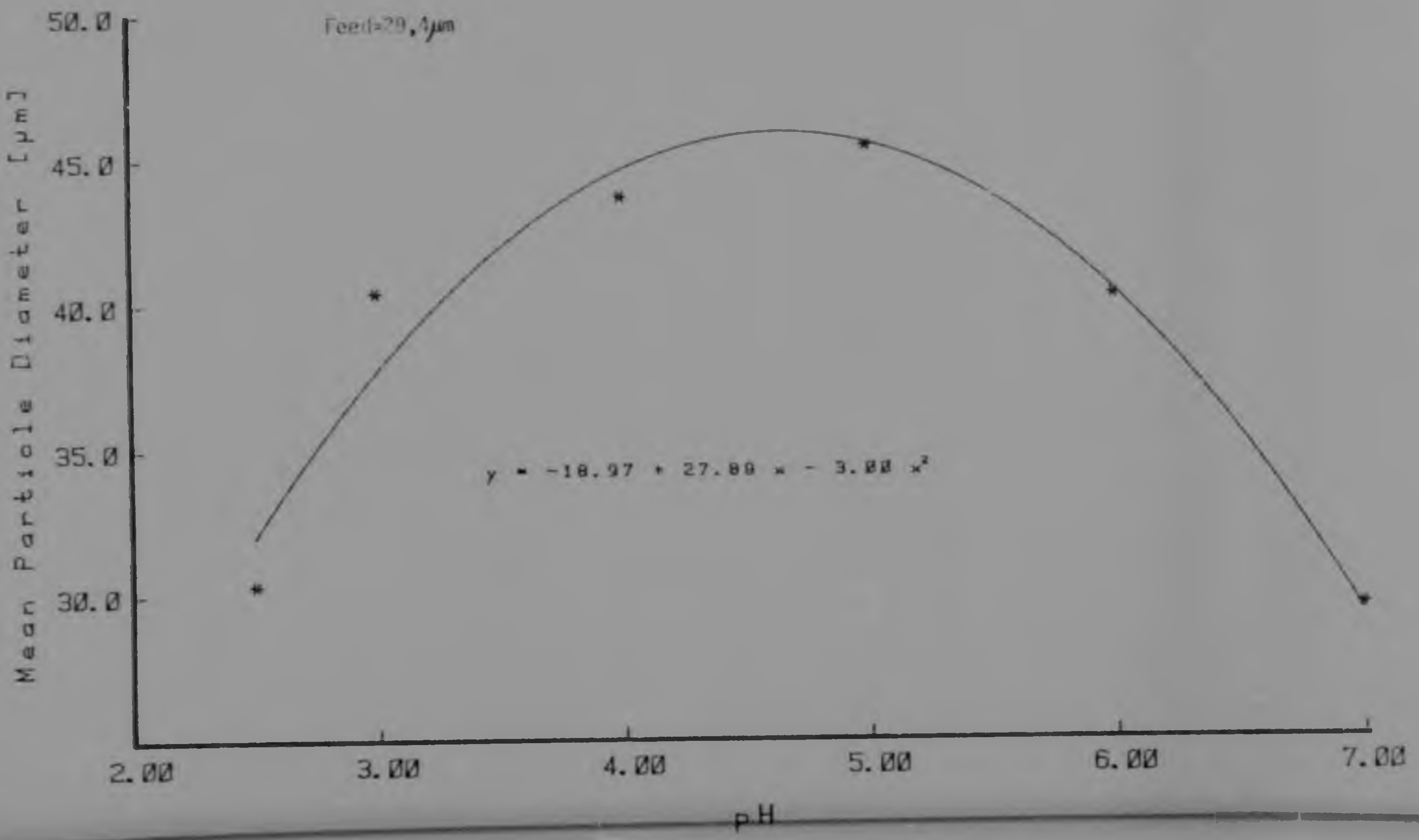

10.11 Calculation of t* from experimental Data for the Unreacted Core Shrinking Model

Example: For Run 1, pH=2,55

From Table 10.9, r_m = 12,77 mol/m^3min

$1 - M_1/M_o$ = 0,959

Now M is defined as the total mass of unreacted manganese per unit volume of fluid, i.e.

$$M = \frac{W_i g_i}{Q_i} \quad (10.39)$$

From Table 10.6

W_1 = 2,87 g/min , W_o = 18,97 g/min

g_1 = 0,146 , g_o = 0,54

Q_1 = 0,6014 l/min, Q_o = 0,5239 l/min

C_m = 27,0 g/l

therefore M = 0,696g/l

C_{ms} is calculated from equation (2.18) (as shown in Appendix 10.8)

therefore C_{ms} = 4,10 X 10^{10} g/l

l is calculated from equation (2.30), i.e.

$$l = (\text{volume of unreacted core})^{1/3}$$

From Figure 10.13, the relationship between the diameter of the unreacted particle and the pH is obtained, i.e.

$$y = -18,97 + 27,89x - 3,00x^2 \quad (10.40)$$

where x is the pH value and y the mean diameter in μm.

therefore $y = -18{,}97 + 27{,}89(2{,}55) - 3{,}00(2{,}55)^2$

$= 32{,}642\ \mu m$

$= 3{,}2642 \times 10^{-3}\ cm$

now $$v = \frac{\pi}{6} d^3 \qquad (10.41)$$

therefore $v = 1{,}82 \times 10^{-\text{[illegible]}}\ cm^3$

now $l = (v)^{1/3}$

$= 2{,}63 \times 10^{-3} cm$

Thus $\frac{M}{l}(C_{ms} - C_m) = 1{,}09 \times 10^{13}\ \frac{g^2}{cm\, l^2}$

From equation (6.2) it can be seen that a plot of $-r_m$ vs $M/l(C_{ms} - C_m)$ is a straight line passing through the origin. Hence the slope of this line, $k\phi/\rho_B$ is simply

$$\frac{-r_m - 0}{M/l(C_{ms} - C_m) - 0} \qquad (10.42)$$

whcih gives $\frac{k\phi}{\rho_B} = 1{,}18 \times 10^{-12}\ \frac{mol}{m^3 min}\ \frac{cm\, l^2}{g^2}$

Since $$t^* = 3\,\frac{\rho_B}{k\phi}\left(\frac{M_o}{M}\right)^{1/3} \frac{1}{C_{ms} - C_m} \qquad (6.3)$$

the only additional information required to calculate t^* is M_o. M_o is defined as

$$M_o = \frac{N_o q_o}{N_o} \qquad (10.43)$$

i.e. $M_0 = 19{,}554$ g/l

$$\text{therefore } t^* = 3\left(\frac{1}{1{,}18 \times 10^{-[illegible]}}\right)\left(\frac{19{,}554}{0{,}696}\right)^{1/3} \frac{2{,}63 \times 10^{-3}}{4{,}10 \times 10^{10}} \times \frac{1000}{54{,}938}$$

$$= 9{,}04 \text{ min}$$

(1000/54,938 converts the units from g/l to mol/m^3)

From equation (6,4)

$$\tau = \frac{V_1}{Q_1} = 23{,}28 \text{ min}$$

$$\frac{\tau}{t^*} = 2{,}57$$

Thus $1 - M_1/M_0$ versus τ/t^* can be plotted and compared with the theoretically predicted values. These values are given in Tables 10.13 - 10.15 below

Table 10.13

Comparison of the Theoretical and Experimental Values of the Unreacted Core Shrinking Model- Run 1

pH	τ/t^*	$1-M_1/M_0$ theoretical	$1-M_1/M_0$ experimental	% error
2,55	2,57	0,910	0,959	5,4
2,62	2,85	0,918	0,965	5,1
2,66	2,93	0,921	0,967	4,9
2,84	2,46	0,906	0,956	5,5
2,85	2,87	0,919	0,964	4,9
2,94	1,98	0,885	0,942	6,4
2,99	2,34	0,902	0,953	5,7
3,08	2,45	0,906	0,956	5,5

Table 10.13 continued

pH	τ/t^*	$1-M_1/M_0$	$1-M_1/M_0$	% error
3,25	2,13	0,395	0,951	6,2
3,39	2,14	0,893	0,950	6,4
3,48	1,63	0,864	0,924	7,0
3,75	2,07	0,8	0,949	6,6
4,02	1,99	0,836	0,947	6,9
4,10	1,68	0,867	0,933	7,6
4,30	1,56	0,858	0,924	7,7
4,60	1,85	0,878	0,943	7,4
4,80	1,42	0,846	0,918	8,5
5,10	1,74	0,871	0,938	7,6
5,23	1,80	0,875	0,938	7,2
5,25	1,32	0,836	0,906	8,4
5,50	1,55	0,857	0,930	8,5
5,60	1,79	0,875	0,939	7,4
5,70	1,19	0,821	0,898	9,4
5,34	0,99	0,791	0,864	9,2
6,05	1,42	0,846	0,915	8,1
6,13	1,31	0,835	0,906	8,5
6,17	0,98	0,789	0,863	9,3
6,18	1,17	0,818	0,8[illegible]	9,0
6,23	1,51	0,854	0,922	7,9
6,27	0,86	0,766	0,839	9,6
6,40	1,41	0,845	0,916	8,4
6,44	0,90	0,774	0,851	9,9
6,46	1,18	0,820	0,894	9,1

Table 10.13 continued

pH	τ/t^*	$1-M_1/M_0$ theoretical	$1-M_1/M_0$ experimental	% error
6,54	0,85	0,764	0,841	10,1
6,63	1,38	0,842	0,918	9,0
6,80	0,88	0,770	0,861	11,8
6,93	0,90	0,774	0,873	12,8
			mean % error :	7,8

The results above are plotted in Figure 10.14 and are presented in the main report as Figure 6.1.

Table 10.14

Comparison of Theoretical and Experimental Values of the Unreacted Core Shrinking Model - Run 2

pH	τ/t^*	$1-M_1/M_0$ theoretical	$1-M_1/M_0$ experimental	% error
7,05	0,58	0.684	0.774	13.2
7,10	0,70	0,725	0,826	14,0
7,20	0,59	0,687	0,776	12,9
7,26	0,72	0,731	0,831	13,7
7,31	0,59	0,687	0,773	12,5
7,35	0,64	0,706	0,805	14,1
7,40	0,48	0,639	0,721	12,9
7,42	0,67	0,716	0,816	14,0
7,50	0,31	0,525	0,594	13,1
7,70	0,27	0,488	0,575	17,9
			mean % error :	13,3

These results are plotted in Figure 10.15

Table 10.15

Comparison of Theoretical and Experimental Values of the Unreacted Core Shrinking Model - Run 3

pH	τ/t^*	$1-M_1/M_0$ theoretical	$1-M_1/M_0$ experimental	% error
2,01	4,11	0,942	0,983	4,4
2,50	3,36	0,930	0,977	5,1
2,88	3,00	0,922	0,971	5,3
2,93	2,51	0,908	0,964	6,2
3,20	2,40	0,904	0,963	6,5
3,22	1,55	0,857	0,928	8,2
3,27	1,99	0,886	[illegible]	9,5
3,35	2,09	0,891	,947	6,3
3,50	1,80	0,875	0,943	7,7
4,02	1,84	0,878	0,944	7,6
4,10	1,92	0,882	0,948	7,5
4,40	1,68	0,867	0,937	8,0
4,97	2,22	0,897	0,958	6,8
5,42	1,62	0,863	0,934	8,2
5,60	1.60	0,861	0,934	8,4
5,87	1,35	0,839	0,918	9,4
5,90	1,47	0,851	0,925	8,7
5,92	1,23	0,826	0,894	8,3
6,05	0,74	0,736	0,872	18,4
6,13	0,90	0,774	0,866	11,9
6,17	1,57	0,859	0,929	8,1

Table 10.15 continued

pH	τ/t*	$1-M_1/M_0$ theoretical	$1-M_1/M_0$ experimental	% error
6,20	1,14	0,814	0,908	11,5
6,25	1,32	0,836	0,912	9,1
6,30	1,28	0,832	0,918	10,4
6,36	1,15	0,816	0,897	10,0
6,40	1,01	0,794	0,888	11,3
6,42	0,85	0,764	0,858	12,4
6,50	1,51	0,854	0,927	8,5
6,53	1,14	0,814	0,904	11,0
6,57	1,05	0,801	0,882	10,1
6,68	1,55	0,857	0,936	9,2
6,83	0,85	0,764	0,847	10,9
6,91	0,76	0,742	0,842	13,5
6,97	0,67	0,716	0,806	12,6
7,00	1,28	0,832	0,919	10,5
7,32	0,45	0,622	0,712	14,5
7,35	0,58	0,684	0,777	13,7
			mean % error	9,5

These results are plotted in Figure 10.16

FIG. 10.14: Comparison of Theoretical and Experimental Values of the Unreacted Core Shrinking Model - Run 1

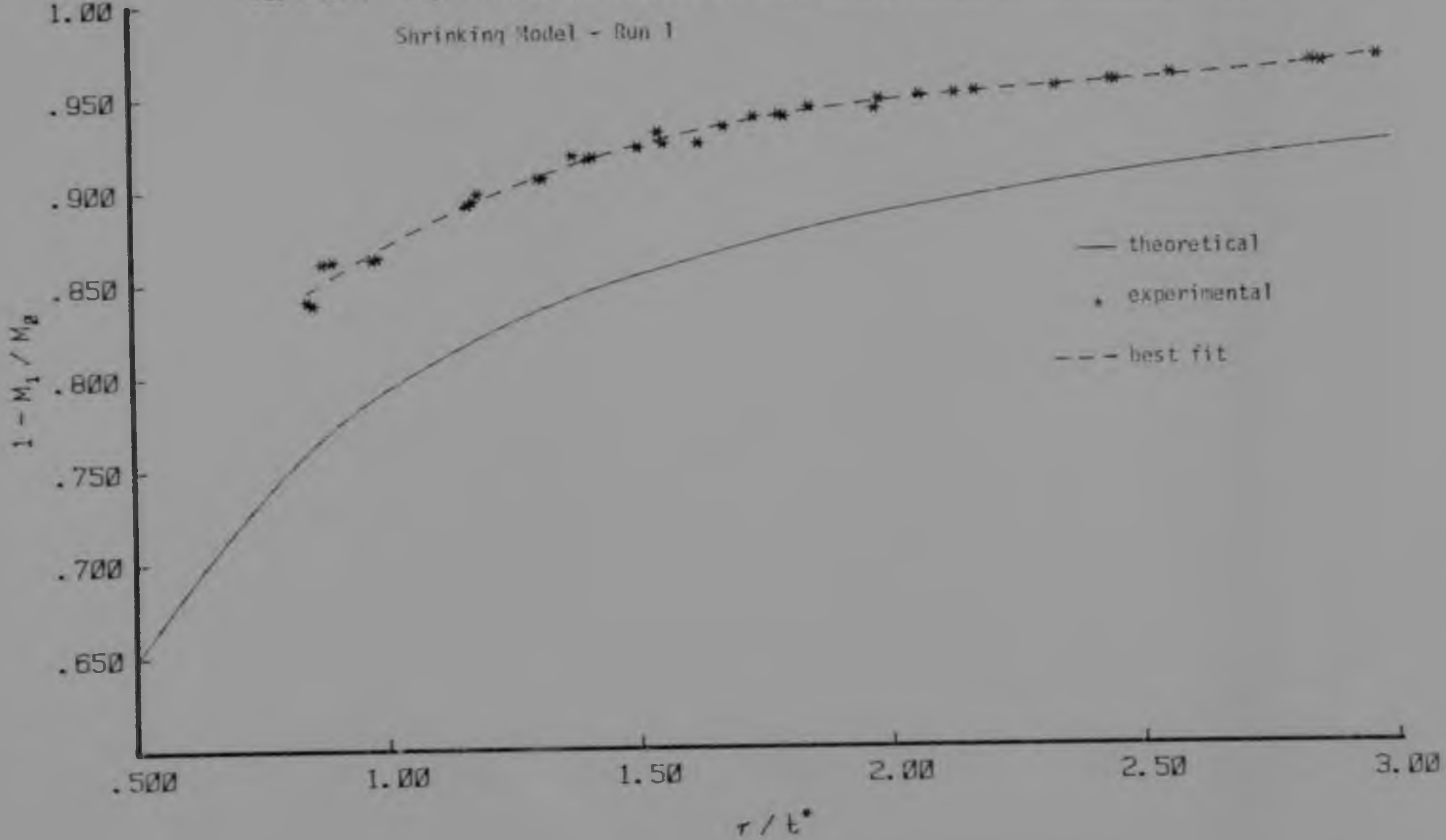

FIG.10.15: Comparison of Theoretical and Experimental Values of the Unreacted Core

Shrinking Model - Run 2

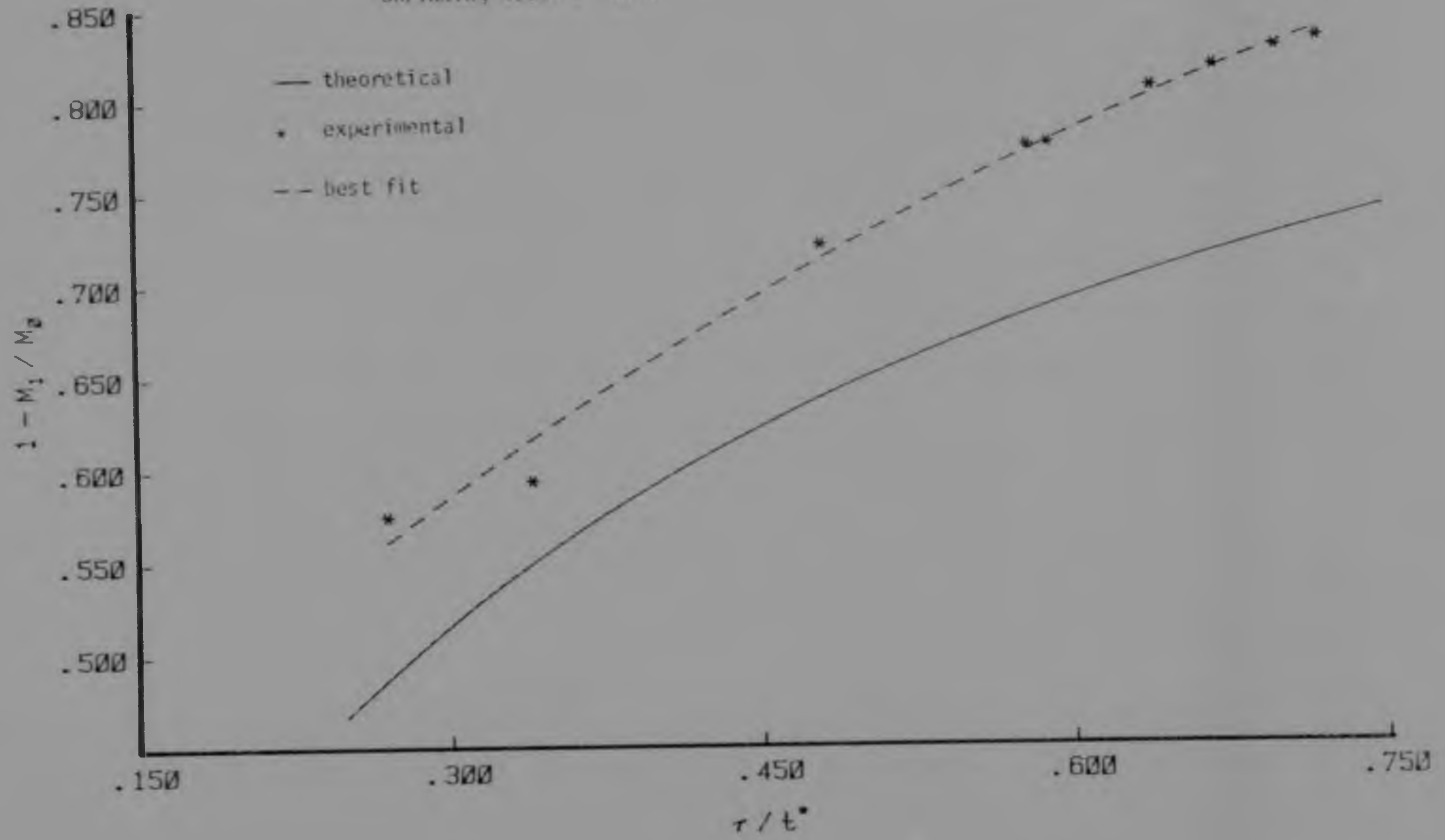

FIG.10.16: Comparison of Theoretical and Experimental Values of the Unreacted Core Shrinking Model - Run 3 .

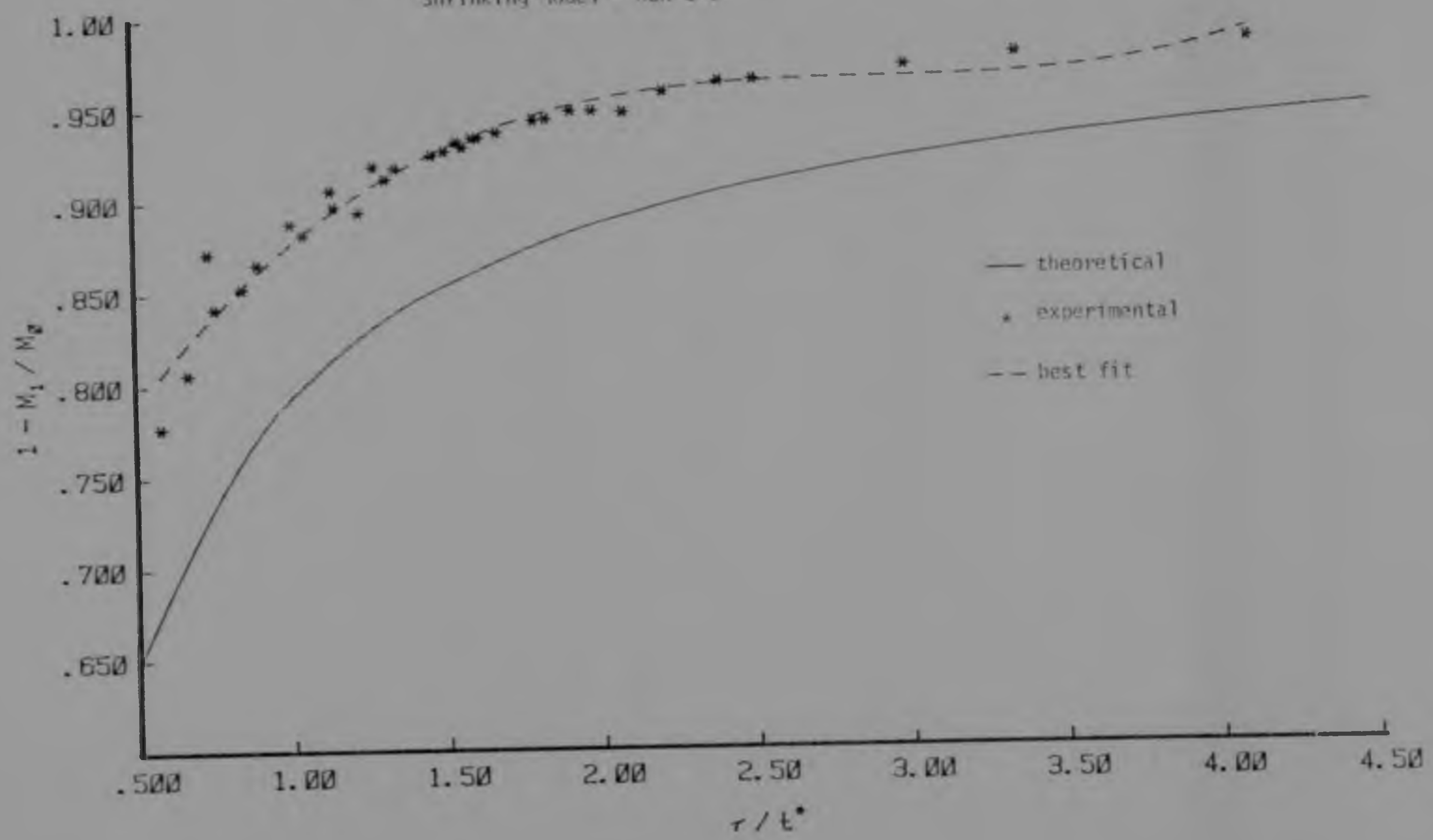

10.12 Calculation of λ from Experimental Data for the Porous Solid Model

Example: For Run 1, pH = 2,55

From Table 10.9, $r_m = 12{,}77\ \text{mol/m}^3\text{min}$

$$1 - M_1/M_o = 0{,}959$$

From Table 10.6

$$W_1 = 2{,}87\ \text{g/min}$$

$$q_1 = 0{,}146$$

$$Q_1 = 0{,}6014\ \text{l/min}$$

$$C_m = 27{,}0\ \text{g/l}$$

Equation (12.39) i.e.

$$M = \frac{W_1 q_1}{Q_1}$$

gives $M = 0{,}696$ g/l

C_{ms} is calculated from equation (2.18) (as shown in Appendix 10.8)

therefore $C_{ms} = 4{,}10 \times 10^{10}$ g/l

Since a plot of $-r_m$ versus $M(C_{ms} - C_m)$ is a straight line passing through the origin, the slope kp/ρ_B is simply

$$\frac{-r_m - 0}{M(C_{ms} - C_m) - 0} \qquad (10.44)$$

i.e.

$$\frac{kp}{\rho_B} = 4{,}48 \times 10^{-10}\ \frac{\text{mol}}{\text{m}^3\text{min}}\ \frac{\text{l}^2}{\text{g}^2}$$

Now, from equation (2.40) i.e.

$$\lambda = \frac{kp}{\rho_B}(C_{ms} - C_m)$$

$$\lambda = 4{,}48 \times 10^{-10} \; (4{,}10 \times 10^{10})$$

$$\lambda = 18{,}35 \; \frac{mol}{m^3 \, min} \; \frac{1}{g}$$

$$= 1{,}01 \; min^{-1}$$

From equation (6.4)

$$\tau = \frac{V_1}{Q_1} = 23{,}28 \; min$$

$$\therefore \lambda.\tau = 23{,}48$$

Thus, the fractional leach efficiency, $1 - M_1/M_0$, can be plotted against $\lambda\tau$ and compared with theoretically predicted values. These values are given in Tables 10.16 - 10.18 below.

Table 10.16

Comparison of the Theoretical and Experimental Values of the Porous Solid Model - Run 1

pH	λ min^{-1}	$\lambda\tau$	$1-M_1/M_0$ theoretical	$1-M_1/M_0$ experimental	% error
2,55	1,01	23,48	0,959	0,959	0,0
2,62	1,20	27,59	0,965	0,965	0,0
2,66	1,20	28,94	0,967	0,967	0,0
2,84	0,89	21,76	0,956	0,956	0,0
2,85	1,07	26,97	0,964	0,964	0,0
2,94	0,68	16,30	0,942	0,942	0,0
2,99	0,80	20,25	0,953	0,953	0,0
3,08	0,84	21,71	0,956	0,956	0,0
3,25	0,84	19,50	0,951	0,951	0,0
3,39	0,81	19,07	0,950	0,950	0,0
3,48	0,46	12,23	0,924	0,924	0,0

Table 10.16 continued

pH	λ min^{-1}	$\lambda\tau$	$1-M_1/M_0$ theoretical	$1-M_1/M_0$ experimental	% error
3,75	0,79	18,79	0,950	0,949	-0,1
4,02	0,71	17,70	0,947	0,947	0,0
4,10	0,54	13,95	0,933	0,933	0,0
4,30	0,42	12,16	0,924	0,924	0,0
4,60	0,63	16,42	0,943	0,943	0,0
4,80	0,42	11,19	0,918	0,918	0,0
5,10	0,53	15,23	0,938	0,938	0,0
5,23	0,51	15,21	0,938	0,938	0,0
5,25	0,44	[illegible]	0,910	0,906	-0,4
5,50	0,50	13,19	0,930	0,930	0,0
5,60	0,53	15,42	0,939	0,939	0,0
5,70	0,33	8,85	0,898	0,898	0,0
5,94	0,20	6,34	0,864	0,864	0,0
6,05	0,34	10,72	0,915	0,915	0,0
6,13	0,30	9,62	0,906	0,906	0,0
6,17	0,19	6,32	0,863	0,863	0,0
6,18	0,27	8,28	0,829	0,802	0,0
6,23	0,37	11,89	0,922	0,922	0,0
6,27	0,15	5,22	0,839	0,839	0,0
6,40	0,35	10,96	0,916	0,916	0,0
6,44	0,17	5,73	0,851	0,851	0,0
6,46	0,26	8,46	0,894	0,894	0,0
6,54	0,15	5,27	0,841	0,841	0,0
6,63	0,35	11,15	0,918	0,918	0,0

Table 10.16 continued

pH	λ min^{-1}	$\lambda\tau$	$1-M_1/M_o$ theoretical	$1-M_1/M_o$ experimental	% error
6,80	0,13	6,17	0,861	0,861	0,0
6,93	0,18	6,85	0,873	0,873	0,0
				mean % error:	-0,01

These results are plotted on Figure 10.17

Table 10.17

Comparison of the Theoretical and Experimental Values of the Porous Solid Model- Run 2.

pH	λ min^{-1}	$\lambda\tau$	$1-M_1/M_o$ theoretical	$1-M_1/M_o$ experimental	% error
7,05	0,14	3,42	0,774	0,774	0,0
7,10	0,23	4,75	0,826	0,826	0,0
7,20	0,14	3,47	0,776	0,776	0,0
7,26	0,23	4,92	0,831	0,831	0,0
7,31	0,13	3,41	0,773	0,773	0,0
7,35	0,19	4,14	0,805	0,305	0,0
7,40	0,09	2,58	0,721	0,721	0,0
7,42	0,20	4,44	0,816	0,816	0,0
7,50	0,05	1,46	0,593	0,594	0,2
7,70	0,06	1,35	0,574	0,575	0,2
				mean % error	0,[illegible]

These results are plotted on Figure 10.18.

Table 10.18

Comparison of Theoretical and Experimental Values for the Porous Solid Model - Run 3

pH	λ min^{-1}	λt	$1-M_t/M_o$ theoretical	$1-M_t/M_o$ experimental	% error
2,01	4,47	56,52	0,983	0,983	0,0
2,50	3,26	42,02	0,977	0,977	0,0
2,88	2,37	34,05	0,971	0,971	0,0
2,93	1,86	26,61	0,964	0,964	0,0
3,20	1,86	25,72	0,963	0,963	0,0
3,22	0,83	12,83	0,928	0,928	0,0
3,27	1,17	13,37	0,948	0,948	0,0
3,35	0,93	17,91	0,947	0,947	0,0
3,50	1,11	16,40	0,943	0,943	0,0
4,02	1,15	16,72	0,944	0,944	0,0
4,10	1,22	18,20	0,948	0,948	0,0
4,40	0,99	14,05	0,937	0,937	0,0
4,97	1,55	22,90	0,958	0,958	0,0
5,42	0,93	14,10	0,934	0,934	0,0
5,60	0,95	14,10	0,934	0,934	0,0
5,87	0,74	11,23	0,918	0,918	0,0
5,90	0,75	12,28	0,926	0,925	0,0
5,92	0,39	8,41	0,894	0,894	0,0
6,05	0,22	4,61	0,822	0,872	6,1
6,13	0,33	6,46	0,866	0,866	0,0
6,17	0,59	13,04	0,929	0,929	0,0

Table 10.18 continued

pH	λ min^{-1}	$\lambda\tau$	$1-M_1/M_0$ theoretical	$1-M_1/M_0$ experimental	% error
6,20	0,57	9,21	0,902	0,908	0,7
6,25	0,45	10,35	0,912	0,912	0,0
6,30	0,63	11,19	0,918	0,918	0,0
6,36	0,38	8,68	0,897	0,897	0,0
6,40	0,42	7,89	0,888	0,888	0,0
6,42	0,31	6,07	0,859	0,858	-0,1
6,50	0,55	12,7[illegible]	0,927	0,927	0,0
6,53	0,50	9,40	0,904	0,904	0,0
6,57	0,31	7,47	0,882	0,882	0,0
6,68	0,77	14,60	0,936	0,936	0,0
6,83	0,23	5,54	0,847	0,847	0,0
6,91	0,23	5,33	0,842	0,842	0,0
6,97	0,18	4,18	0,807	0,806	-0,1
7,00	0,58	11,38	0,919	0,919	0,0
7,32	0,10	2,47	0,712	0,712	0,0
7,32	0,14	3,48	0,777	0,777	0,0
				mean % error	0,2

These results are plotted on Figure 10.19

FIG. 10.17: Comparison of Theoretical and Experimental Values of the Porous Solid Model - Run 1

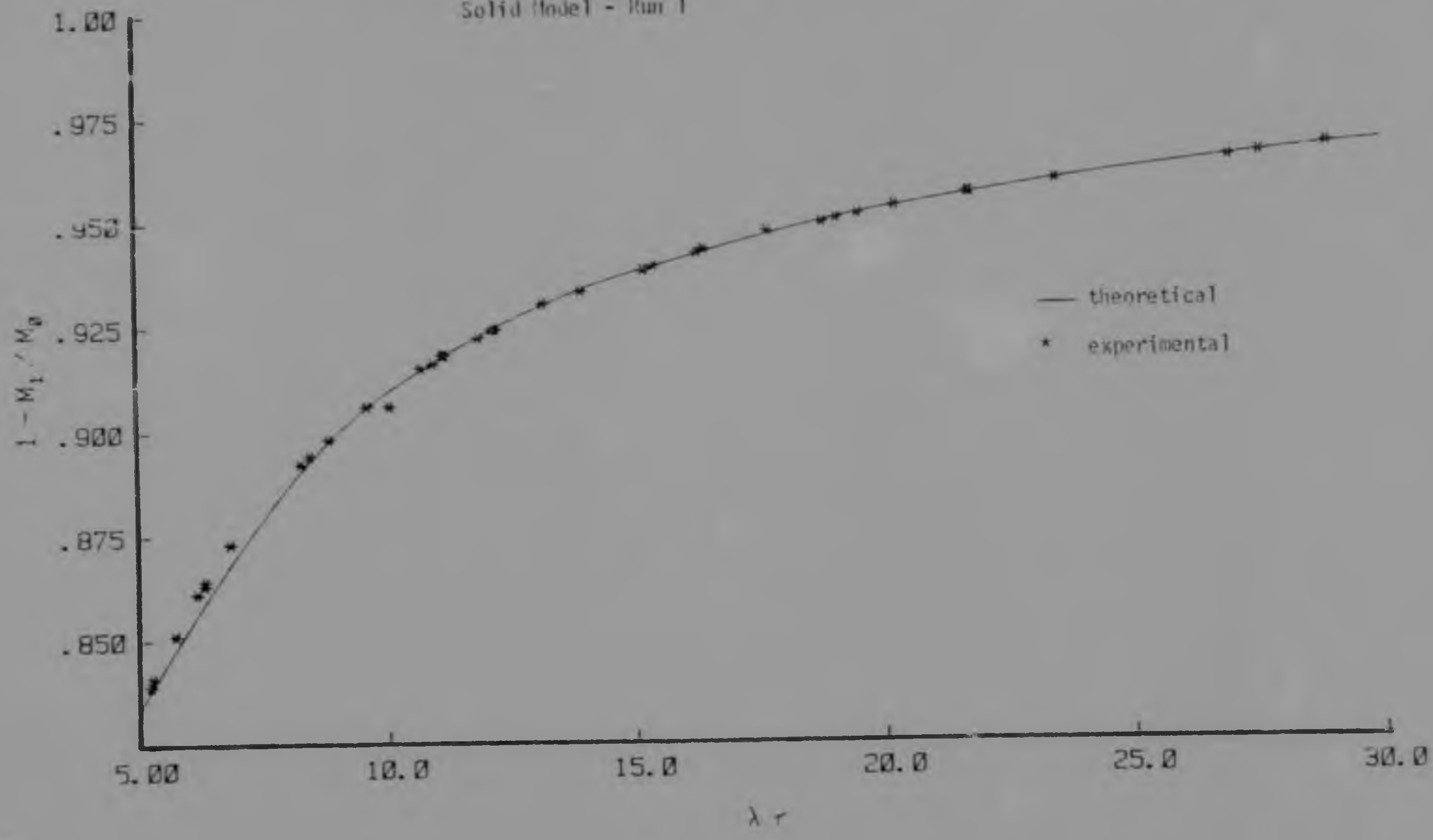

FIG. 10.18: Comparison of Theoretical and Experimental Values of the Porous Solid Model - Run 2

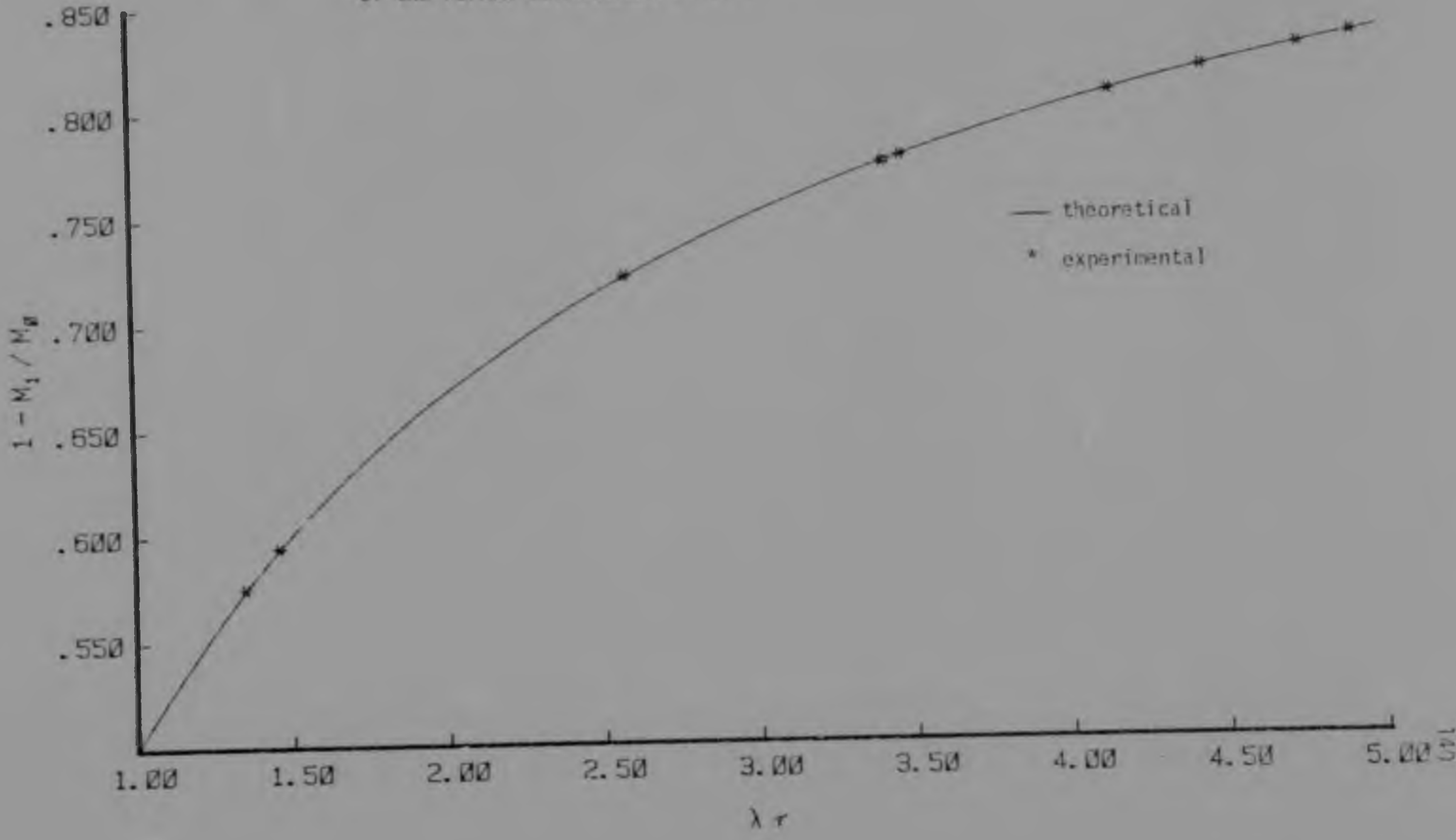

FIG. 10.19: Comparison of Theoretical and Experimental Values of the Porous Solid Model - Run 3

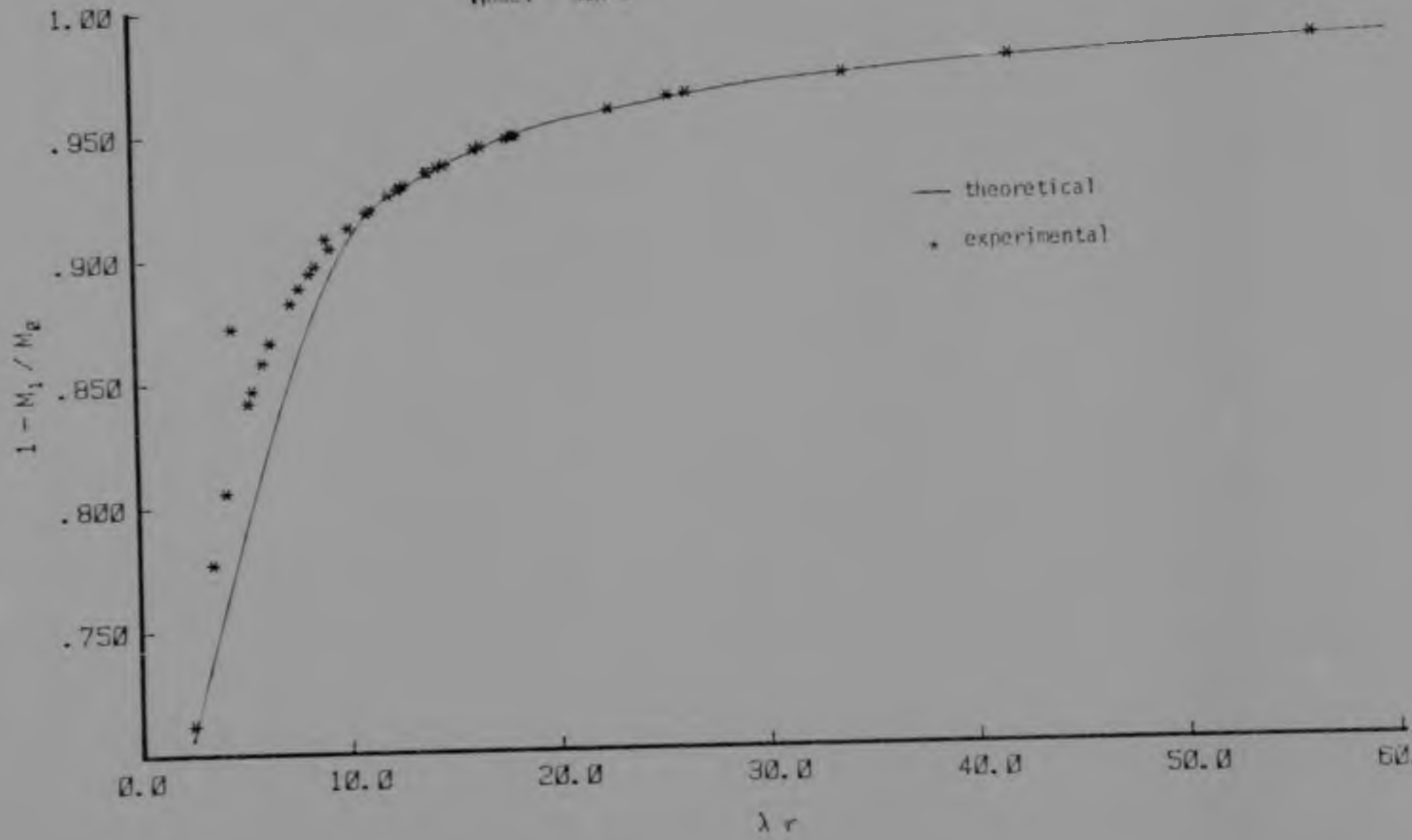

10.13 Relationship between r, M and C_m

From equation (10.39), i.e.

$$M = \frac{W_1 g_1}{Q_1}$$

and equation (10.36), i.e.

$$W_o g_o + C_o Q_o = W_1 g_1 + C_1 Q_1$$

it is found that

$$W_1 g_1 = W_o g_o + C_o Q_o - C_1 Q_1$$

or

$$\frac{W_1 g_1}{Q_1} = \frac{W_o g_o + C_o Q_o - C_1 Q_1}{Q_1}$$

i.e.

$$M = \frac{W_o g_o}{Q_1} + \frac{Q_o}{Q_1} C_o - C_1 \qquad (10.45)$$

But since

$$r = \frac{Q_1}{V_1} (C_1 - \frac{Q_o}{Q_1} C_o) \qquad (2.43)$$

this gives

$$M \frac{Q_1}{V_1} = \frac{W_o g_o}{Q_1} \frac{Q_1}{V_1} + \frac{Q_1}{V_1} (C_1 - \frac{Q_o}{Q_1} C_o)$$

or

$$M \frac{Q_1}{V_1} = \frac{W_o g_o}{Q_1} + r$$

therefore

$$r = \frac{W_o g_o}{Q_1} - \frac{M}{\tau} \qquad (10.46)$$

where

$$\tau = \frac{V_1}{Q_1}$$

Thus, r versus M/τ can be plotted for each of the experimental runs and the theoretical and experimental values compared for the slope and the intercept. (The theoretical value of the slope is in all cases -1 and the intercept $V_0 q_0/V_1$). This comparison is given in Table 10.19

Table 10.19

Comparison of Theoretical and Experimental Values of the Slope and intercept

Run no.	Slope		Intercept	
	Theoretical	Experimental	Theoretical	Experimental
1	-1,00	-1,00	13,32	13,32
2	-1,00	-1,00	20,36	20,36
3	-1,00	-1,00	23,73	23,75

(see Figures 10.20 - 10.22)

FIG.10.20: Experimental Leaching Rates - Run 1

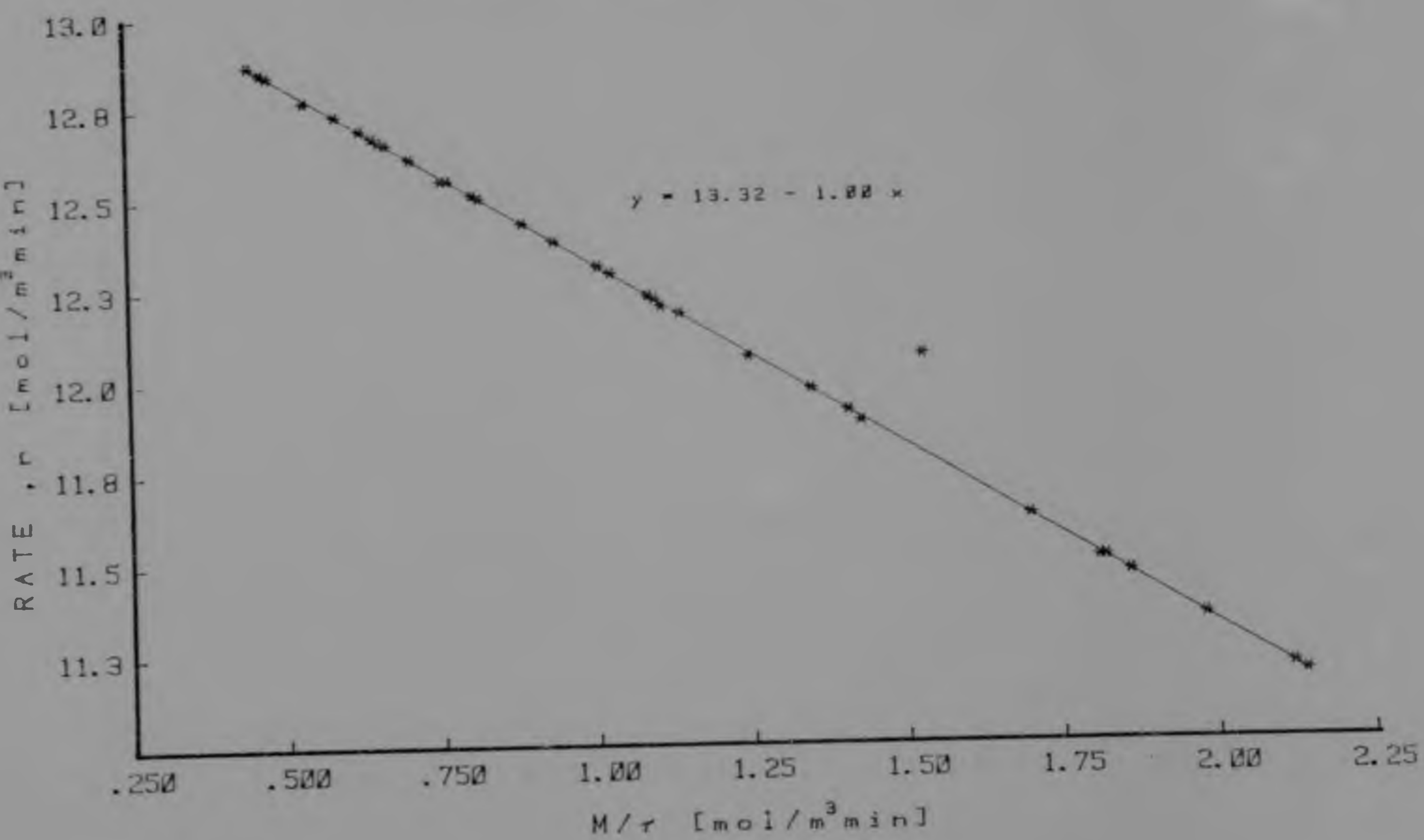

FIG.10.21: Experimental Leaching Rates - Run 2

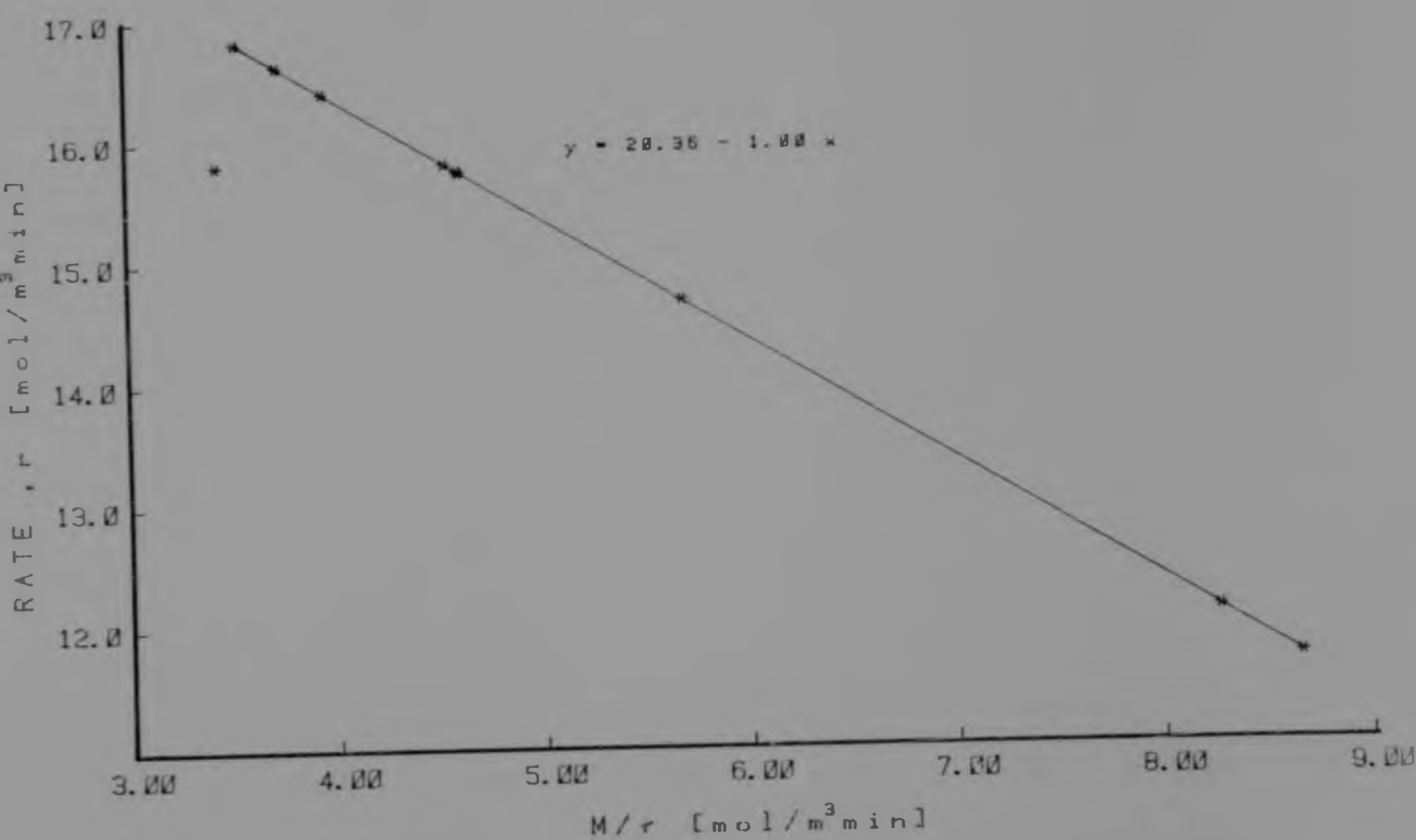

FIG.10.22: Experimental Leaching Rates - Run 3

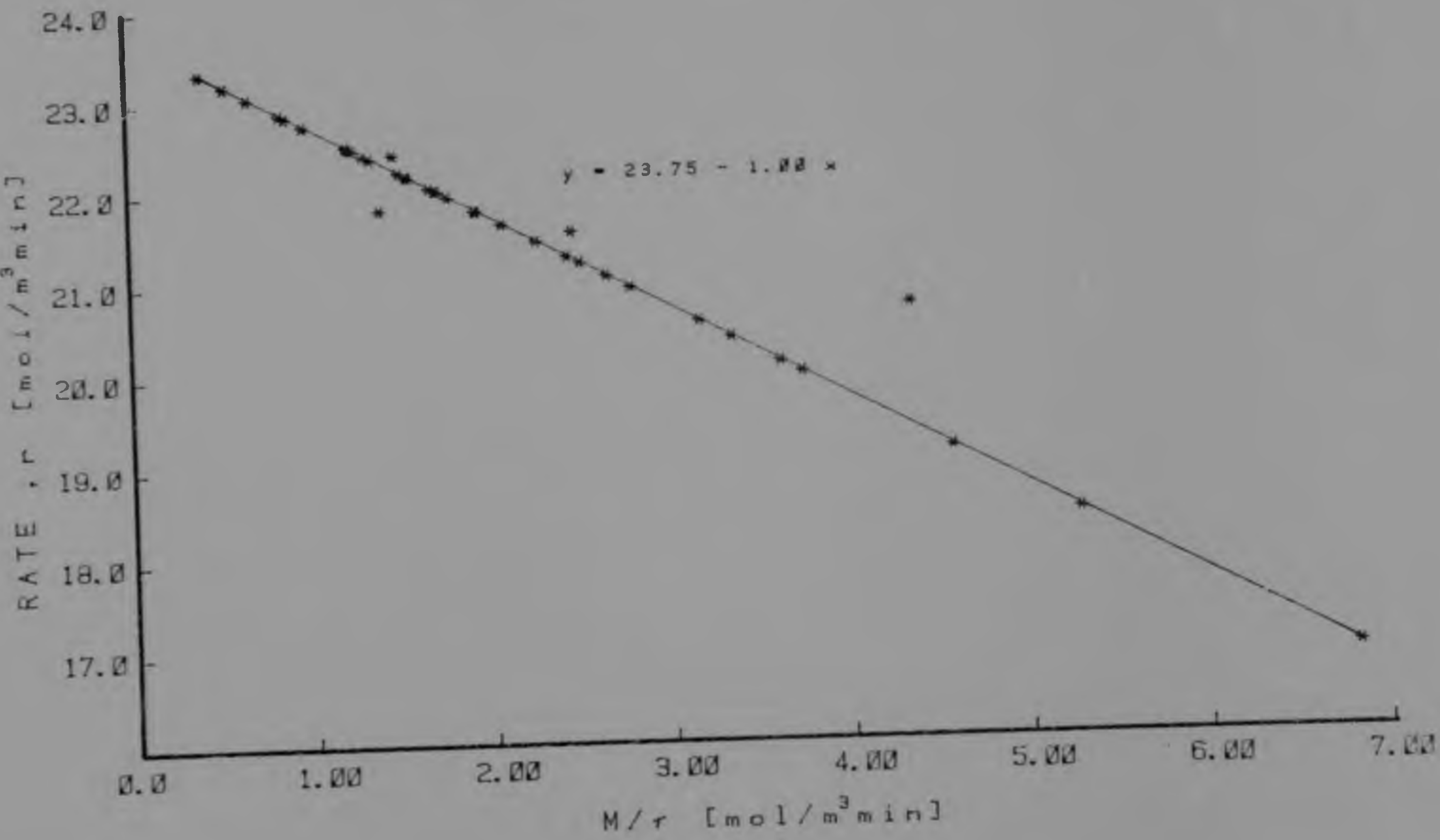

10.14 Leaching of the Minor Elements

The results of the continuous leaching experiments for each of the minor elements are given in Tables 10.20 - 10.22.

Table 10.20

Leaching of the Minor Elements - Run 1

pH	Iron		Silicon		Zinc		Cobalt		Nickel	
	Liquid (ppm)	Solid (%)	Liquid (ppm)	Solid (%)	Liquid (ppm)	Solid (ppm)	Liquid (ppm)	Solid (ppm)	Liquid (ppm)	Solid (ppm)
2,55	1080	32,1	610	5,9	7,9	185	8,0	41	10,0	22
2,62	1195	35,9	710	5,3	11,3	338	8,3	31	11,1	15
2,66	1250	35,4	970	5,4	11,1	147	8,5	47	11,3	21
2,84	871	22,9	610	8,9	8,1	173	8,2	39	10,3	22
2,85	991	31,7	750	6,5	7,3	232	8,5	39	10,5	23
2,94	827	31,6	450	6,5	8,4	180	7,8	44	10,5	22
2,99	870	34,3	940	6,2	11,0	187	8,7	45	11,8	20
3,08	828	29,1	520	7,8	7,3	[illegible]	8,3	42	10,3	22
3,25	699	27,8	350	8,0	7,5	230	7,4	41	9,9	19
3,39	666	29,0	460	7,5	7,5	375	7,5	37	10,0	20
3,43	870	29,2	460	7,6	11,0	239	8,6	48	11,4	18
3,75	585	27,5	240	9,5	5,2	475	7,3	38	9,9	18

Table 10.20 continued

pH	Iron		Silicon		Zinc		Cobalt		Nickel	
	Liquid (ppm)	Solid (%)	Liquid (ppm)	Solid (%)	Liquid (ppm)	Solid (ppm)	Liquid (ppm)	Solid (ppm)	Liquid (ppm)	Solid (ppm)
4,02	600	27,4	290	9,4	6,4	336	7,5	66	9,9	20
4,10	632	29,8	220	6,9	6,5	290	7,6	41	9,9	23
4,30	737	28,3	190	8,8	9,2	306	8,3	40	11.1	18
4,60	570	26,8	250	9,3	6,2	348	7,5	39	10,0	19
4,30	615	24,6	190	8,6	5,7	395	7,4	43	9,9	17
5,10	537	25,6	150	10,2	4,8	440	7,3	40	9,8	19
5,23	657	26,2	84	9,7	5,4	806	8,2	39	11,2	17
5,25	556	23,1	90	8,1	4,7	378	7,3	38	9,6	16
5,50	417	24,7	87	9,7	3,8	469	7,3	42	9,7	20
5,60	542	26,3	74	9,1	6,6	517	8,0	49	11,0	17
5,70	327	23,6	68	9,8	3,3	456	7,2	41	9,6	20
5,94	345	24,7	45	9,0	2,3	524	8,0	52	10,1	27
6,05	389	23,9	45	9,3	2,4	559	8,3	52	10,3	28

Table 10.20 continued

pH	Iron Liquid (ppm)	Iron Solid (%)	Silicon Liquid (ppm)	Silicon Solid (%)	Zinc Liquid (ppm)	Zinc Solid (ppm)	Cobalt Liquid (ppm)	Cobalt Solid (ppm)	Nickel Liquid (ppm)	Nickel Solid (ppm)
6,13	127	23,1	35	8,7	1,8	541	7,8	63	10,0	34
6,17	73	23,3	30	8,5	1,5	561	7,6	66	9,8	32
6,18	29	22,6	38	9,0	1,6	605	8,0	66	10,8	22
6,25	28	24,2	50	9,4	1,7	586	8,0	64	10,1	35
6,27	35	22,9	15	8,2	1,9	470	7,7	74	10,0	34
6,40	61	25,6	15	8,0	2,2	560	7,6	59	10,0	37
6,44	38	22,6	15	8,8	2,2	446	7,5	76	9,7	40
6,46	35	24,3	15	8,8	3,3	585	8,4	45	11,2	32
6,54	27	23,1	14	8,3	3,3	553	8,2	68	11,0	34
6,63	22	21,9	14	7,5	2,6	500	7,3	76	9,9	37
6,80	11	21,8	11	7,8	3,1	415	6,9	80	9,7	33
6,93	12	20,3	9	7,2	4,2	317	7,1	90	10,0	29

Table 10.21

Leaching of the Minor Elements - Run 2

pH	Iron		Silicon		Zinc		Cobalt		Nickel	
	Liquid (ppm)	Solid (%)	Liquid (ppm)	Solid (%)	Liquid (ppm)	solid (ppm)	Liquid (ppm)	Solid (ppm)	Liquid (ppm)	Solid (ppm)
7,05	139	20,3	23	8,5	2,7	303	5,8	82	6,5	25,7
7,10	141	22,2	48	9,2	1,7	412	5,[illegible]	61	5,6	21,0
7,20	94	19,6	21	8,0	3,4	274	5,8	87	6,7	24,5
7,26	93	22,4	30	9,1	1,5	412	5,8	60	5,8	21,2
7,31	87	18,9	21	7,7	4,2	227	5,6	103	6,8	26,4
7,35	83	22,1	29	9,1	1,7	396	5,7	60	5,6	20,2
7,40	38	18,2	17	7,3	4,6	214	5,3	100	6,7	27,3
7,42	32	22,0	20	9,1	[illegible]	417	5,8	63	5,7	20,1
7,50	28	13,2	17	5,2	5,4	145	5,0	92	6,5	20,6
7,70	30	10,6	17	4,1	5,5	116	4,3	86	6,0	18,3

Table 10.22

Leaching of the Minor Elements - Run 3

PH	Iron Liquid (ppm)	Iron Solid (%)	Silicon Liquid (ppm)	Silicon Solid (%)	Zinc Liquid (ppm)	Zinc Solid (ppm)	Cobalt Liquid (ppm)	Cobalt Solid (ppm)	Nickel Liquid (ppm)	Nickel Solid (ppm)
2,01	948	36,4	797	4,9	7,8	110	7,0	27	9,3	15
2,50	925	33,3	678	5,3	7,7	151	6,9	33	9,1	16
2,88	748	29,1	557	6,4	5,1	212	6,7	43	7,3	22
2,93	703	31,2	545	6,9	7,4	208	7,3	34	9,4	16
3,20	652	28,6	340	8,1	6,3	266	7,0	42	9,1	18
3,22	679	26,5	384	6,8	5,0	244	7,2	43	8,5	19
3,27	883	31,0	410	8,4	8,6	565	8,7	53	11,0	51
3,35	1210	31,1	380	9,1	11,1	278	10,2	71	12,9	56
3,50	629	26,9	192	8,2	3,8	390	6,9	45	8,1	18
4,02	591	26,2	149	8,3	3,3	384	6,8	43	8,0	18
4,10	598	26,2	175	8,2	4,0	325	6,8	44	8,0	20
4,40	583	25,7	183	8,1	4,4	298	6,9	41	8,1	15
4,97	593	26,4	180	9,7	4,0	576	7,2	44	9,3	21

Table 10.22 continued

pH	Iron Liquid (ppm)	Iron Solid (%)	Silicon Liquid (ppm)	Silicon Solid (%)	Zinc Liquid (ppm)	Zinc Solid (ppm)	Cobalt Liquid (ppm)	Cobalt Solid (ppm)	Nickel Liquid (ppm)	Nickel Solid (ppm)
5,42	573	23,9	125	8,2	3,5	339	7,0	49	8,1	18
5,60	430	24,2	110	9,7	3,8	447	7,1	45	9,2	19
5,87	308	24,2	60	9,4	2,4	471	6,9	51	8,9	19
5,90	438	23,5	46	8,7	1,9	370	6,7	41	7,1	17
5,92	482	25,3	63	9,5	4,5	480	6,9	75	12,3	56
6,05	522	25,2	26	9,6	2,5	658	6,[illegible]	79	12,0	62
6,13	468	25,5	41	8,9	2,7	712	6,1	71	10,3	56
6,17	155	24,6	8	9,8	2,3	816	9,5	73	11,6	67
6,20	148	23,8	33	8,7	2,7	527	7,9	69	9,4	64
6,25	80	19,6	9	13,8	1,4	1320	7,6	50	11,6	38
6,30	77	22,6	33	7,6	1,5	374	6,1	71	6,9	30
6,36	73	24,6	13	9,4	1,5	617	6,3	74	11,6	64
6,40	44	21,9	27	7,6	1,8	314	6,1	71	7,0	26
6,42	42	23,5	20	8,3	2,3	643	8,1	102	10,8	73

Table 10.22 continued

pH	Iron Liquid (ppm)	Iron Solid (%)	Silicon Liquid (ppm)	Silicon Solid (%)	Zinc Liquid (ppm)	Zinc Solid (ppm)	Cobalt Liquid (ppm)	Cobalt Solid (ppm)	Nickel Liquid (ppm)	Nickel Solid (ppm)
6,50	23	23,3	8	25,0	0,6	692	8,4	69	10,9	45
6,53	27	21,2	8	7,1	2,2	307	6,0	74	6,9	25
6,57	22	22,6	10	18,1	0,7	635	5,6	140	10,6	84
6,68	20	21,9	17	8,0	2,1	374	7,0	65	8,2	28
6,83	7	21,5	10	8,0	1,3	554	5,2	174	9,1	110
6,91	4	22,3	22	7,7	2,1	660	6,8	142	9,5	92
6,97	17	20,5	23	10,1	1,0	480	6,0	181	9,7	83
7,00	9	20,5	14	7,0	3,0	280	6,3	83	8,9	28
7,32	7	19,1	29	7,1	0,6	349	6,2	163	10,0	58
7,35	8	19,5	8	11,1	0,5	474	4,7	213	9,4	83

The above results are presented graphically below in Figures 10.23 - 10.37.

FIG.10.23: Leaching of Iron - Run 1

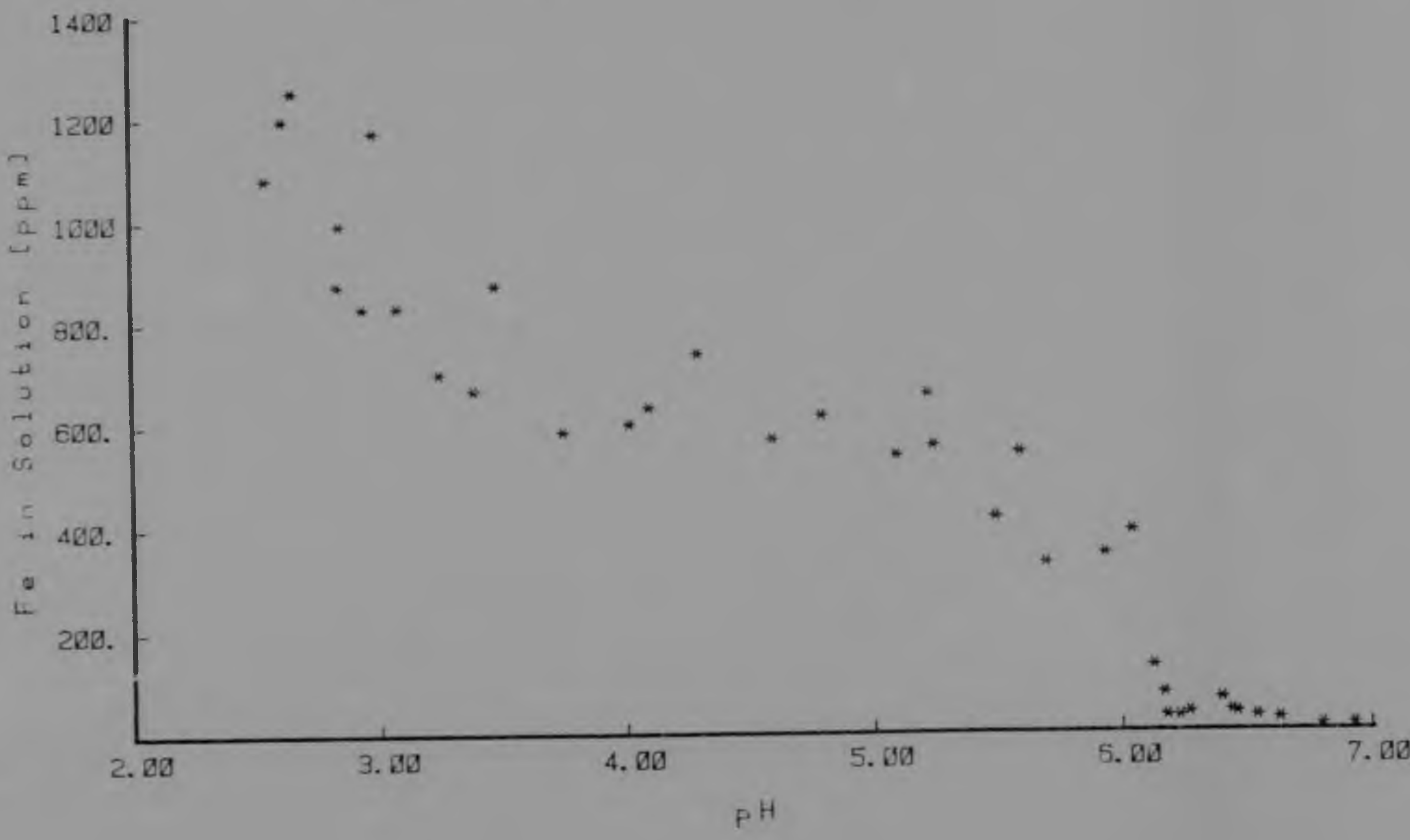

FIG.10.24: Leaching of Iron - Run 2

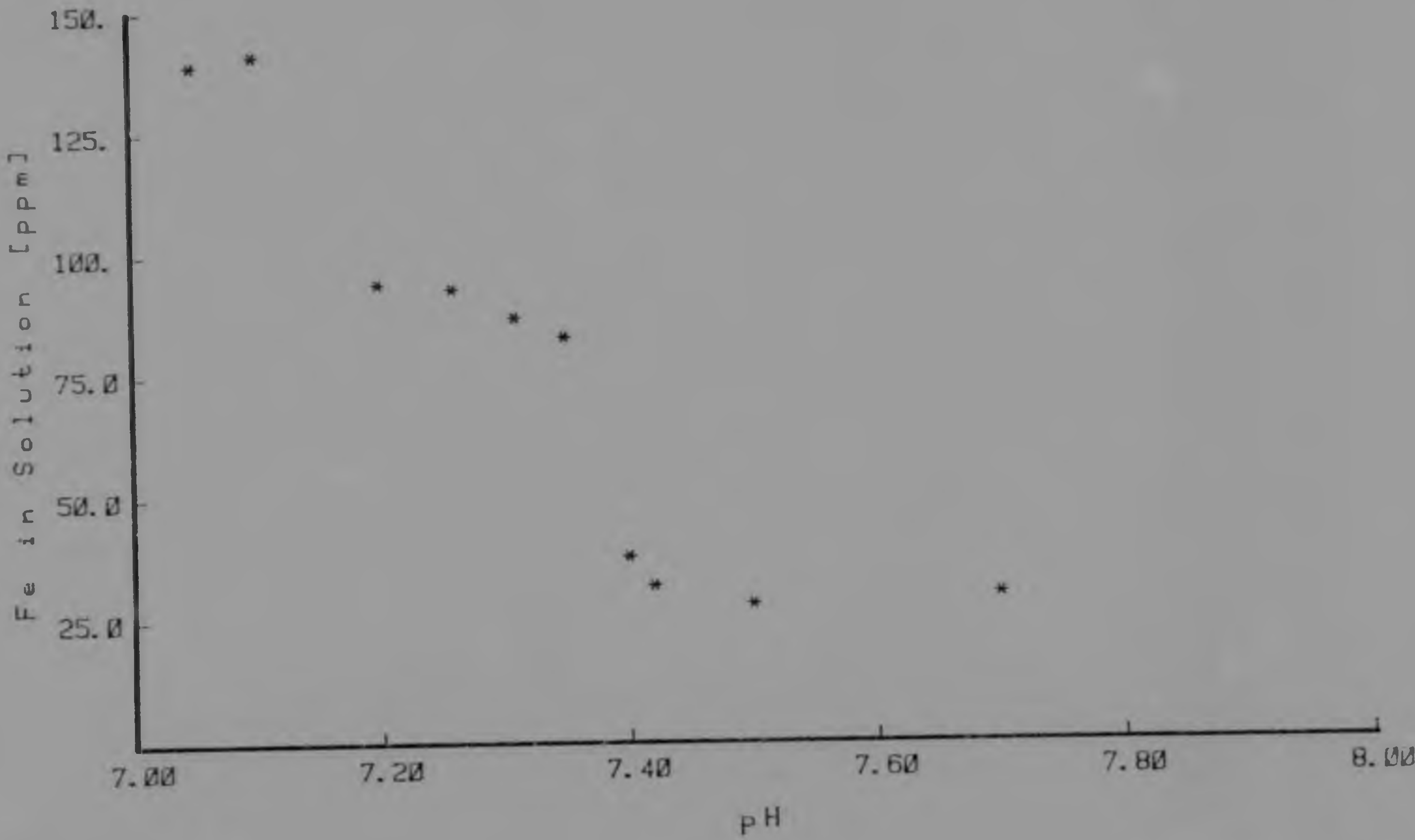

FIG.10.25 Leaching of Iron - Run 3

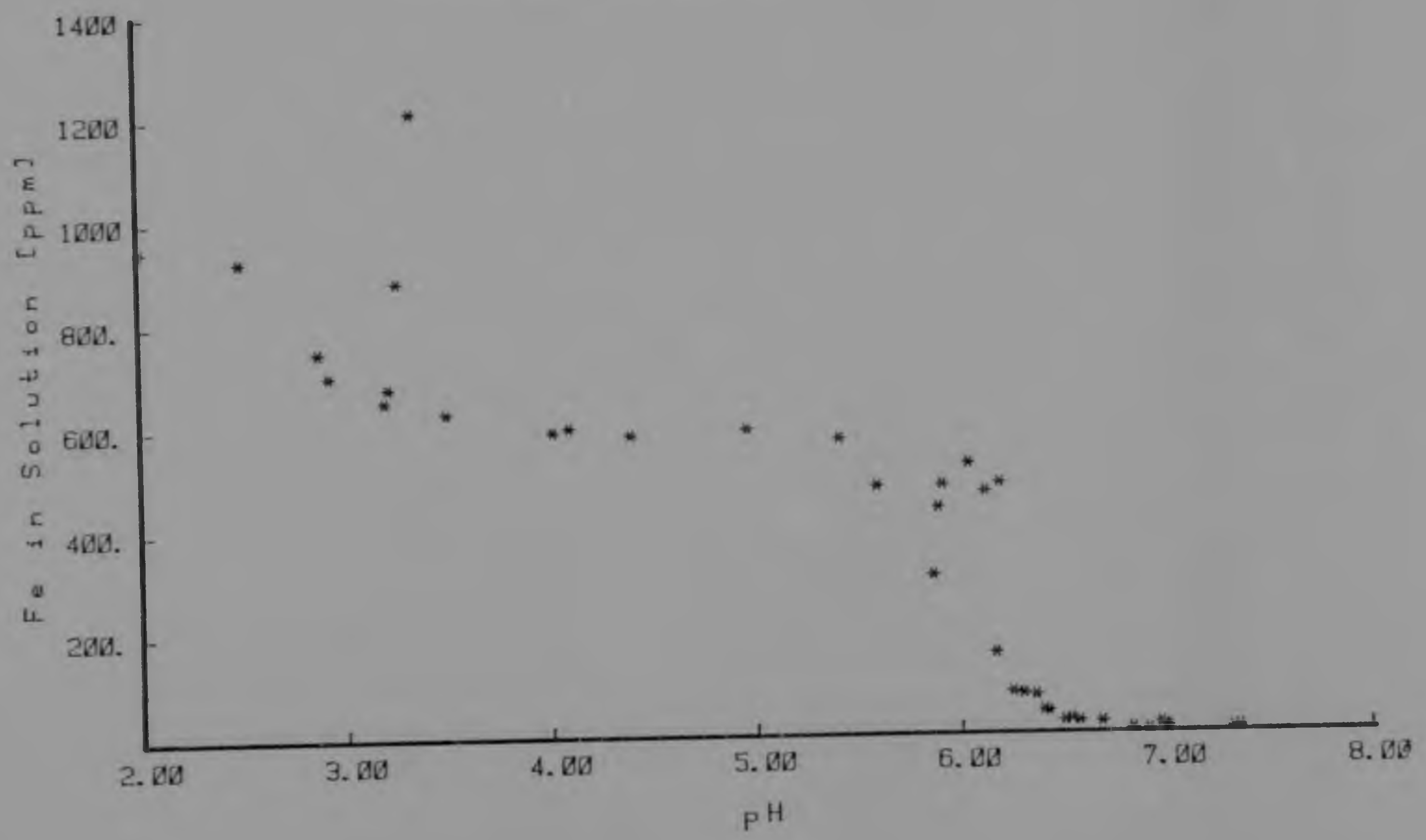

FIG.10.26: Leaching of Silicon - Run 1

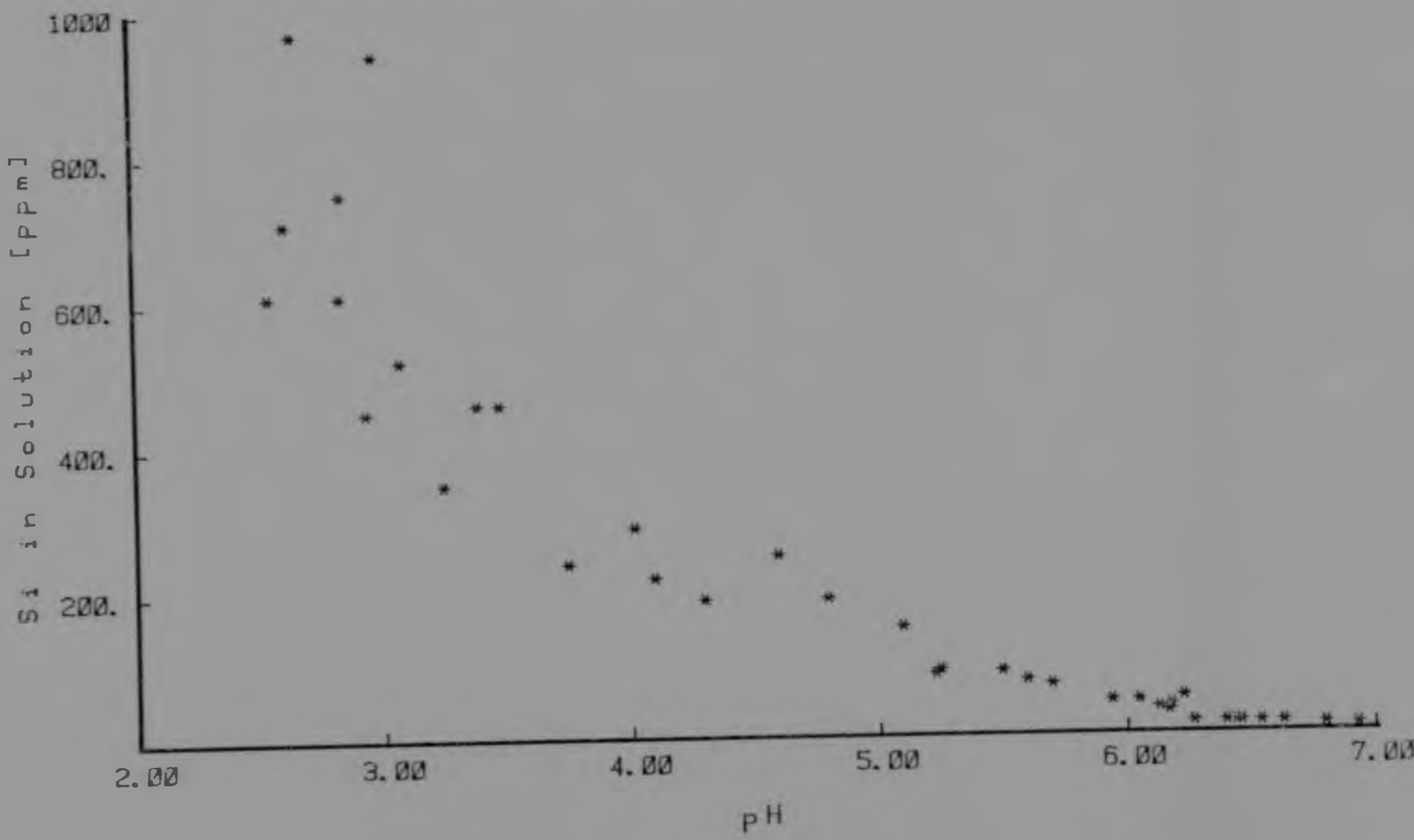

FIG.10.26: Leaching of Silicon - Run 1

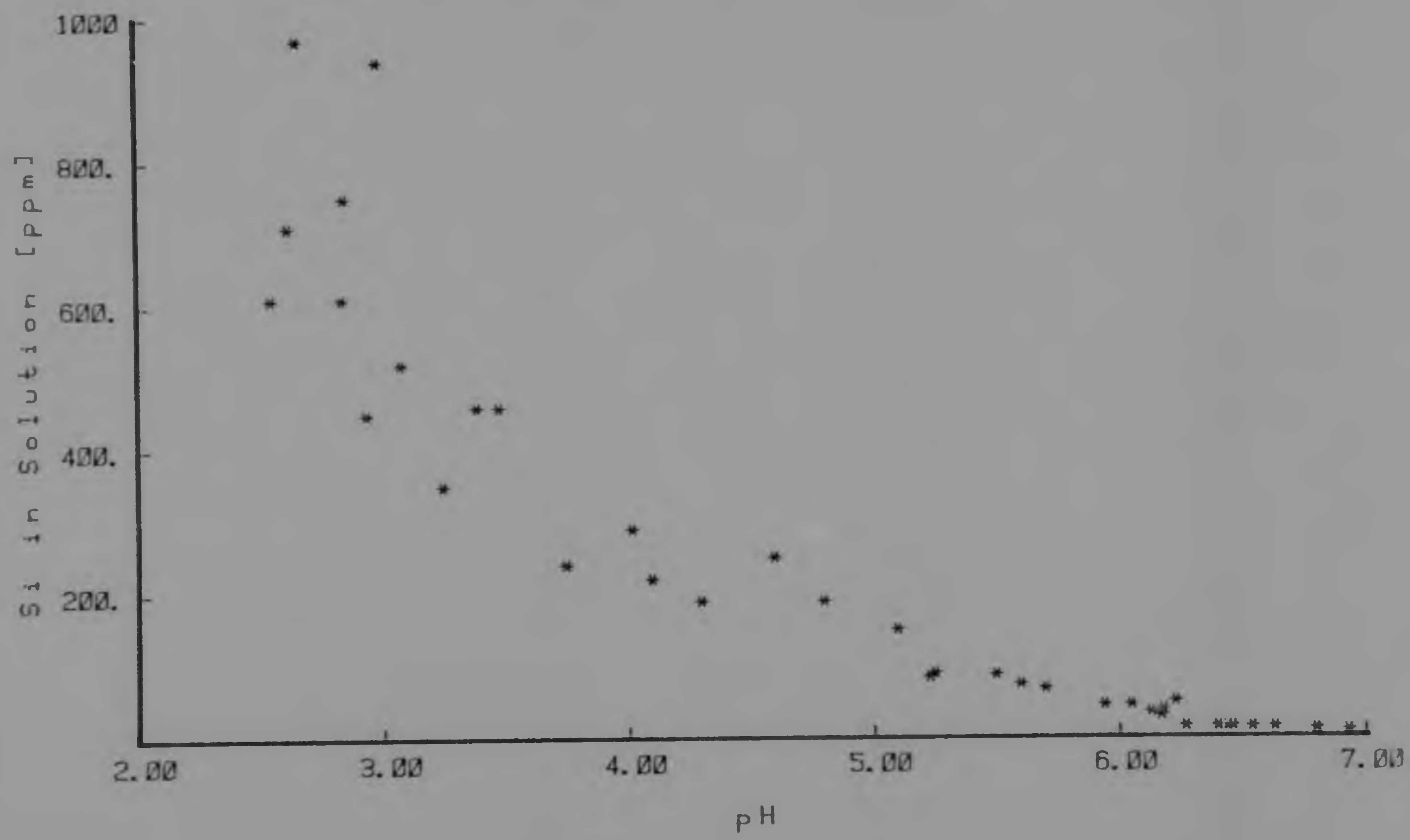

FIG.10.27 Leaching of Silicon - Run 2

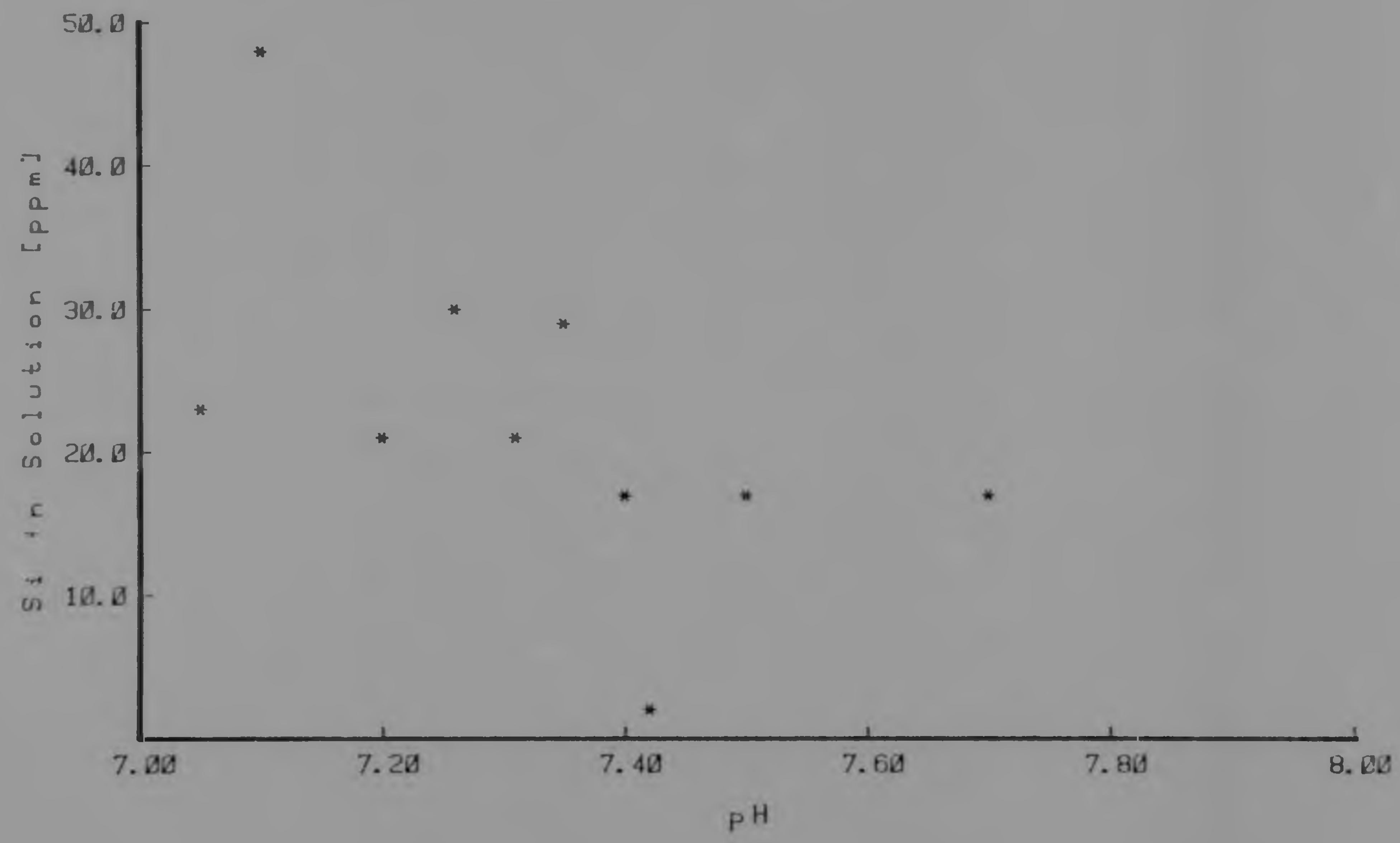

FIG.10.28: Leaching of Silicon - Run 3

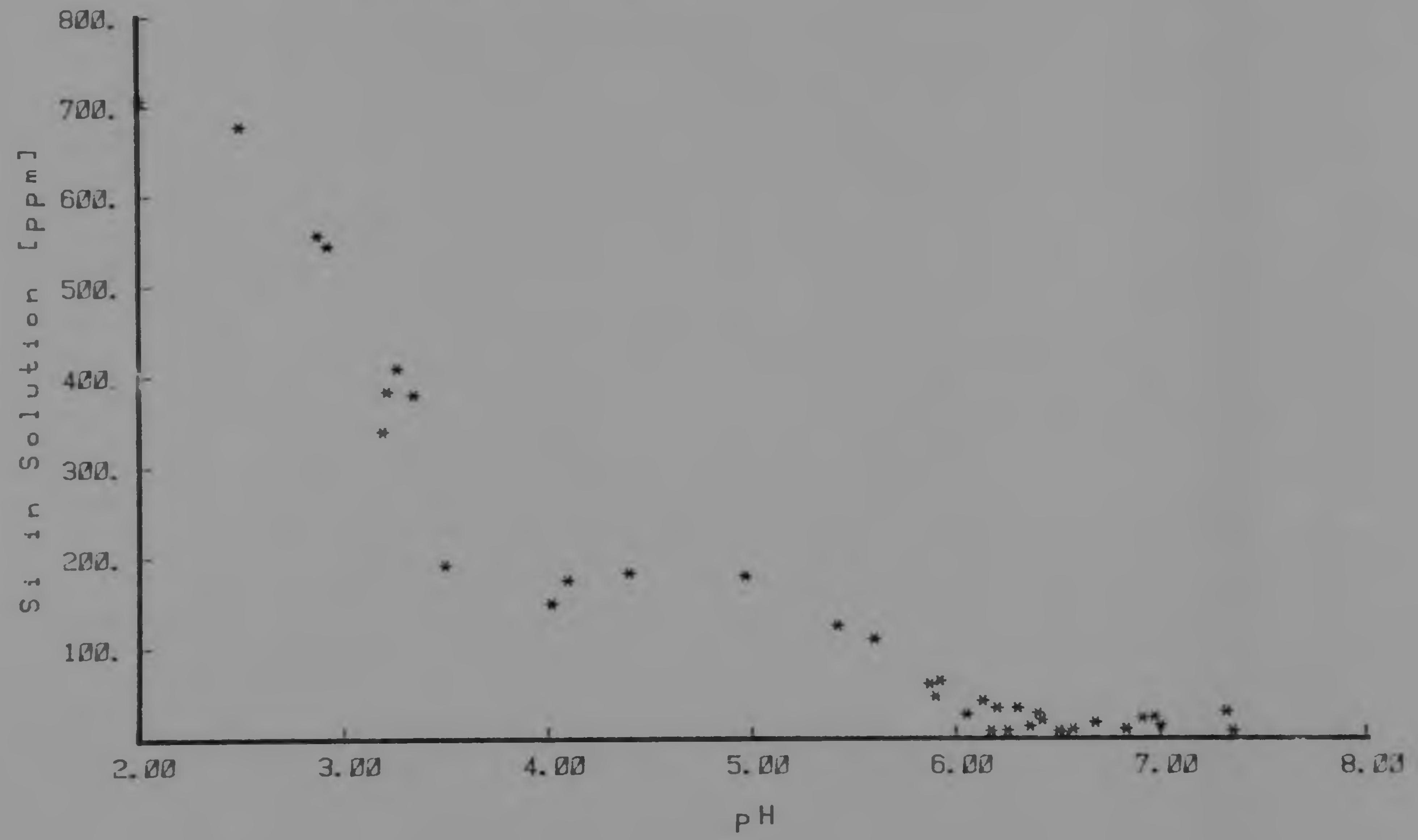

FIG.10.29: Leaching of Zinc - Run 1

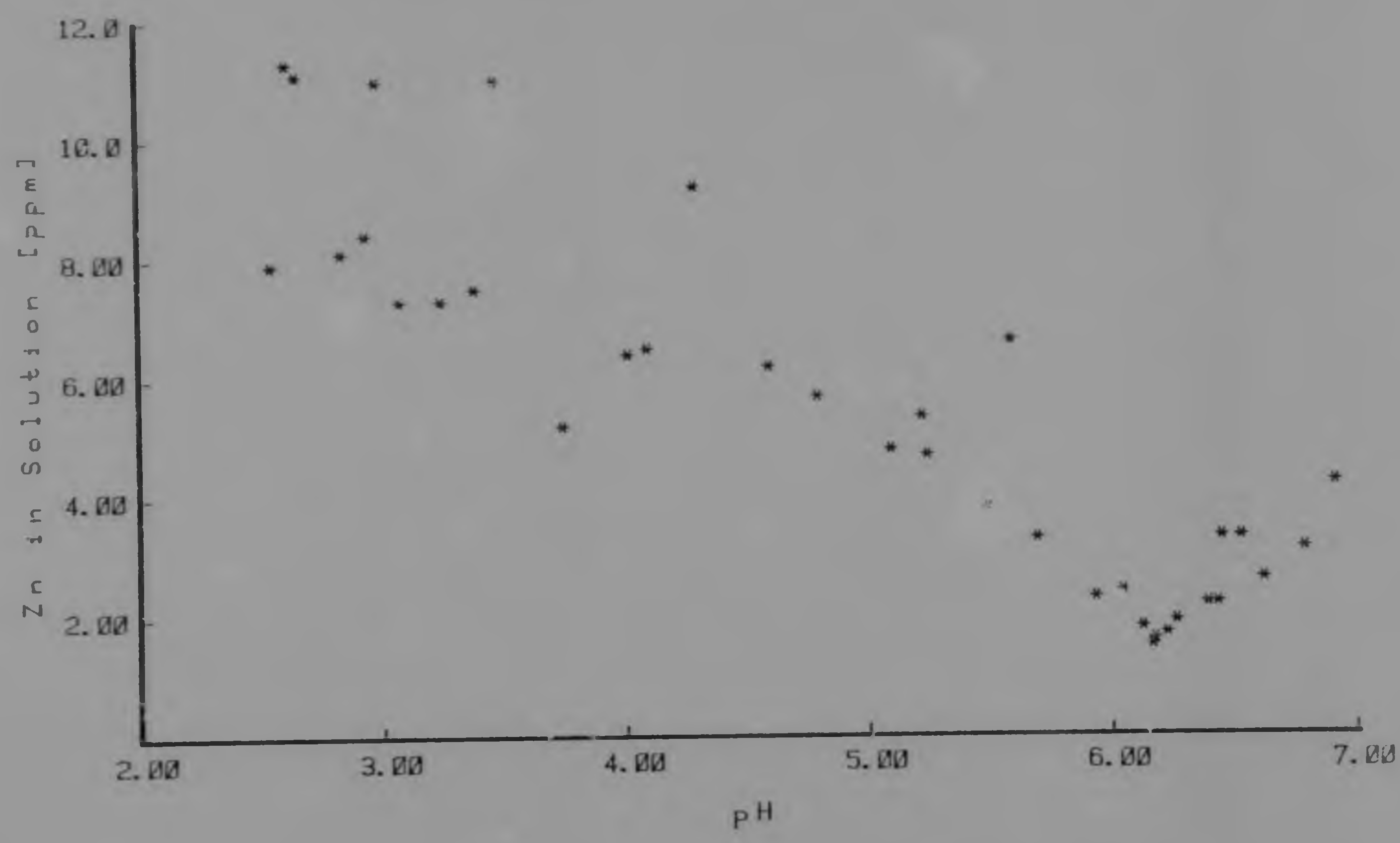

FIG.10.30: Leaching of Zinc - Run 2

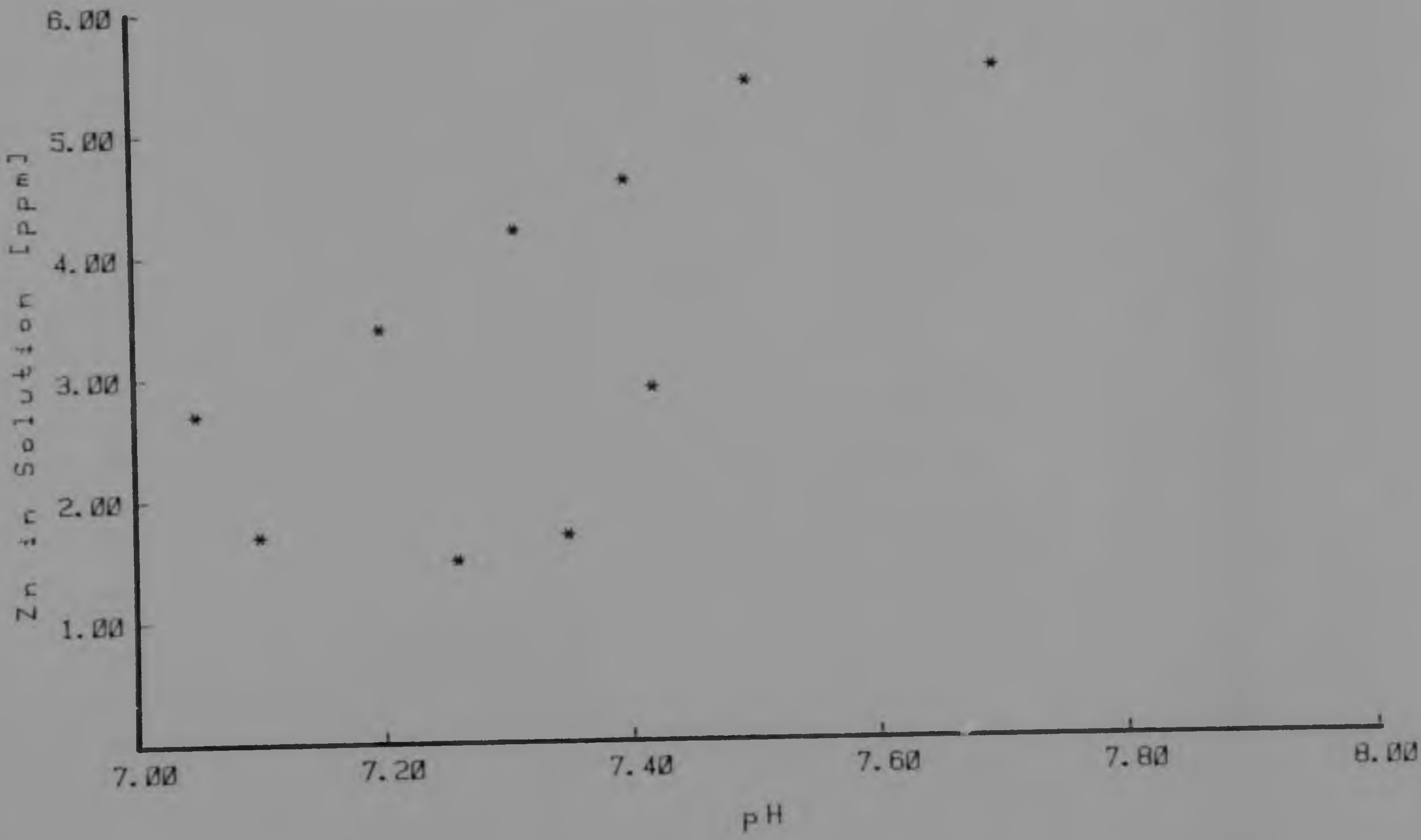

FIG.10.31: Leaching of Zinc - Run 3

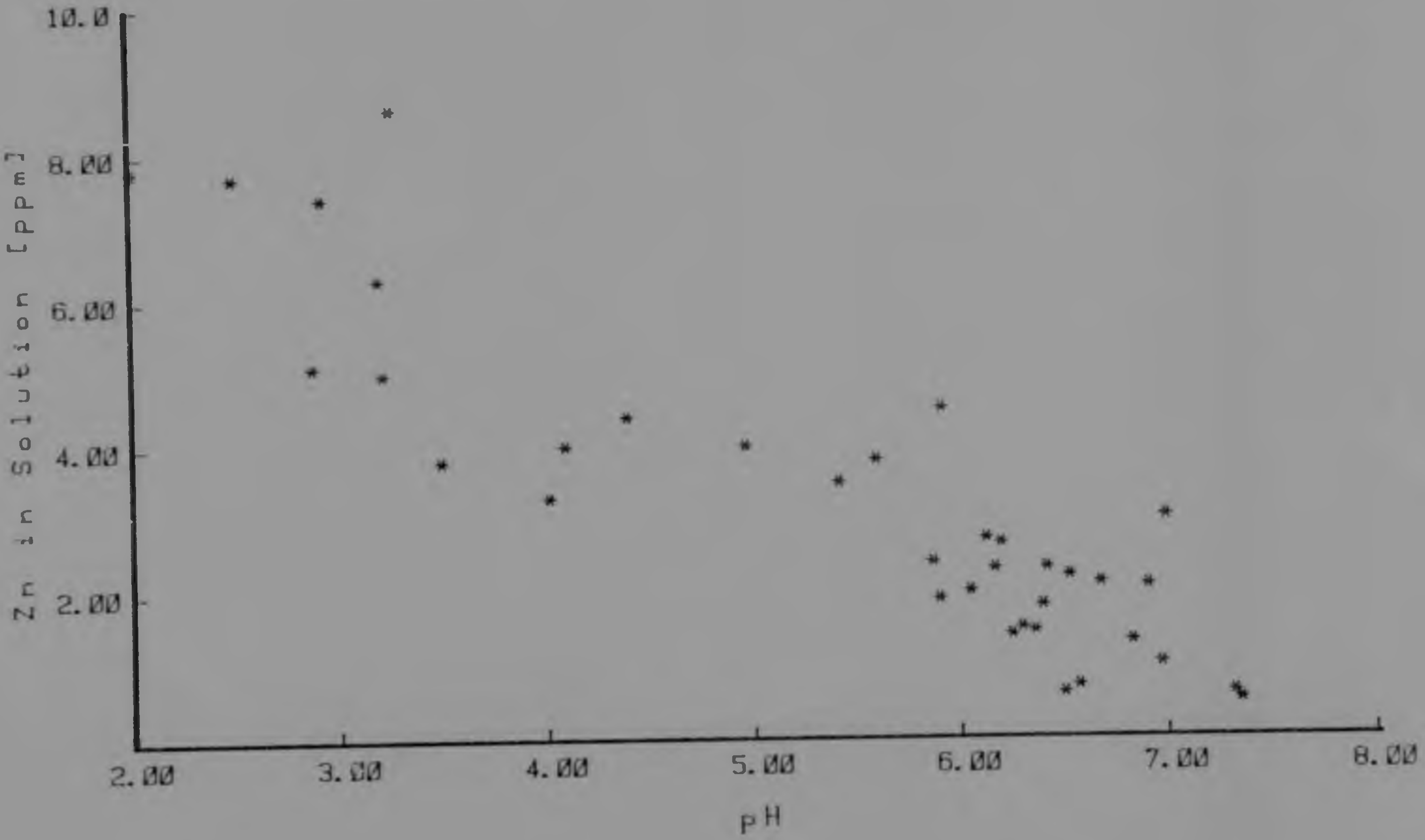

FIG. 10.32: Leaching of Cobalt - Run 1

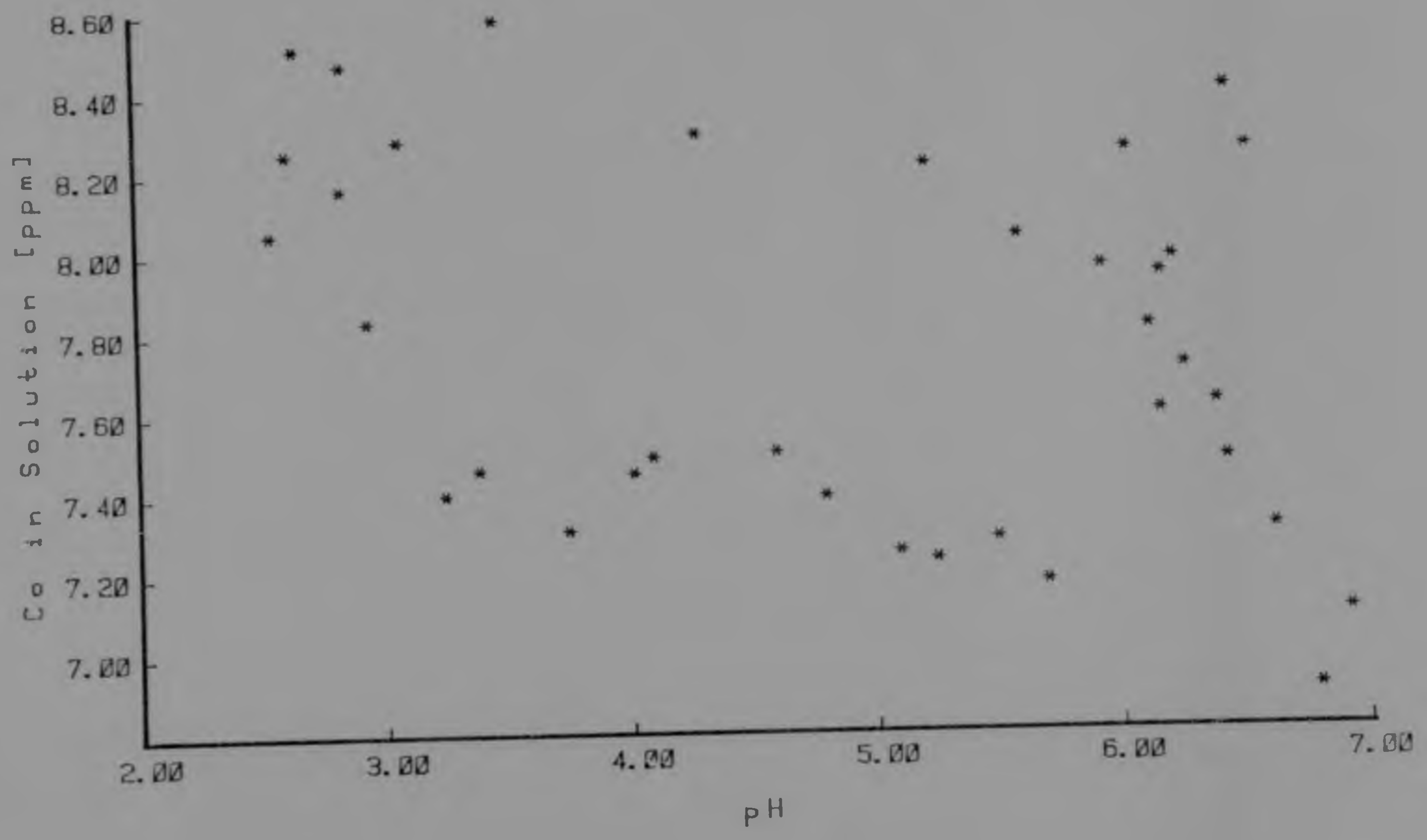

FIG.10.33: Leaching of Cobalt - Run 2

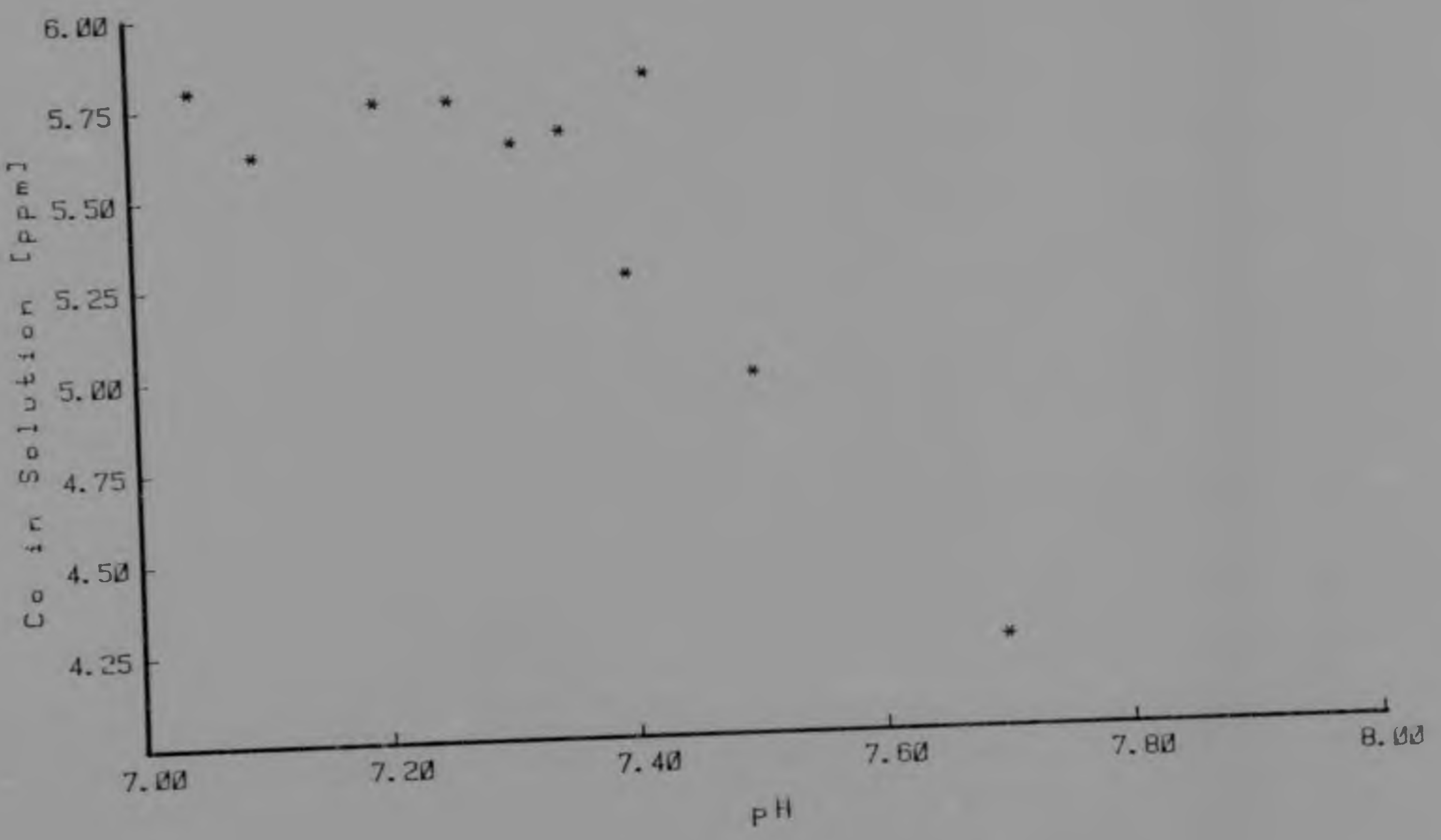

FIG. 10.34: Leaching of Cobalt - Run 3

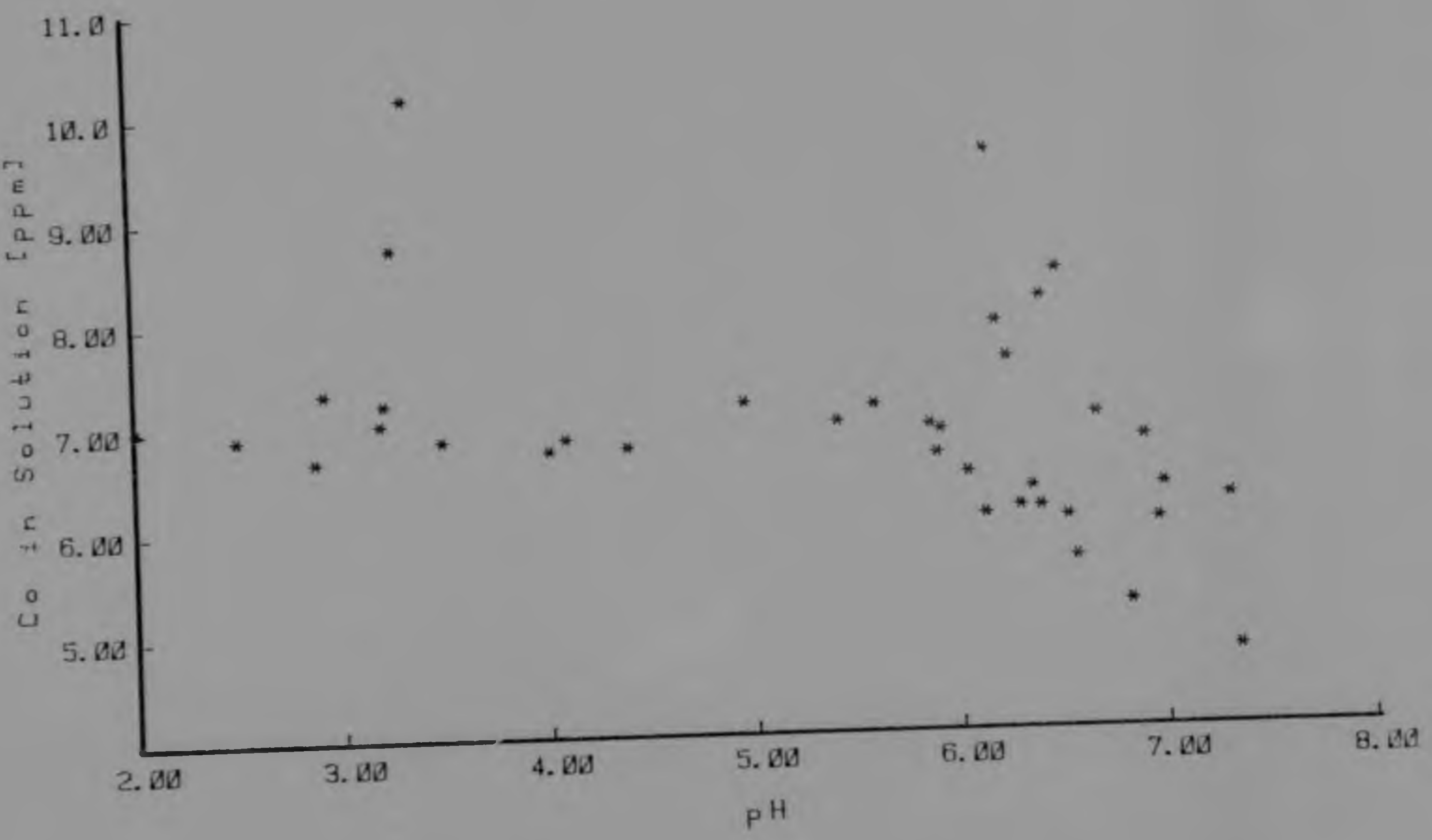

FIG 10.35: Leaching of Nickel - Run 1

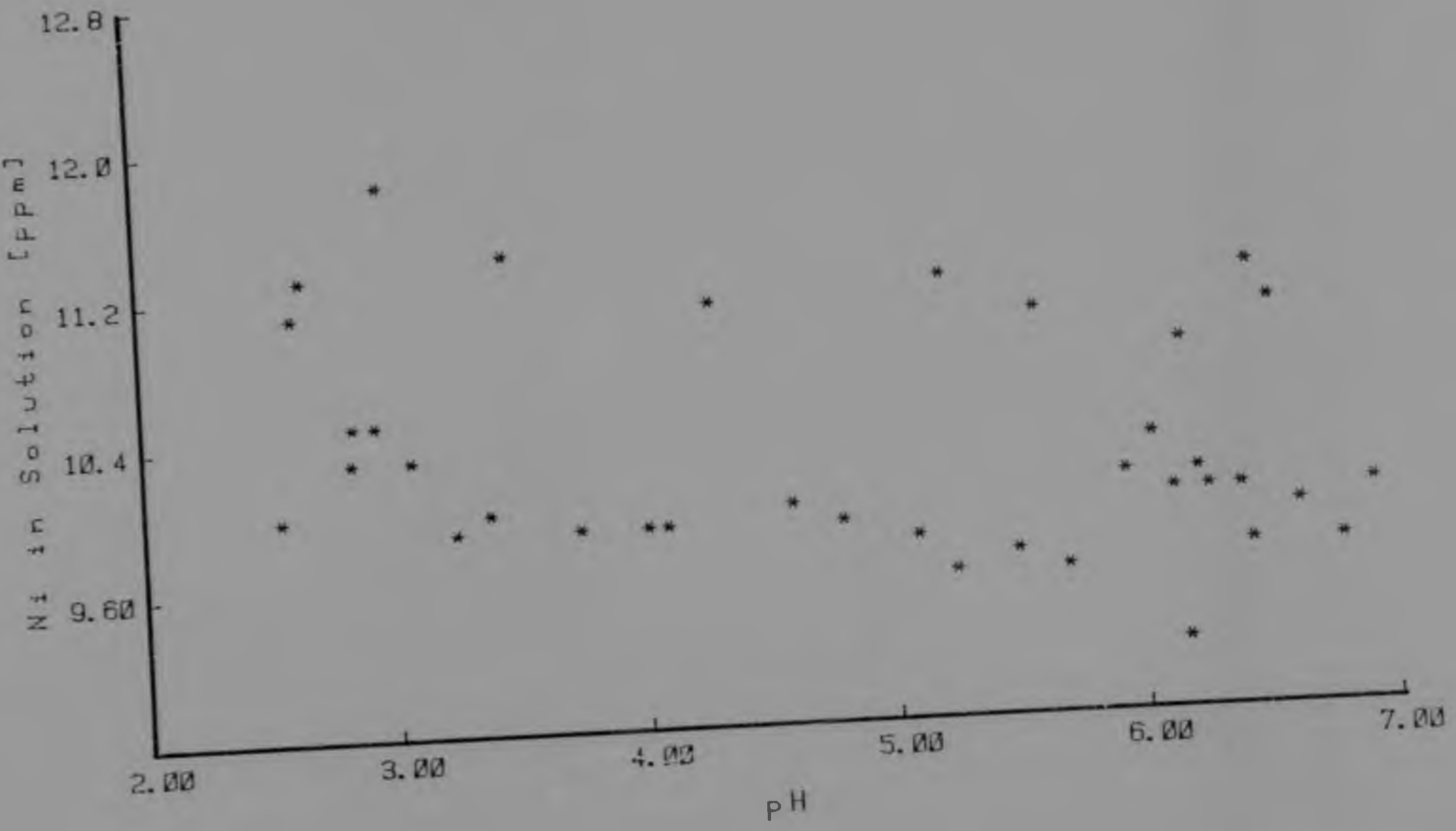

FIG 10.36: Leaching of Nickel - Run 2

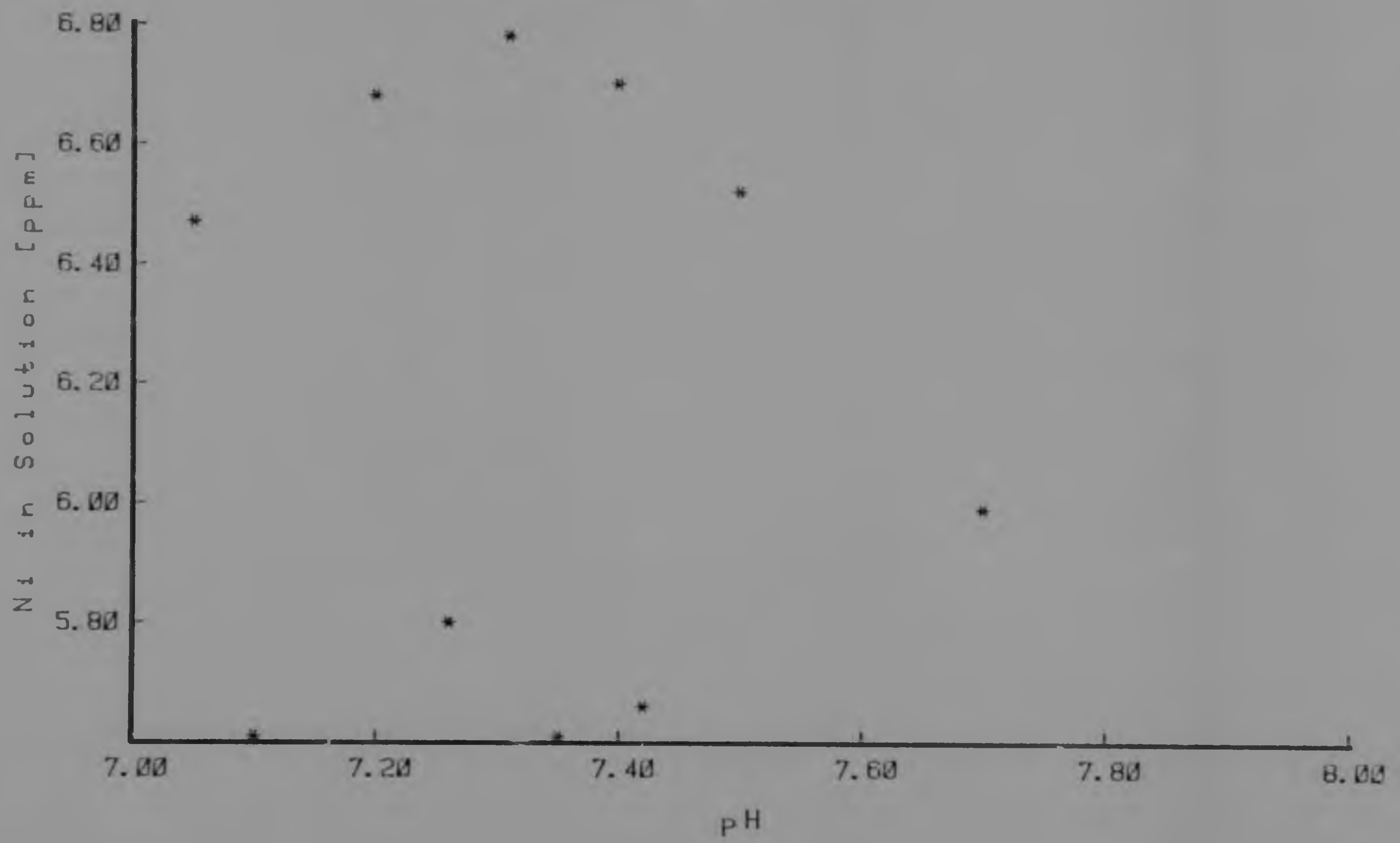

FIG.10.37: Leaching of Nickel - Run 3